12-1-2014

AN IMBRICATE MID CRUSTAL SUTURE ZONE: THE MOJAVE-YAVAPAI PROVINCE BOUNDARY IN GRAND CANYON, ARIZONA

Mark Holland

Mark Holland

Candidate

Earth and Planetary Sciences

Department

This thesis is approved, and it is acceptable in quality and form for publication:

Approved by the Thesis Committee:

Dr. Karl Karlstrom , Chairperson

Dr. Laura Crossey

Dr. Yemane Asmerom

AN IMBRICATE MID CRUSTAL SUTURE ZONE: THE MOJAVE-YAVAPAI PROVINCE BOUNDARY IN GRAND CANYON, ARIZONA

by

MARK E. HOLLAND

B.S. GEOLOGY, UNIVERSITY OF MASSACHUSETTS, AMHERST, 2012

THESIS

Submitted in Partial Fulfillment of the
Requirements for the Degree of

Master of Science
Earth and Planetary Sciences

The University of New Mexico
Albuquerque, New Mexico

December, 2014

ACKNOWLEDGEMENTS

I would like to acknowledge several institutions and individuals that have made this research possible. First I would like to extend my thanks to the University of New Mexico Department of Earth and Planetary sciences for the financial support that has made my graduate education possible. Second, I would like to thank the University of New Mexico Office of Career Services for financial support that allowed me to present this research at both the Geological Society of America Annual Meeting in 2013, and the American Geophysical Union Fall Meeting in 2013. Next, I acknowledge the National Science Foundation for providing funds to Dr. Karl Karlstrom and Dr. George Gehrels through NSF grant EAR-1145247. These funds provided the wherewithal to analyze dozens of samples and expand our understanding of the Proterozoic assembly of the North American continent. In addition, I am grateful to have had the Arizona Laserchron Center at my disposal. The ALC is a top notch analytical facility with an exceptionally knowledgeable and helpful staff. A special to thanks to the Laserchron staff who must be well sick of the Karlstrom/Holland group by now.

As for professional acknowledgements, I must acknowledge my committee, but first and foremost extend my sincerest gratitude to my principal advisor, Dr. Karl Karlstrom. Karl has always been eager to answer questions, consider new ideas or interpretations, conduct fieldwork, and has been a powerful inspiration both personally and professionally. I look forward to continuing my graduate career as his student. I would also like to thank Dr. Laura Crossey, whose quick wit extends beyond geology and makes field excursions hilarious and unpredictable. Dr. Yemane Asmerom has been one of the most influential instructors I have ever had. He has challenged me intellectually and I have always felt stronger for it. Furthermore, I must extend my thanks to faculty at the University of Massachusetts, Dr. Michael Williams and Dr. Sheila Seaman, whose academic nurturing enabled me to pursue a graduate degree in geosciences. Thanks to Mike for his contagious enthusiasm for geology, and to Sheila who was quite right when she told me that majoring in geology would be a wonderful idea.

Next, I thank my fellow students for support, comradery, and numerous discussions of our research and geology in general. I acknowledge: Brad Jeffry, Chris McGibbon, Shannon Miller, Phil Ragonese, Jason Ricketts, Jesse Roberston, and Rachel Weiss (Texas Tech). I must extend a very special thanks to Sean Regan, who is as inspiring as he is kind. Were it not for his passion for geology and his friendship I would not be where I am today.

Finally, I would like to thank my family for more than could possible fit on this page. I extend the warmest thanks to Laura Burkemper, to whom I have said all of this already, but thank you for your love and support.

AN IMBRICATE MID CRUSTAL SUTURE ZONE: THE MOJAVE-YAVAPAI PROVINCE BOUNDARY IN GRAND CANYON, ARIZONA

by

Mark E. Holland

B.S., Geology, University of Massachusetts, Amherst, 2012

M.S., Earth and Planetary Sciences, University of New Mexico, 2014

ABSTRACT

The Mojave and Yavapai provinces in southwestern Laurentia contain evolved and juvenile crust respectively, but the nature of their boundary remains uncertain. This paper analyzes the U-Pb-Hf isotopic composition of zircons from both the oldest plutons and metasedimentary rocks in Grand Canyon. My results show that the Vishnu Schist does not support suturing. Paradoxically, plutons east and west of the Crystal shear zone support suturing based on different U-Pb-Hf isotopic characteristics across the shear zone. I interpret the nature of this boundary to be the existence of an Archean substrate which is sampled by plutons west of the shear zone. The overlapping Vishnu Schist suggests a more complicated architecture. The Vishnu Schist was deposited across Mojave and Yavapai crust, and imbricated during the Yavapai orogeny. The ultimate architecture is a distributed boundary with slivers of plutons carrying the isotopic signature of their respective provinces imbricated within metasediments.

LIST OF FIGURES

LIST OF TABLES

INTRODUCTION

The core of the North American continent was assembled by collision of Archean cratons during the 1.83-1.80 Ga Trans-Hudson system (Hoffman, 1988; Corrigan et al., 2005; 2009) followed by progressive southward (present coordinates) addition of lithosphere in accretionary orogens of southwestern Laurentia (Karlstrom and Bowring, 1988; Windley, 2003) beginning ~1.8 Ga and culminating with the Grenville orogeny and assembly of Rodinia (e.g. Whitmeyer and Karlstrom, 2007). In this model, southern Laurentia is an important field laboratory for studies of continent formation processes because it has been interpreted as an amalgamation of dominantly juvenile Paleoproterozoic terranes that were added to the Archean and 1.8 Ga nucleus (Figure 1 inset) (DePoalo, 1981; Hoffman, 1988; Karlstrom and Bowring, 1988; Bowring and Karlstrom, 1990; Duebendorfer, 2007). Further, this region may represent one of the largest additions of juvenile continental crust in Earth history (Reymer and Schubert, 1986). Alternatively, new models suggest that many orogens previously thought to be predominantly accretionary can contain hybridized and metasomatized lithosphere where cryptic substrates of older lower crust and mantle lithosphere underlie younger crust (Begg et al., 2007; 2009; Griffin et al., 2008; 2011; Belousova et al., 2009; 2010).

The Mojave Province of southwestern Laurentia (Figure 1) has long been known to include older crustal material (Bennett and DePaolo, 1987; Wooden and Miller, 1990; Chamberlain and Bowring, 1990; Wooden and DeWitt, 1991; Ramo and Calzia, 1998; Ilg et al., 1996; Hawkins et al., 1996; Iriondo et al., 2004; Barth et al., 2000, 2009; Wooden et al., 2012), but the age, origin, and distribution of this material remains uncertain. A parallel debate has involved the boundary between the Mojave province and the Yavapai

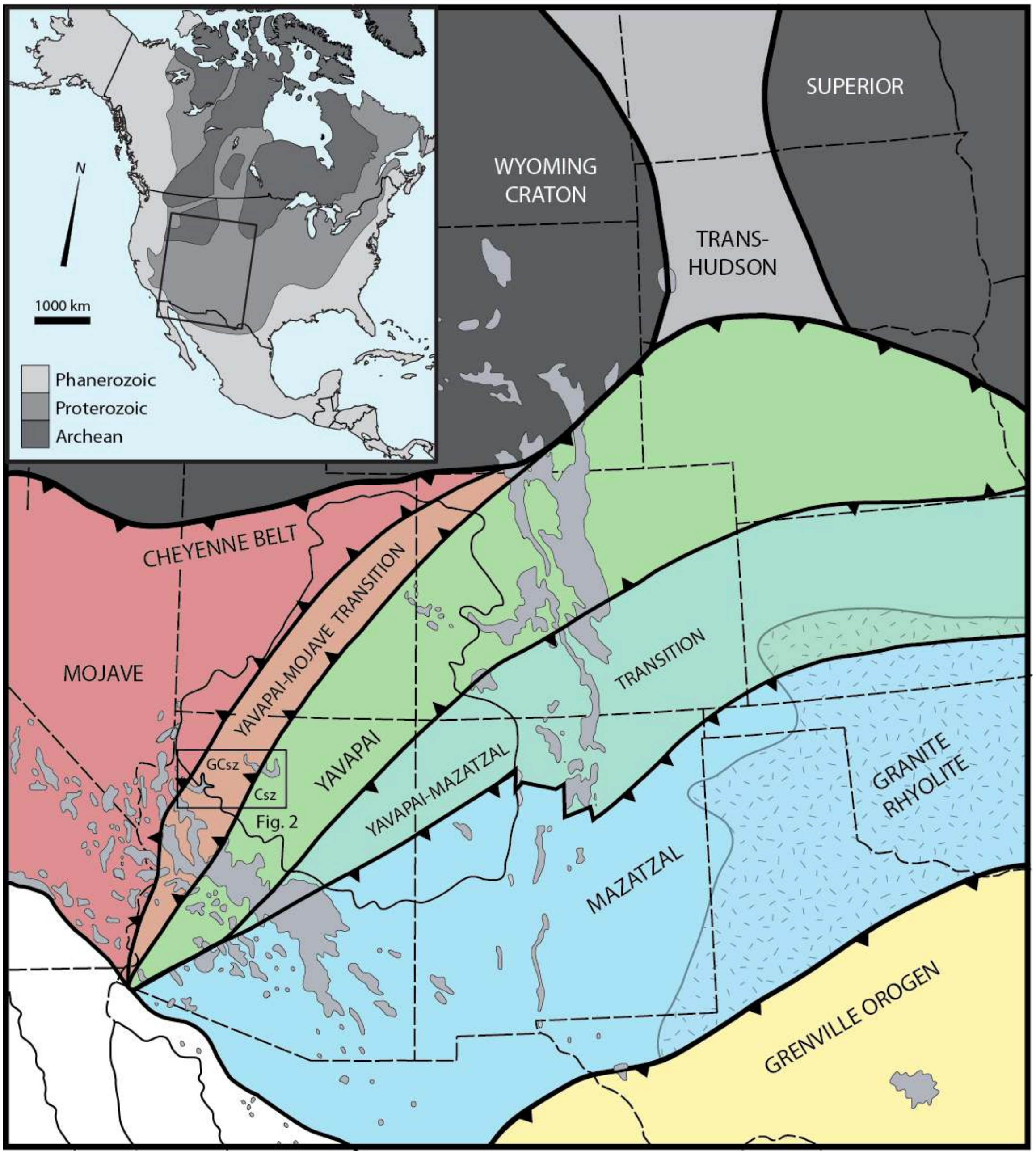

Figure 1. Regional map of Proterozoic provinces of western Laurentia modified after Karlstrom et al., 2004. Outcrops of Proterozoic rocks are shown in gray. Box shows location of Figure 2. Csz (Crystal shear zone), GCsz (Gneiss Canyon shear zone).

province, which contains 1.8-1.7 Ga juvenile crust (Wooden and DeWitt, 1991; Karlstrom and Bowring, 1993; Bennett and DePaolo, 1987; Duebendorfer et al., 2006). Previous models of the nature of the Mojave province's inherited signature and the Mojave-Yavapai boundary include: 1) subducted Archean detritus as the source of the evolved isotopic signature of the Mojave, with inherited signature decreasing with distance from the Archean Wyoming province (Bennett and DePaolo, 1987; Ramo and Calzia, 1998), 2) a ~75 km wide boundary zone defined by whole-rock and feldspar Pb isotopic data that was interpreted to be the result of post 1.73 Ga modification of the Mojave-Yavapai boundary by deformation and plutonism after the provinces were tectonically juxtaposed (Wooden and DeWitt, 1991), 3) a distributed tectonic suture centered at the Crystal shear zone in Grand Canyon (Ilg et al., 1996; Hawkins et al., 1996) that extends ~130 km to the Gneiss Canyon shear zone in western Grand Canyon (Karlstrom et al., 2003), 4) Duebendorfer et al. (2006) interpreted similar Pb isotopic data to represent a wide isotopically mixed zone resulting from rifting and hybridization of older crust, and 5) the presence of Archean crust in middle to lower crustal subcrops of the Mojave province that contributed detritus to the Vishnu Schist (Shufeldt et al., 2010).

A recent detrital zircon study was conducted on the Vishnu Schist in the Grand Canyon, which spans over 30 km on both sides of the proposed Crystal suture zone (Shufeldt et al., 2010). Laser ablation-multicollector-inductively coupled plasma-mass spectrometry (LA-MC-ICP-MS) analysis of >1000 grains separated from 12 spatially distributed samples along a 180-km-long cross-strike transect revealed a uniform bimodal detrital zircon age population with peaks at 1.8 Ga and 2.5 Ga. This surprising result lead Shufeldt et al. (2010) to conclude that: 1) any collision of Yavapai crust with Mojave either pre-dated or was synchronous with Vishnu deposition at 1.75 Ga because the turbidite succession overlaps the proposed crustal boundary at Crystal shear zone, 2) these sediments were not derived from juvenile terranes as only 13% were 1.75 Ga grains, 3) the ~1.85 Ga peak in the metasediments was derived from the underlying 1.84 Ga Elves Chasm gneiss, and 4) that an older Mojave crustal substrate contributed detritus to the Vishnu Schist.

The purpose of this paper is to present new Hf and U-Pb data from the oldest rocks in the Grand Canyon and use a synthesis of all available age and isotopic data to test models to explain the nature of the Mojave-Yavapai boundary. The goal is to resolve the nature of the Crystal shear zone by comparing the U-Pb and Hf isotopic composition of zircons from the Vishnu metaturbidite with those from plutons that intrude on both sides of the Crystal shear zone. This methodology will test the hypotheses of Hawkins et al. (1996) and Shufeldt et al. (2010) that the crystal shear zone represents a Mojave-Yavapai crustal boundary, and that there exists an older crustal substrate in the Mojave province. The excellent exposure of a 180-km-long cross-strike basement transect, the uniform detrital zircon population of the Vishnu Schist, and the well described structural, geochronologic, and thermobarometric history of the Granite Gorges make the Grand Canyon an ideal field locality for exploring and resolving the timing and character of the Mojave-Yavapai crustal boundary.

New data includes paired U-Pb and Hf isotopic analyses of 187 detrital zircons from the Vishnu Schist, and 233 igneous zircons from 10 plutons that intrude the Vishnu Schist, from east to west across the entire transect. Our approach of applying paired U-Pb dating and Hf isotopic analysis to both the oldest metasedimentary rocks and the oldest plutons in the orogen provides a powerful dataset on earliest evolution of the Mojave and Yavapai provinces. These data provide both "top-down" and "bottom-up" views of the crust in the region. U-Pb and Hf composition of zircons collected from metasedimentary rocks provide information about the age and chemical maturity of crust exposed in the provenance region during the time of deposition. Conversely, the U-Pb and Hf composition of zircons separated from intrusive lithologies provide information about the character of their lower crustal melt source regions. The concept of using plutons as probes of the lower crustal melt reservoirs has been applied to many orogens in the North American cordillera, (Farmer and DePaolo, 1983; Samson et al., 1989; 1991; Friedman et al., 1995) the Variscan orogen (Finger et al., 1997) Alpine orogeny (Kohút and Nabelek, 2008), and the Central Asian Orogenic Belt (Jahn et al., 2000; Kovalenko et al., 2004). Hf isotopes of plutonic zircons have been used to evaluate the participation of juvenile versus evolved crust in Proterozoic terranes (Andersen et al., 2002), and to discern terrane boundaries and infer crustal architecture (Cecil et al., 2011).

GEOLOGIC BACKGROUND

Basement rocks are exposed from River Mile (RM measured downstream from Lees Ferry) 78 to 260 within both the Upper Granite Gorge (RM 78-116) and Lower Granite Gorge (RM 208-260) segments. The Upper Granite Gorge in particular is characterized by a block type architecture, consisting of six ~10-km-scale tectonic blocks bounded by five discrete high strain zones, the deformational and metamorphic character of which have been studied extensively (Ilg et al., 1996 Hawkins et al., 1996; Karlstrom et al., 2003; Dumond et al., 2007). These six blocks, from east to west are the Mineral Canyon, Clear Creek, Trinity Creek, Topaz Canyon, Tuna Creek, and Walthenberg Canyon blocks. Two blocks are sampled in the Lower Granite Gorge: the Travertine Grotto and Spencer Canyon blocks, separated by the Gneiss Canyon shear zone (Karlstrom et al., 2003). These eight blocks all contain Vishnu Schist, and they share a similar 1.75-1.69 Ga tectonic history as described below.

Upper Granite Gorge contains about half supracrustal and half plutonic rocks (Figure 2). The supracrustal Granite Gorge Metamorphic Suite is composed of three intimately interlayered but mappable units: the 1740 ± 2 Ma Rama Schist, the 1750 ± 1 Ma Brahma Schist, and Vishnu Schist. These felsic and mafic metavolcanic, and metaturbidite units respectively were interpreted to represent juvenile marine volcanic-arc rocks (Hawkins et al., 1996; Ilg et al., 1996). These are in a transposed depositional contact with underlying basement of the 1840 ± 1 Ma Elves Chasm Gneiss, an orthogneiss that ranges from hornblende biotite tonalite to granodiorite (Hawkins et al., 1996). This is the oldest presently known rock in southwestern North America and is ~90 Ma older than all other lithologies in the Grand Canyon region.

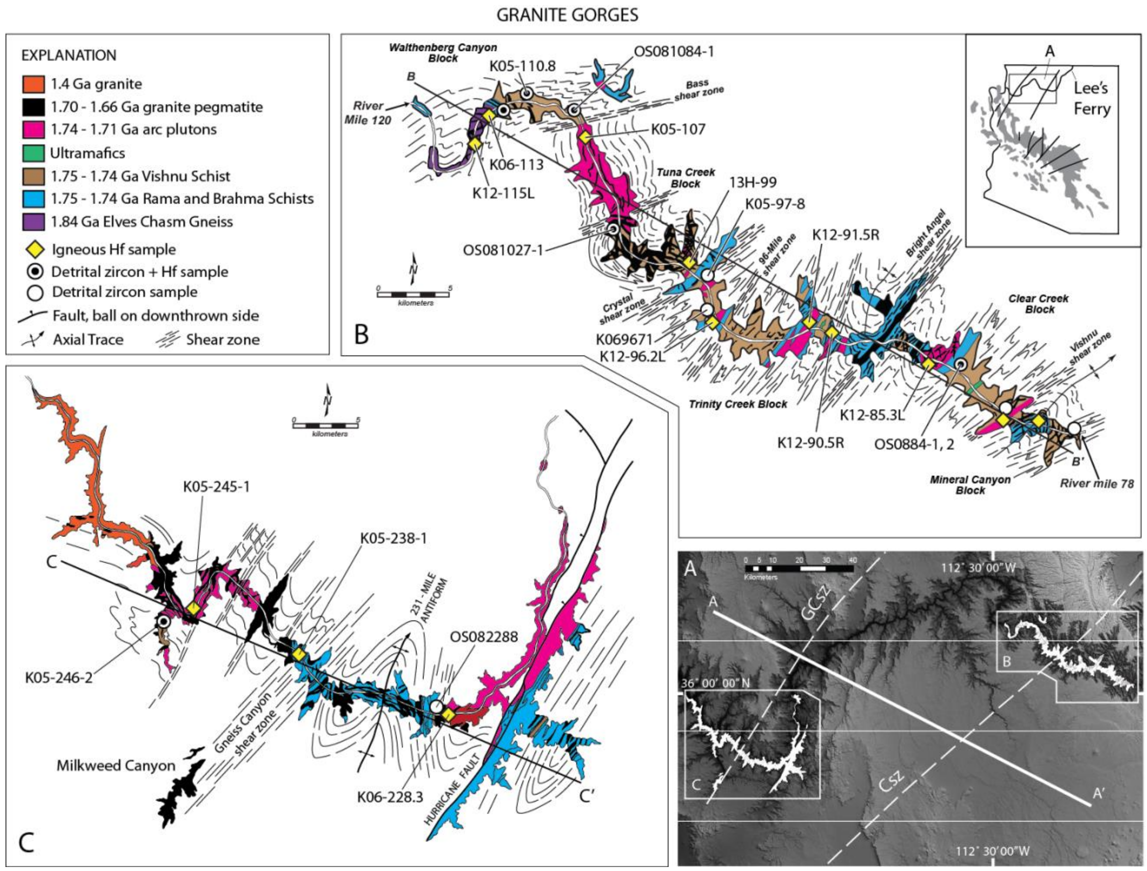

Figure 2. A: Digital elevation model of the Grand Canyon region. Paleoproterozoic outcrops are shown in white. Csz (Crystal shear zone), GCsz (Gneiss Canyon shear zone). Line of section A to A' is keyed to Figure 13. **B:** Geologic map of the Upper Granite Gorge after Ilg et al. (1996). Line of section B to B' is keyed to Figure 3A. Inset shows the Colorado River and outcrops of Proterozoic rocks in the Arizona Transition Zone are shown in gray. Sample locations are projected orthogonally from their location along the river corridor to the line of section. **C:** Geologic map of the Lower Granite Gorge after Karlstrom et al. (2003). Line of section C to C' is keyed to Figure 3B. Sample locations are projected orthogonally from their location along the river corridor to the line of section.

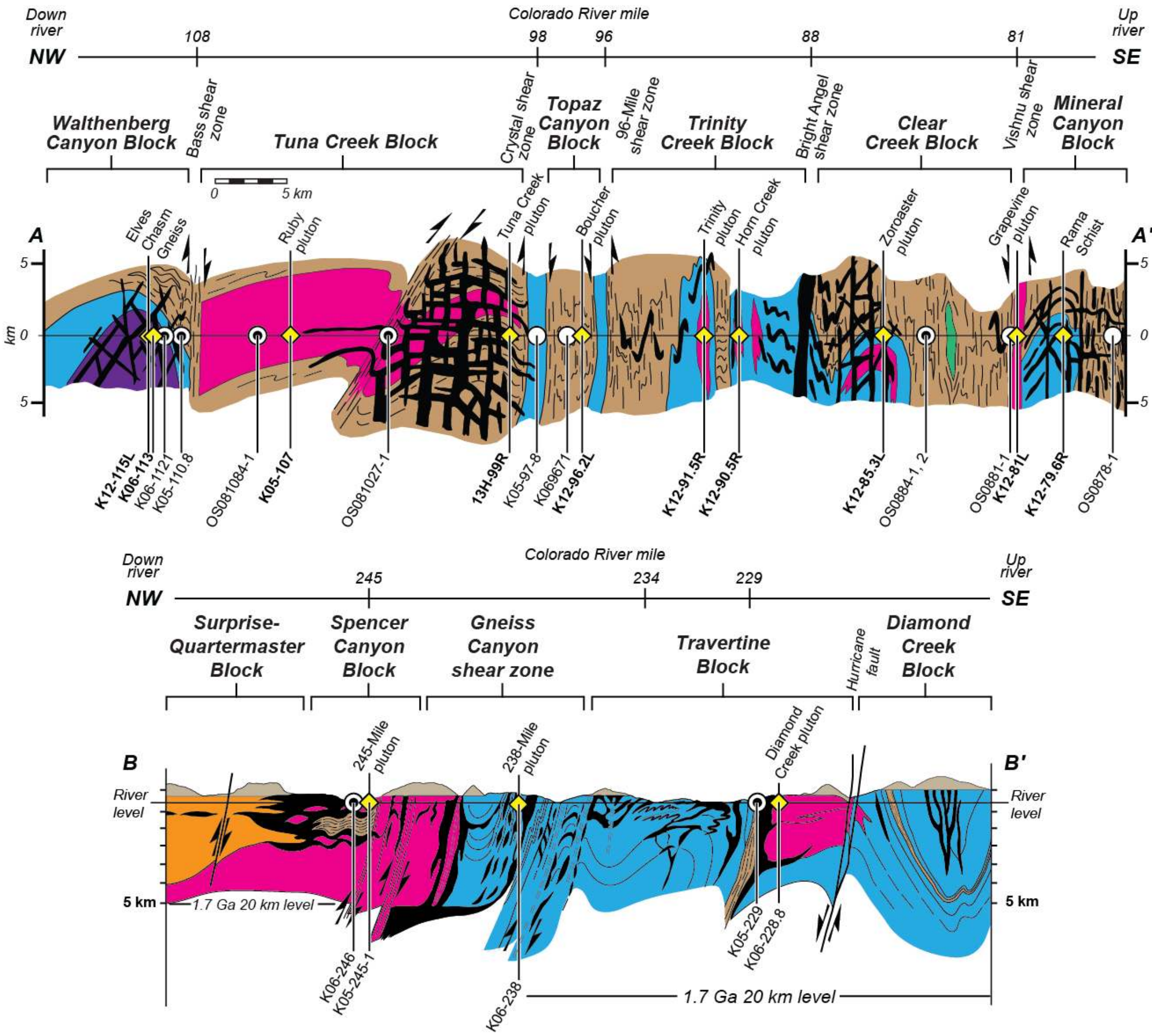

Figure 3. Geologic cross sections of the Granite Gorges in Grand Canyon**.** Sample locations are projected orthogonally from the river corridor to the line of section. The block-type architecture and block-bounding high strain zones are shown along with river mile downstream of Lee's Ferry.**A:** Geologic cross section of the Upper Granite Gorges modified after Dumond et al., 2007. **B:** Geologic cross section of the Lower Granite Gorge modified after Karlstrom et al., 2003 respectively.

The plutonic rocks of the Granite Gorges are calc-alkaline plutons of 1741-1713 Ma (Hawkins et al., 1996), interpreted as subduction-related arc plutons, are primarily granodiorite and commonly have gabbro-diorite enclaves that record varying degrees of magma mixing (Ilg et al., 1996; Karlstrom et al., 2003). Some contacts with the country rock are intrusive with cross cutting fabric relations, but many are tectonic contacts (Table 1). The largest plutons are ten-km-scale large F_2-folded sheet-like bodies, while others are km-wide subvertical tabular bodies that suggest tectonic slices (Figure 3). Ultramafic cumulates also occur as lenses within turbidites and are interpreted as dismembered roots of arc magma chambers (Seaman et al., 1997; Low et al., in progress). In addition, several 1.70-1.66 Ga granite-pegmatite dike swarms are interpreted to be syncollisional granites derived from partial melting of a tectonically thickened crust (Ilg et al., 1996; Hawkins et al., 1996).

The tectonic history of the Upper Granite Gorge involves multi-stage deformation and metamorphism culminating in the 1.72-1.68 Ga Yavapai orogeny (Ilg et al., 1996; Dumond et al., 2007). Structural, geochronologic, and metamorphic studies suggest that the two main stages of deformation overlap locally, and peak metamorphism occurred synchronously with the transition between D_1 and D_2 (Ilg et al., 1996). D_1 involved early thrusting and isoclinal folding, preserved in domains of NW-striking S_1 fabric developed between 1730-1698 Ma (Ilg et al., 1996). D_2 involved km-scale upright, isoclinal to open F_2 folds and development of a penetrative NE striking subvertical S_2 foliation from 1713-1685 Ma (Ilg et al., 1996; Dumond et al., 2007). This subvertical foliation is the dominant fabric throughout the transect. The block-bounding high strain zones (Figure 2) are in D_2 orientations but probably accommodated multiple slip events, including earlier D_1

movements and much later brittle displacement of Grand Canyon Supergroup (Huntoon, 1980; Elston, 1989). Metamorphic studies indicate variable peak temperatures of 520-770 °C with the high strain zones serving as 100 – 200 °C thermal discontinuities between tectonic blocks at near isobaric ~0.7 GPa pressure (~25 km depth; Ilg et al., 1996; Dumond et al., 2007). Dumond et al. (2007) proposed that changes in peak metamorphic temperature across shear zones were the result of magma-enhanced metamorphic field gradients and that the entire transect decompressed from ~0.7 to ~0.3-0.4 GPa (~12 km depths) mainly during the end of D_2 by 1680 Ma, and certainly by 1.4 Ga.

Shear zones are primarily D_2 shortening high strain zones, however some have been proposed to have earlier histories, like the Crystal shear zone. It is a ~1 km-wide, NE-striking zone of strong foliation with stretching lineations plunging steeply to the west (Ilg et al., 1996). Based on macroscopic fold asymmetries, and a ~0.1 GPa higher pressure to the west (Ilg et al., 1996; Dumond et al., 2007), the shear zone is interpreted as west side up. The presence of possible mélange-like rocks, a step to more radiogenic common Pb isotopic composition west of the shear zone, and the presence of xenocrystic >2.0 Ga zircons to the west of the shear zone suggest the Crystal shear zone represents an early (D_1) structure that was reactivated and transposed during D_2 deformation (Ilg et al., 1996; Hawkins et al., 1996). However, as mentioned above, the uniform detrital zircon population of the Vishnu Schist across this boundary suggests that any juxtaposition of crustal blocks across this boundary must have occurred before or during Vishnu Schist deposition at 1750 Ma (Shufeldt et al., 2010).

METHODS

Samples for this study were collected over the course of several field seasons from 2005-2014, and U-Pb and Hf isotopic analyses were conducted at two different laboratories. Plutonic samples from western Grand Canyon were taken by Dr. Graham Begg and Dr. Karl Karlstrom during two field seasons in 2005 – 2006 and analyzed at the Geochemical Evolution and Metallogeny of Continents (GEMOC) Key Centre at Macquarrie University in Sydney, Australia. Samples of Vishnu Schist from across the entire Grand Canyon transect were taken on field seasons in 2005 – 2006 and 2008 and detrital zircon U-Pb analyses were conducted at the Arizona Laserchon Center (ALC) at the University of Arizona in Tucson by Owen Schufeldt. Subsequent Hf isotopic analysis of the Vishnu Schist was carried out on these samples by Dr. George Gehrels at the ALC in 2010 and I carried out new U-Pb and Hf isotopic analyses from 2012-2014. I collected plutonic samples from the eastern Grand Canyon and performed U-Pb and Hf isotopic analyses on them at the ALC during 2012-2014. Analytical methods at both laboratories are detailed in Appendix A (see also: Belousova et al., 2001; Griffin et al., 2000, 2002, 2004; Jackson et al., 2004; Gehrels et al., 2006, 2008; Cecil et al., 2011; Gehrels and Pecha, 2014).

As detailed in the data repository, both laboratories employ broadly similar sample preparation and analytical methods and report similar precision and accuracy in both U-Pb and Hf isotopic analyses. Both laboratories perform standard heavy mineral separation techniques and mount unknowns together with zircon standards. Prior to analysis, backscattered electron (BSE) or cathodoluminescent (CL) images of all unknown grains were obtained to guide spot selection and identify potential xenocrystic cores. All εHf values were calculated using the bulk silicate earth composition of Bouvier et al. (2008), and we compare the results to the depleted mantle composition of Vervoort and Blichert-Toft (1999).

U-Pb AND Hf ICPMS RESULTS FROM GRAND CANYON

Table 1 provides a synthesis of new and published U-Pb geochronologic and Hf isotopic analyses from the basement rocks of the Grand Canyon. The results of all analyses are presented in Appendix A. Table A1 contains all new Vishnu Schist and Rama Schist U-Pb geochronologic analyses. Table A2 contains all Vishnu Schist and Rama Schist Hf isotopic analyses. Table A3 contains all plutonic U-Pb geochronologic analyses conducted at the ALC. Table A4 contains all plutonic Hf isotopic analyses conducted at the ALC. Table A5 contains all plutonic U-Pb analyses conducted at the GEMOC Key Centre. Table A6 contains all plutonic Hf isotopic analyses conducted at the GEMOC Key Centre. Supporting data are presented in more detail in Appendices B and C; analytical methods are detailed in Appendix B, and descriptions of individual plutonic sample zircon ages, morphology, and internal textures are provided in Appendix C.

Interlaboratory Comparison

Samples of the Tuna Creek pluton, and the Elves Chasm gneiss were independently analyzed at both laboratories. Before discussion and interpretation of the U-Pb-Hf isotopic data discussed herein, we compare the results from these very different samples. The Tuna Creek pluton and the Elves Chasm gneiss provide an excellent means of inter-laboratory comparison; the Tuna Creek pluton contains a complex zircon population with varied U-Pb ages and Hf isotopic compositions, and has never been precisely dated. In contrast, the age of the Elves Chasm gneiss is precisely known (Hawkins et al., 1996), and results from both laboratories show that it is juvenile at 1840 Ma. Therefore, as discussed in more detail below, similar U-Pb-Hf characteristics

Table 1. Geochronologic summary of Paleoproterozoic Grand Canyon rocks

	Rock Name	River Mile	Weighted Mean U-Pb Age (Ma)	MSWD	Deformational Context	Contact Relations	Metamorphic Block	Lab
K12-79.6R	Rama Schist	79.6	1751 ± 16 1741 ± 1[1]	0.2	Pre D_1; from hinge of Sockdolager antiform	Interlayered with Vishnu Schist	Mineral Canyon	ALC
K12-81L	Grapevine Camp Pluton	81	1756 ± 16 1737 ± 1[1]	0.3	Contains S_1; alligned along S_2 Vishnu shear zone. Pre D_1	Cross cuts compositional layering in Vishnu Schist on eastern contact; western contact is the Vishnu shear zone.	Mineral Canyon	ALC
K12-85.3L	Zoroaster Pluton	85.3	1755 ± 14 1740 ± 2[1]	0.6	Contains S_1, folded by F_2. Pre- or syn-D_2	Contains screens of Grand Canyon Metamorphic Suite	Clear Creek	ALC
K12-90.5R	Horn Creek Pluton	90.5	1719 ± 14 1713 ± 1[1]	0.3	Contains magmatic S_1, solid state S_2. Syn-D_1	Intrudes parallel to compositional layering in Vishnu Schist	Trinity Creek	ALC
K12-901.5R	Trinity Gneiss	91.5	1755 ± 16 1730 ± 3[1]	0.4	Contains S_1 and S_2. Pre-D_1	Contacts between Brahma amphibolites are folded and sheared; intrusive contacts locally preserved	Trinity Creek	ALC
K12-96.2L	Boucher Pluton	96.2	1730 ± 15 1714 ± 1[2]	0.5	Weakly foliated. Pre or syn-D_1	Eastern margin is 96-mile shear zone; western margin is intrusive into metasupracrustals	Topaz Canyon	ALC
13H-99R	Tuna Pluton	99	1751 ± 15 < 1750[1]	1.1	Contains S_1 and S_2. Pre- to syn-D_1	Folded sheet-like body intrudes Vishnu Schist	Tuna Creek	ALC
K05-100.5-105	Tuna Pluton	100.5	1737 ± 7 < 1750[1]	0.7	Contains S_1 and S_2. Pre- to syn-D_1	Folded sheet-like body intrudes Vishnu Schist	Tuna Creek	GEMOC
K05-107	Ruby Pluton	107	1726 ± 15 1716.6 ± 0.5[1]	0.1	Contains S_1 as magmatic layering. Syn-D_1	Eastern margin is tectonized, but locally preserves intrusive relations to supracrustal rocks, western margin is cut by the Bass shear zone.	Tuna Creek	GEMOC

K06-113	Elves Chasm Gneiss	113	1842 ± 5 1840 ± 1[1]	0.9	Contains S_1 and S_2. Pre-D_1 basement to Vishnu Schist	Transposed depositional contact between Brahma Schist and Elves Chasm Gneiss	Walthenberg Canyon	GEMOC
K12-115L	Elves Chasm Gneiss	115	1850 ± 18 1840 ± 1[1]	1.4	Contains S_1 and S_2. Pre-D_1 basement to Vishnu Schist	Transposed depositional contact between Brahma Schist and Elves Chasm Gneiss	Walthenberg Canyon	ALC
K06-228.3	Diamond Creek pluton	228.3	1738 ± 14 1736 ± 1[3]	0.2	Contains magmatic S_1 and solid-state S_2 shear zones. Syn-D_1	Intrudes Vishnu Schist on western margin, eastern margin covered by Phanerozoic rock	Travertine Block	GEMOC
K06-238-1	Granitic Gneiss from Gneiss Canyon shear zone	238	1731 ± 14	0.1	Cuts S_1, contains weak to strong and magmatic S_2. Syn-D_2	Sheet like intrusions into mixed para and orthogneisses	Gneiss Canyon shear zone	GEMOC
K06-245-2	245-mile pluton	245	1741 ± 13 1720 ± 5[3]	0.6	Contains S_1 and S_2. Pre-D_2	Intrudes into Vishnu Schist on western margin, eastern margin is intruded by the younger Seperation pluton	Spencer Canyon Block	GEMOC

reported from each laboratory show consistent results and the data can be presented and interpreted together.

Elves Chasm Gneiss

Sample K05-113 was analyzed by Dr. Graham Begg at the GEMOC Key Centre, and I analyzed sample K12-115L at the ALC. The results of each sample analysis are compared in Figure 4. 20 grains separated from sample K05-113 (GEMOC lab) yields a weighted mean age of 1841 ± 5 Ma (MSWD = 0.7). Likewise, 12 ages from sample K12-115L (ALC lab) yielded a weighted mean age of 1855 ± 18 Ma (MSWD = 0.2). The results from both laboratories are in good agreement with the 1840 ± 1 Ma TIMS age of the Elves Chasm gneiss (Hawkins et al., 1996).

Both samples yield juvenile $\varepsilon Hf_{(t)}$ values for the Elves Chasm gneiss. The $\varepsilon Hf_{(t)}$ of the depleted mantle at 1840 Ma is +9.8. $\varepsilon Hf_{(t)}$ values from sample K05-113 range from +12.5 to +8.7 with an average of +10.5. Similarly, K12-115L yields $\varepsilon Hf_{(t)}$ values from +11.3 to +6.1 with an average of +8.6. $\varepsilon Hf_{(t)}$ values from the GEMOC sample (K05-113) are consistently higher than those from the ALC sample (K12-115L), but there is substantial overlap between the two data sets and all zircons yield $\varepsilon Hf_{(t)}$ values that are within analytical error of the depleted mantle array.

Tuna Creek Pluton

Two samples of the Tuna Creek pluton were collected; K05-100.5 was analyzed by Dr. Graham Begg at the GEMOC Key Centre, and I analayzed 13H-99R at the ALC (Figure 5). Both samples show excellent agreement in terms of zircon ages; with a 1740 Ma age peak, and a xenocrystic population of 2480-2485 Ma. The presence of inheritance in the Tuna Creek pluton has been documented previously (Hawkins et al., 1996), but the age constraints were limited to crystallization at 1750-1710 Ma with >2.0 Ga inheritance. These results corroborate prior findings, and provide more complete geochronologic constraints on the age of inherited grains.

There is somewhat more disparity between $\varepsilon Hf_{(t)}$ values in the Tuna Creek pluton than the Elves Chasm gneiss. GEMOC $\varepsilon Hf_{(t)}$ values for six ~1.74 Ga zircons plot in a tight cluster at ~+2.8. Two additional grains yield lower values; one zircon yields an $\varepsilon Hf_{(t)}$ value of -11.3 at 1853 Ma. This grain overlaps at 2σ with the age of the Elves Chasm gneiss, but has a substantially lower $\varepsilon Hf_{(t)}$ value. The 2.48 Ga xenocrystic population in the GEMOC sample also plots in a tight cluster, with an average $\varepsilon Hf_{(t)}$ value of -1.2 for six grains. Conversely, the ALC $\varepsilon Hf_{(t)}$ values for the 1740 Ma population show more of a vertical spread, with $\varepsilon Hf_{(t)}$ values of seven grains ranging from +2.8 to +12.7 and averaging +7.1. Three additional grains that overlap with the age of the Elves Chasm gneiss were identified in sample 13H-99R; two yielded juvenile $\varepsilon Hf_{(t)}$ values, and one yielded an intermediate value of -3.7 at 1851 Ma. Finally, the ~2.48 Ga population of zircons yielded $\varepsilon Hf_{(t)}$ values ranging from +0.9 to +3.7 and averaging at +2.2.

Comparison Summary

Hf isotopic data from each sample show substantial overlap, however average values consistently differ by ~2 espilon units. Typically these differences are within uncertainty of the $\varepsilon Hf_{(t)}$ values. $\varepsilon Hf_{(t)}$ values for the Elves Chasm gneiss were consistently higher from the GEMOC data, however the ALC data yielded higher $\varepsilon Hf_{(t)}$ values for the Tuna Creek pluton. As described by Gehrels and Pecha (2014), the uncertainties reported by the ALC are "not of ideal precision," due to analytical procedures that emphasis accuracy at the expense of internal precision. The result of these procedures is that the

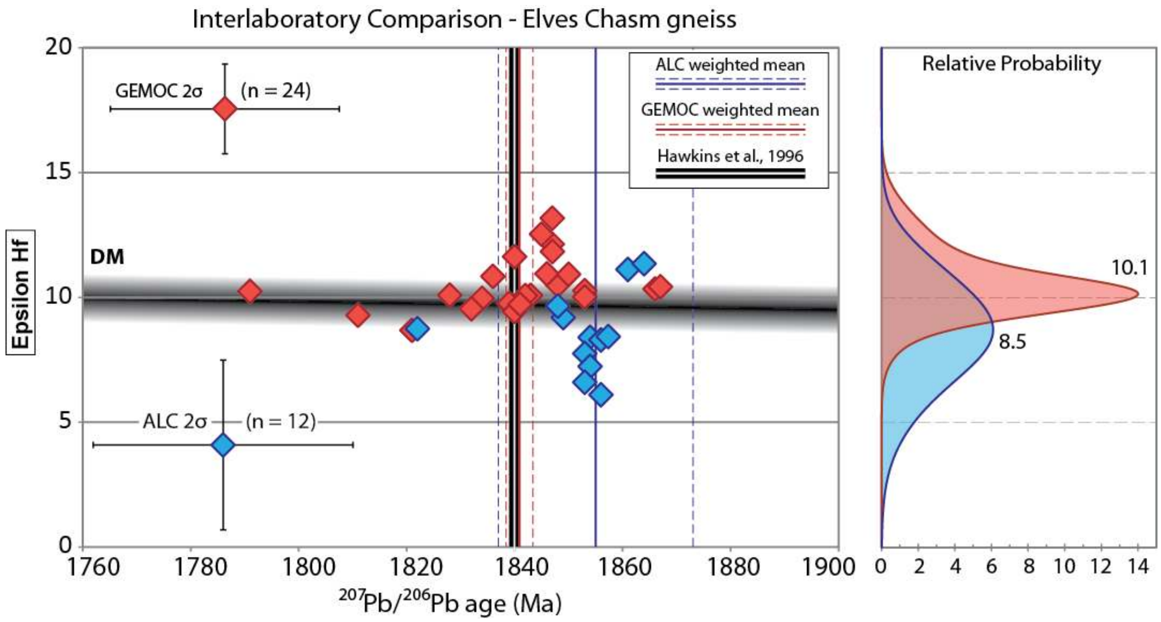

Figure 4. Comparison of results from the Elves Chasm Gneiss as analyzed at the Geochemical Evolution and Metallogeny of Continents (GEMOC) Key Centre, and the Arizona Laserchron Center (ALC). Symbols with error bars represent the average 2 sigma uncertainties for U-Pb and Lu-Hf isotopic analyses from each data set.

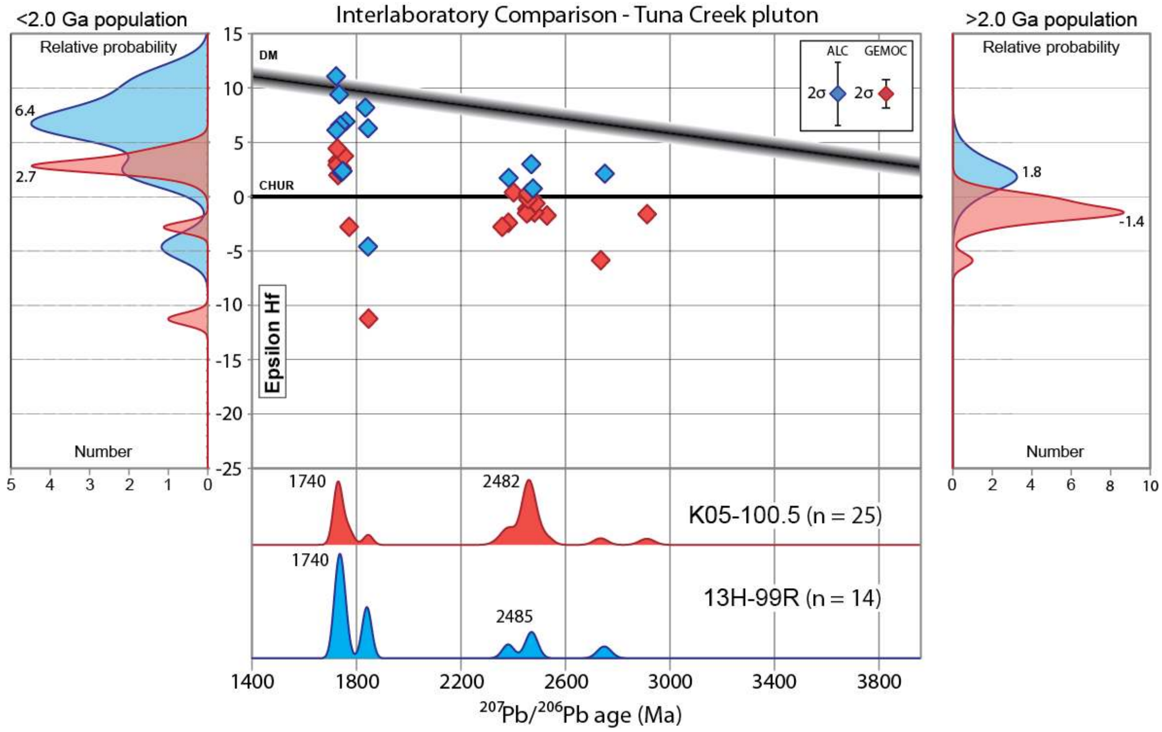

Figure 5. Comparison of ALC and GEMOC results for the Tuna Creek pluton. Coloring and symbols as in Figure 4. Age probability plots are normalized such that the area underneath each curve is equal. These show excellent agreement between U-Pb ages in primary and inherited grains.

$\varepsilon Hf_{(t)}$ values reported by the GEMOC Key Centre are more precise. However, standard analyses from the ALC yielded uncertainties of ± 0.000035 (May 2013) to 0.000040 (May 2014) at 1σ, which result in standard uncertainties of 2 to 3 epsilon units at the 2-sigma level. The uncertainty in standard analyses is consistent with the ~2 epsilon unit disparity between the ALC and GEMOC Key Centre and suggests that all measurements are accurate to within 2-3 epsilon units. However, it must be emphasized that while sample pairs K05-113, K12-115L, and K05-100.5, 13H-99R were obtained from the same plutons, analyses were not conducted on the same zircons. It is possible that one or both plutons may not be isotopically homogenous, and that the observed variation in $\varepsilon Hf_{(t)}$ values reflect real isotopic variation within the plutons. In conclusion, we feel that the results from each laboratory are consistent and the entire data set can be compared within reasonable uncertainty.

Results from Supracrustal Rocks

Vishnu Schist

380 new U-Pb ages from Vishnu Schist were obtained for this study. Analyses were conducted on the same grain mounts prepared by Shufeldt et al. (2010) with the intention of obtaining paired U-Pb and Hf isotopic data. I selected samples that were distributed across the entire length of the Grand Canyon transect (river mile 84 – 246) to obtain data that are representative of the entire population. The results of each analysis are presented in Appendix D, Table A1.

My new data are compiled with the entire dataset of Shufeldt et al. (2010) and presented on order of east to west (river mile downstream of Lee's Ferry) in Figure 6. New samples show the same bimodal Paleoproterozoic and early Archean populations

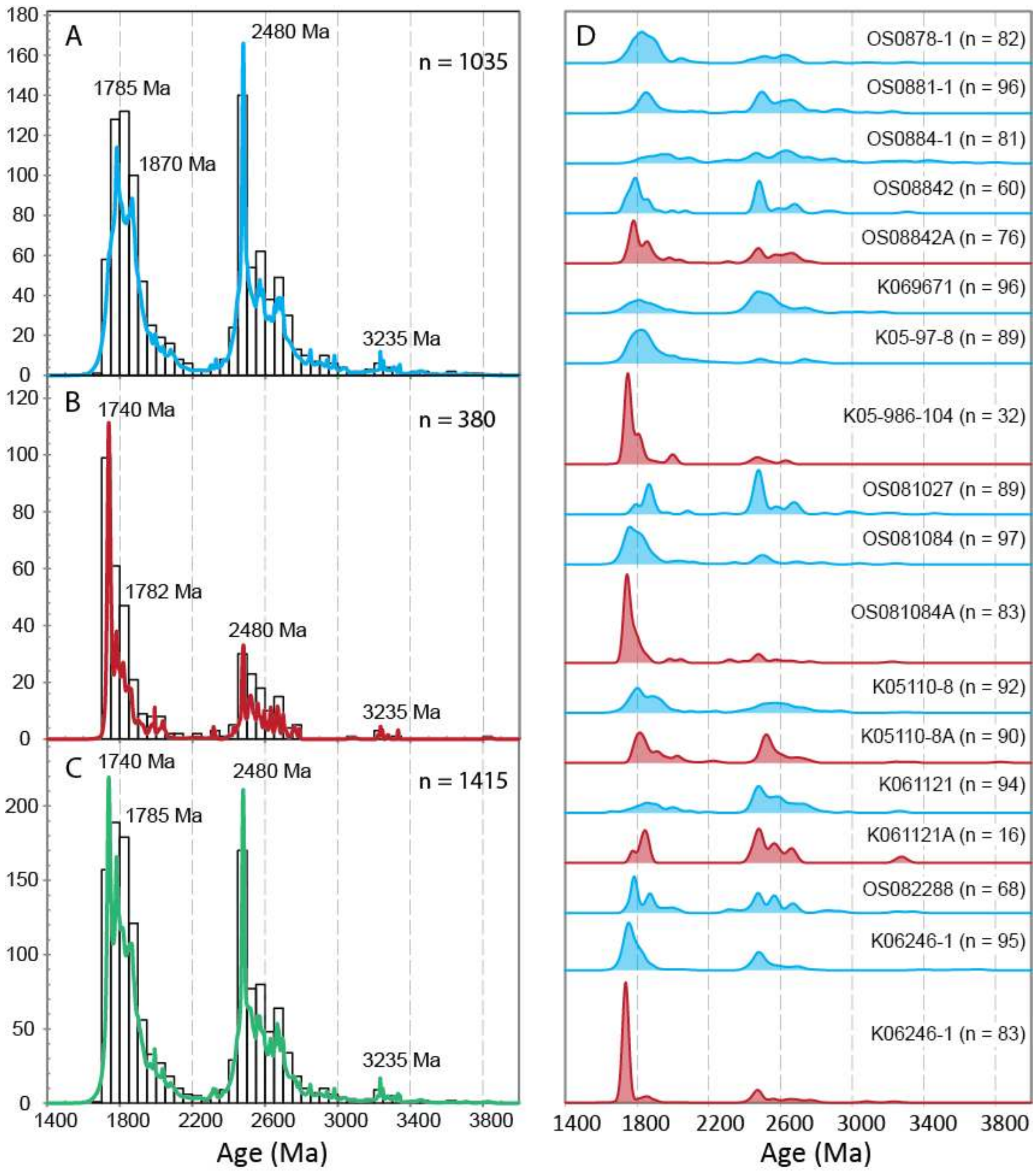

Figure 6. Comparison and synthesis of new and previous Vishnu Schist detrital zircon U-Pb age data. **A:** Composite age probability plot take from Shufeldt et al., 2010. **B:** New detrital zircon ages obtained for this study. **C:** New composite age probability plot with all current Vishnu Schist detrital zircon ages. **D:** Normalized age probability plots of Vishnu Schist detrital zircon samples arranged by river mile (OS0878-1 = Owen Shufeldt, 2008, river mile 78). Results from Shufeldt et al., 2010 are shown in blue, new results obtained in this study are shown in red. See also Table A1 for detrital zircon age data.

with peaks at 1780 Ma and 2480 Ma as identified by Shufeldt (2010), and confirm the observation that, whereas individual samples vary, there is no systematic difference in the relative proportions of the 2.5 and 1.8 Ga age populations from east to west across the Crystal shear zone. Shufeldt et al. (2010) reported that only 13% of all grains overlapped at 2σ with the 1750-1740 Ma depositional age of the Vishnu Schist (Hawkins et al., 1996); new data show more grains of this age (Figure 6), such that the new composite Vishnu distribution has 18% 1740-1750 Ma first-cycle grains. 14% of all ages overlap at 2σ with the 1840 ± 1 Ma Elves Chasm gneiss, and 28% are >2500 Ma in age.

I obtained Hf isotopic information for 187 zircons from six spatially distributed samples of Vishnu Schist (Figure 7). The results of each individual analysis are presented in Appendix D, Table A2. As for the U-Pb ages, there is variation in which mode dominates a given spectrum, but there is no systematic variation in Hf composition with river mile (Figure 7). For example, sample K0598.6-104 did in fact yield Archean U-Pb ages (Table A1), but each of these grains were either too small to withstand the larger spot size and deeper pit depth of Hf analysis, or the Hf analyses did not pass the data reduction process. The apparent difference in detrital zircon age spectra in this case is probably the result of a reduced sample size for this sample (n = 32 for U-Pb, and n = 16 for Hf). However, I do not feel that the Hf isotopic data for the Archean population is underrepresented in the entire dataset.

Detrital zircons from the Vishnu Schist yield a broad range of $\varepsilon Hf_{(t)}$ values from +10.0 to -19.4. For our purposes, only $\varepsilon Hf_{(t)}$ values that overlap within analytical uncertainty (2σ) of the depleted mantle array are considered juvenile. Surprisingly, only 30 grains (16%) of the entire Vishnu Schist dataset yielded juvenile values. However, due

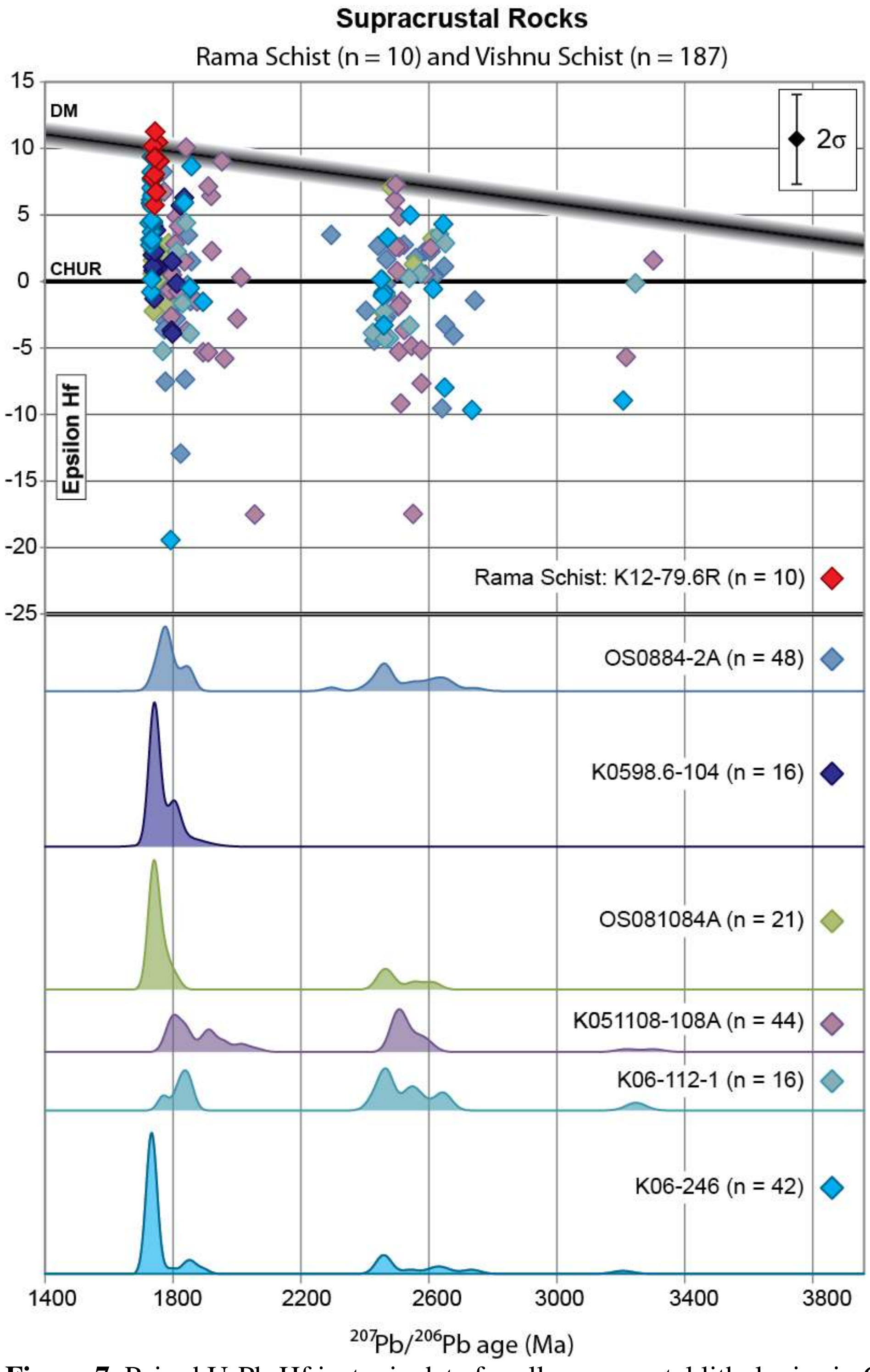

Figure 7. Paired U-Pb-Hf isotopic data for all supracrustal lithologies in Grand Canyon. Each diamond represents a zircon with paired U-Pb and Lu-Hf isotopic data. DM–depleted mantle of Vervoort and Blichert-Toft, 1999; CHUR–chondritic uniform reservoir of Bouvier et al., 2008. Sample K12-79.6R is of the Rama Schist (shown in red), all other data are Vishnu Schist. Below are normalized detrital zircon age probability plots of grains for which we have obtained Lu-Hf isotopic data.

to the time-integrated nature of Hf isotopic information, these terms refer to the zircons themselves compared to depleted mantle rather than compared to depositional age. Thus, for the purpose of this study, only zircons that yield crystallization ages of 1750-1740 Ma as well as $\varepsilon Hf_{(t)}$ values that overlap with the depleted mantle array, and therefore could have been derived from local arc rocks, are considered juvenile. Of the 187 grains for which I have paired U-Pb-Hf data 58 grains (31%) fall in this age range, and only 14 of those grains (6%) yield $\varepsilon Hf_{(t)}$ values that overlap with the depleted mantle array. Therefore, I infer that only 7% of grains could have been derived from juvenile (1.75-1.74 Ga) plutonic sources (see below). The rest were derived from older crust.

Shufeldt et al. (2010) proposed that the 1.8 Ga age peak in the Vishnu Schist was derived from the Elves Chasm Gneiss, a hypothesis which is tested with these new Hf isotopic data. 23 grains for which I have paired U-Pb-Hf isotopic data overlap at 2σ with the 1840 ± 1 Ma Elves Chasm gneiss. However, only 4 yield $\varepsilon Hf_{(t)}$ values that overlap with the depleted mantle array. Therefore the Vishnu Schist was also not significantly sourced by the juvenile Elves Chasm pluton. My data show that very little of the detritus that sourced the Vishnu Schist was derived from local crust. Instead, Vishnu Schist was overwhelmingly derived from older, isotopically evolved crust.

Rama Schist

I collected a sample of the Rama Schist from the same locality sampled by Hawkins et al. (1996). A weighted mean of 12 analyses yielded an age of 1751 ± 16 Ma (MSWD = 0.2), in good agreement with the 1741 ± 1 Ma age of Hawkins et al. (1996).

Interestingly, the 10 grains for which I obtained Hf isotopic data yielded juvenile $\varepsilon Hf_{(t)}$ values that ranged from +5.7 to +11.3 (Figure 7). All but one grain yielded $\varepsilon Hf_{(t)}$

values that overlap with the depleted mantle array. This is essentially the same range of εHf$_{(t)}$ values shown by plutons in eastern Grand Canyon (see below), which suggests that the interlayered metavolcanics were locally derived juvenile arc products and that they became interlayered with far-traveled sedimentary rocks derived from older crustal sources. Interlayering is now parallel to strong S_2 foliation such that it could have been primary or tectonic, an interpretation that would require additional study.

Results from Granodiorite Plutons

East of Crystal Shear Zone

I obtained 134 paired U-Pb-Hf isotopic analyses from zircons separated from five plutons east of the Crystal shear zone from river mile 81-96 (Figure 8). 84 grains (74%) overlap at 2σ with the 1741-1713 Ma timing of arc magmatism described by Hawkins et al. (1996). Although there are individual outliers, and ICPMS precision is considerably less than the previous ID-TIMS dates, weighted mean ages for each pluton are in good agreement with previously published ID-TIMS ages (Table 1).

Hf isotopic data for plutonic zircons east of Crystal shear zone are shown in Figure 8. We obtained paired U-Pb-Hf isotopic data for 97 plutonic zircons. εHf$_{(t)}$ values range from +5.5 to 13.1. Of the 97 analyses, 86 (87%) of them yield εHf$_{(t)}$ values that overlap with the depleted mantle array. They form a very tight cluster that indicates these granodiorites were derived almost entirely from a juvenile source. However, the few grains that yield more evolved εHf$_{(t)}$ values suggest minor involvement of slightly older juvenile crust, such as the Elves Chasm Gneiss, or a crustal component as old as 2.0 Ga.

Two of the grains that do not overlap with the depleted mantle array are core analyses from the Boucher pluton: K12-96.2L-22C, which yielded an εHf$_{(t)}$ value of -5.1

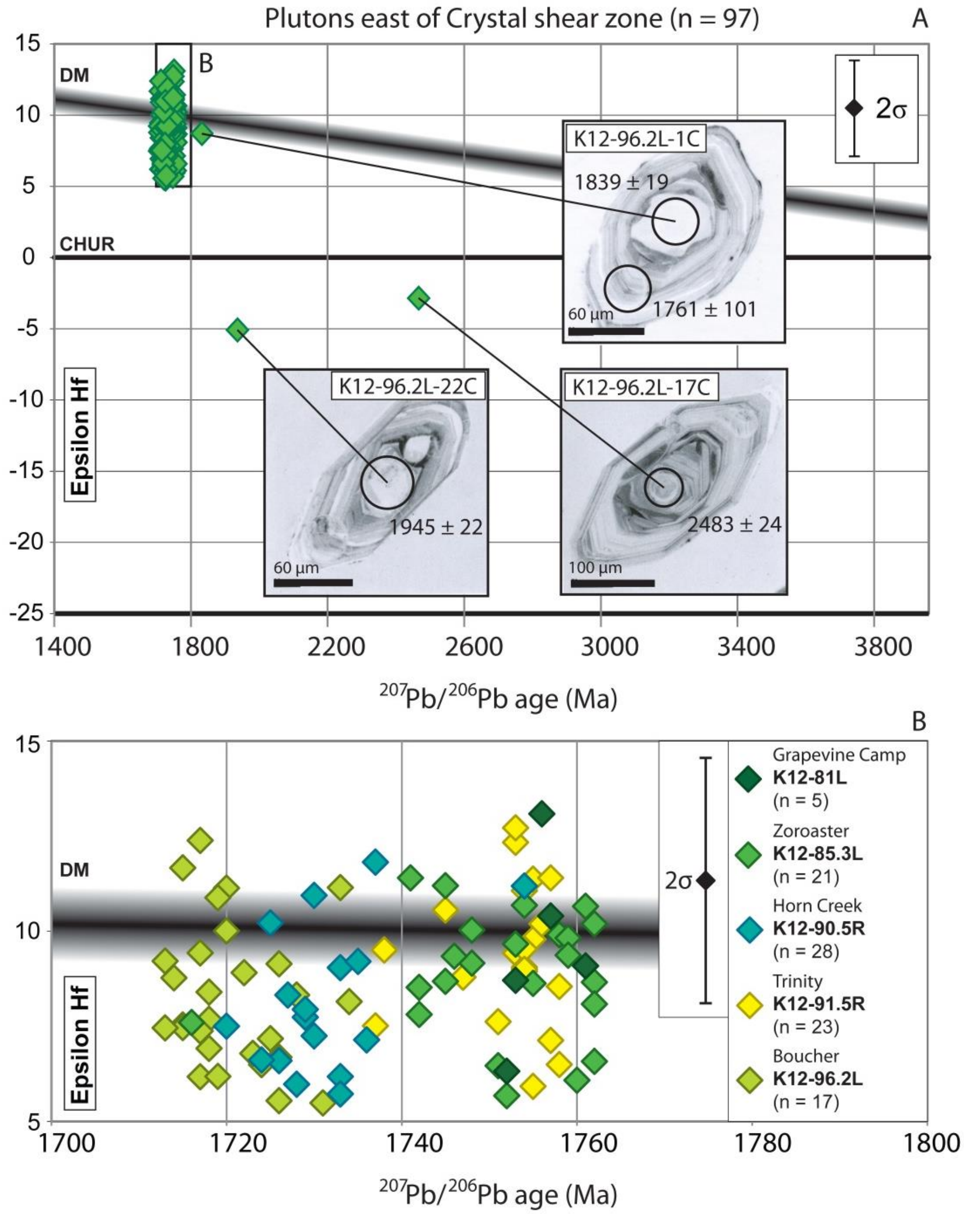

Figure 8. A: Paired U-Pb-Hf results for zircons separated from plutons east of the Crystal shear zone. Shown in green above are all results from igneous zircons east of Crystal shear zone. **B:** Results for each pluton, note change in x-axis scale. Average 2-sigma uncertainty of all epsilon Hf values is shown in the top right.

at 1945 Ma, and K12-96.2L-17C, which yielded an $\varepsilon Hf_{(t)}$ value of -2.9 at 2483 Ma. Grain K12-96.2L-1C yielded a juvenile $\varepsilon Hf_{(t)}$ value of +8.7 at 1839 Ma. The Boucher pluton at river mile 96 (K12-96.2L) contained zircons that displayed inherited cores in CL-texture. 25 core-rim pairs were analyzed, however only 8 core-rim pair analyses passed the data reduction process. Many apparent core-rim pairs ultimately yielded overlapping ages that contributed to the 1730 ± 15 Ma weighted mean age. Only 1 core-rim pair yielded non-overlapping ages. Grain K12-96.2L-3 yielded a core age of 2598 ± 22 Ma, and a rim age of 1727 ± 37 Ma (Figure 8). In addition, grain K12-96.2L-1 yielded core and rim ages of 1839 ± 19 and 1761 ± 101 Ma respectively. The large uncertainty associated with the rim analysis causes these grains to overlap at 2σ, however the similarity between the core age and the Elves Chasm gneiss is noteworthy. I infer that the rims are the same age as the 1730 Ma crystallization age of this pluton. Similarly, despite the lack of reliable rim age data, two additional core analyses yielded ages substantially older than the 1730 Ma population. Grain K12-96.2L-22C yielded an age of 1945 ± 22 Ma, and grain K12-96.2L-17C yielded an age of 2483 ± 24 Ma. The latter age corresponds quite closely to the 2481 Ma age peak defined in the compiled data of the Vishnu Schist (Shufeldt et al., 2010).

Granodiorites West of Crystal Shear Zone

Granodioritic plutons west of the Crystal shear zone are markedly different than those to the east. I obtained 134 paired U-Pb-Hf isotopic analyses from zircons separated from six plutons west of Crystal shear zone from river mile 99-245 (Figure 9). Excluding the 36 zircons from the Elves Chasm Gneiss, a majority of 64 grains (65%) still overlap at 2σ with the 1741-1713 Ma timing of arc-magmatism in the Upper Granite Gorge. However, the remainder of grains yield a semi-continuous spectrum of ages that range

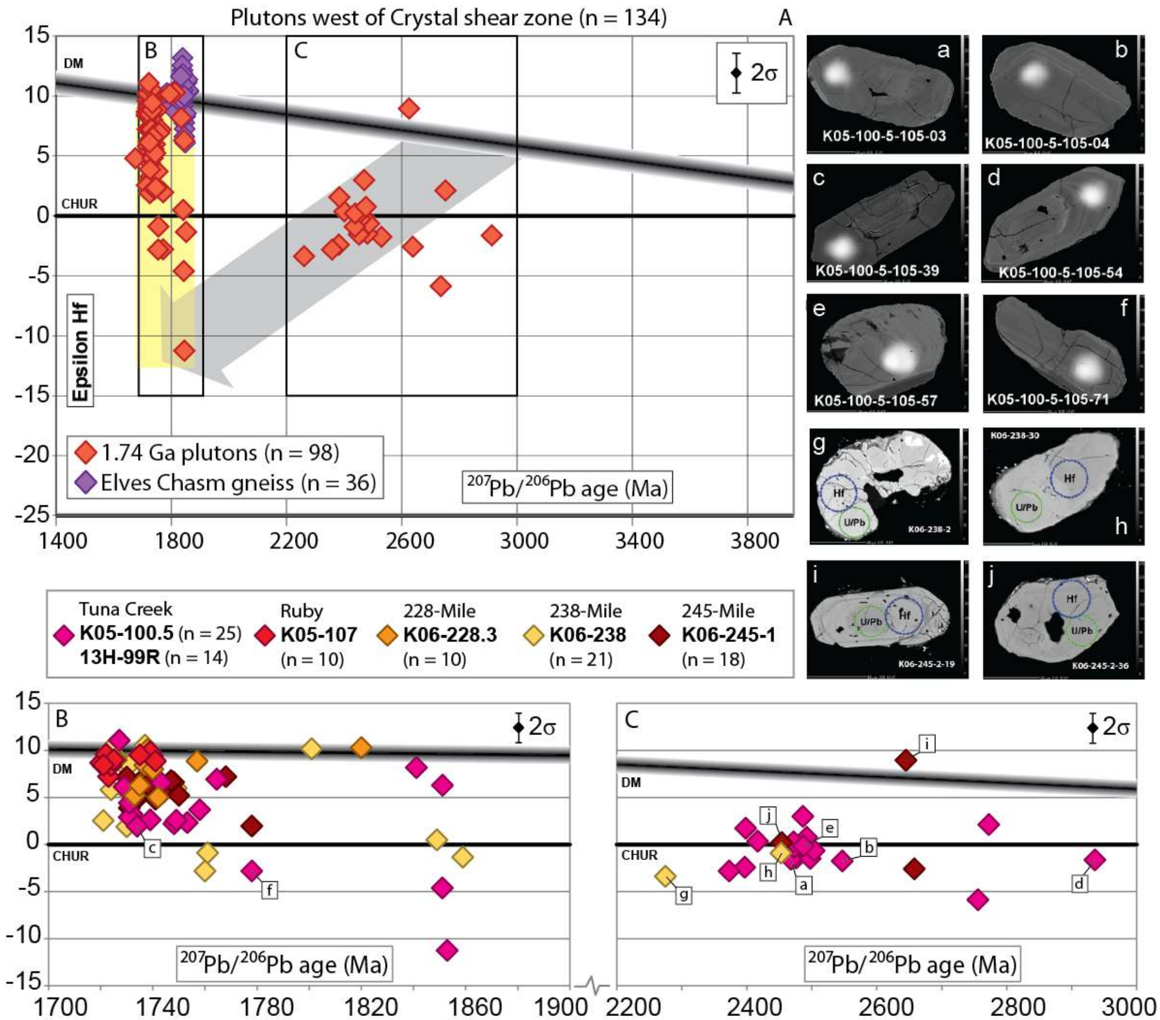

Figure 9. Paired U-Pb-Hf results for zircons separated from plutons west of the Crystal shear zone. **A:** Composite diagram of all paired igneous U-Pb-Hf data west of Crystal shear zone. Elves Chasm Gneiss shown in purple. Average 2-sigma uncertainty of all epsilon Hf values is shown in top right. Gray arrow shows average crustal evolution of Vervoort and Patchett, 1996. Yellow column represents interpreted mixing of crust of varying age. Boxes show area of B and C. **B:** ~1.7 Ga population of zircons shown according to pluton name and sample number. Elves Chasm Gneiss not shown (see Figure 4). **C:** Inherited population of zircons by sample. BSE images of inherited grains and Paleoproterozoic grains with low epsilon Hf values are keyed to B and C.

from 1741-1867 Ma, and a substantially older inherited population that ranges from 2275-2936 Ma. Interestingly, 13 grains (10%) yield ages that overlap at 2σ with the 2480 Ma age peak in the compiled data for the Vishnu Schist, and 8 grains overlap at 2σ with the age of the Elves Chasm gneiss.

Of the 64 grains that overlap with the 1.74-1.71 Ga magmatism, 25 grains (39%) yield juvenile $\varepsilon Hf_{(t)}$ values; the remaining 39 grains yield a spread of more evolved Hf isotopic compositions, with $\varepsilon Hf_{(t)}$ values as low as -2.8 (Figure 9B). Furthermore, the 8 grains that overlapped in age with the Elves Chasm gneiss yielded varied $\varepsilon Hf_{(t)}$ values ranging from +10.3 to -11.3, with four of them juvenile at 1.84 Ga.

The Elves Chasm gneiss itself yielded exclusively juvenile $\varepsilon Hf_{(t)}$ values. Attempts were made to date apparently distinct core and rim age domains in zircons, but all attempts yielded ages of ~1.84 Ga. Along with the Elves Chasm Gneiss, the Ruby pluton, and Diamond Creek pluton yielded only juvenile grains, with the exception of one zircon from the Diamond Creek pluton that yielded a juvenile Elves Chasm-aged grain.

The 2275-2936 Ma population of inherited zircons is derived from the Tuna Creek, 238-Mile, and 245-Mile plutons. These xenocrystic grains are generally more evolved than most of the primary Paleoproterozoic grains (Figure 9).

DISCUSSION

Comparison of Igneous and Metasedimentary Zircons

My approach of applying paired U-Pb dating and Hf isotopic analysis to both the oldest metasedimentary rocks and the oldest plutons in the orogen provides insight into the earliest evolution of the Mojave and Yavapai provinces. These two datasets provide initially contradictory information: metasedimentary rocks are the same across the proposed Crystal shear zone, whereas plutons are markedly different. The following discussion addresses this apparent conundrum.

Detrital zircons from the Vishnu Schist show a broad range of juvenile and evolved Hf isotopic compositions but are uniform across the entire Grand Canyon transect. The vertical spread of data in epsilon space suggests that the Vishnu Schist was derived from crust that experienced substantial mixing of older crustal material with juvenile magmas, including: ~3.3-3.2 Ga crust, ~2.8-2.4 Ga crust, and 2.0-1.7 Ga crust all characterized by mixing of juvenile material with older crust (Figure 10). Few zircons of any age are juvenile ($\varepsilon Hf_{(t)}$ values that overlap at 2-sigma with the depleted mantle array) at the time of their crystallization (16%), and most late Archean grains are dominated by εHf values that suggest the involvement of ~3.0 Ga crust. The Paleoproterozoic population of zircons predominantly suggest the involvement of 2.0-2.2 Ga crust, but the lack of crust of that age in our data set, and globally, might suggest instead that the abundance of Paleoproterozoic grains with $\varepsilon Hf_{(t)}$ values between +5.0 and 0.0 are the result of mixing between juvenile ~1.8 and ~2.5 Ga crust.

Conversely, interlayered volcanic deposits of the Rama schist in eastern most Grand Canyon are juvenile at 1.74 Ga. The similarity between plutonic and volcanic

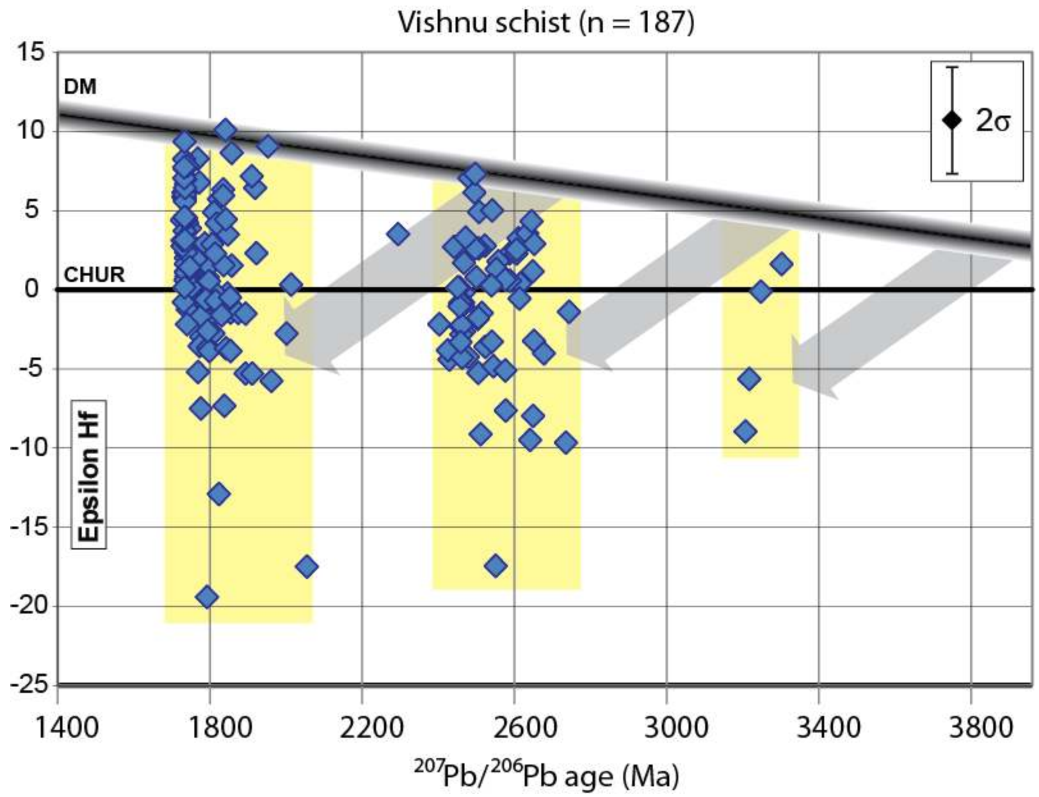

Figure 10. Compiled Vishnu Schist U-Pb-Hf data show that the Vishnu Schist was sourced by an Archean craton characterized by extensive crustal reworking at ~1.8 Ga, ~2.5 Ga, and ~3.2 Ga.

$\varepsilon Hf_{(t)}$ values suggests that the Rama Schist in the eastern part of the transect is locally derived from similarly aged, but slightly older, arc magmatism.

The age and Hf isotopic composition of plutonic zircons, summarized in Figure 11, are in stark contrast to the detrital grains of the Vishnu Schist. Plutons east of Crystal shear zone are uniformly juvenile at 1.74-1.71 Ga. Very few detrital zircons of this age and Hf isotopic composition are found in the Vishnu Schist suggesting a dearth of local juvenile Yavapai province derived crust contributing to the Vishnu basin. However, the xenocrystic grains and Paleoproterozoic grains with more evolved Hf isotopic compositions found in plutons west of the Crystal shear zone are more similar to Vishnu detritus, which suggests that these plutons interacted with crust similar to that which sourced the Vishnu basin. Moreover, this may suggest that the Vishnu Schist was sourced from the west (present coordinates).

Two important first-order observations are as follows: (1) granodioritic arc plutons include both juvenile and inherited zircons, (2) there is a dramatic change in igneous zircon ages and Hf composition across the Crystal shear zone: plutons east of Crystal shear zone yield almost exclusively juvenile $\varepsilon Hf_{(t)}$ values, and a lack of inherited grains. The only exceptions are the two inherited cores found in the Boucher pluton (sample K12-96.2L) at river mile 96, which is the western-most pluton still east of the Crystal shear zone at river mile 97 (see below). Conversely, west of the Crystal shear zone some plutons yield abundant xenocrystic zircons, inherited cores, and more evolved $\varepsilon Hf_{(t)}$ values, while other plutons are predominantly juvenile. Juvenile plutons include the 1.84 Ga Elves Chasm gneiss (K06-113, and K12-115L), and 1.74-1.71 Ga Grapevine Camp (K12-81L), Zoroaster (K12-85.3L), Horn (K12-90.5R), Trinity (K12-91.5R), Ruby

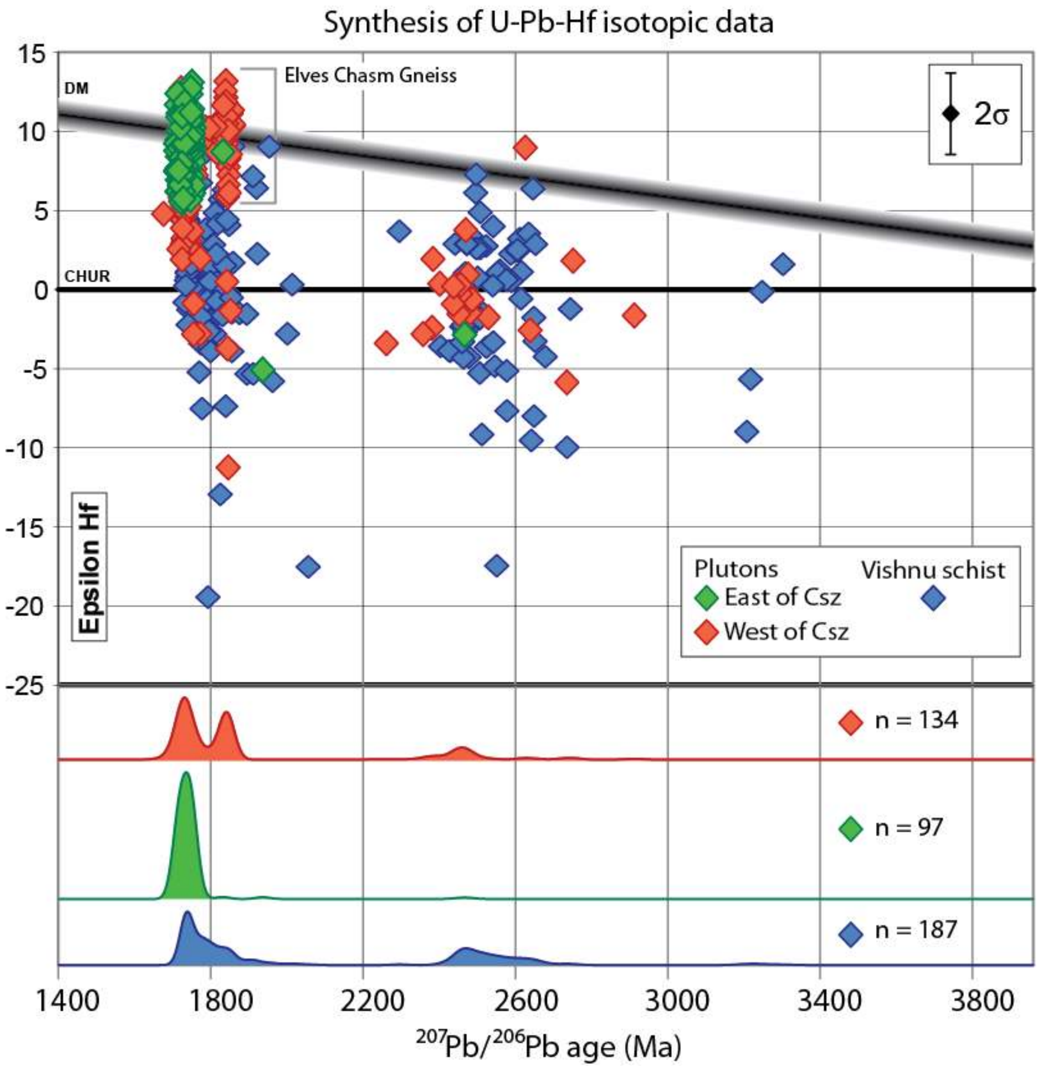

Figure 11. Synthesis of all U-Pb-Hf data from plutonic and detrital samples in Grand Canyon. Vishnu Schist is shown in blue, plutons east of the Crystal shear zone in green, and plutons west of the Crystal shear zone in red. The dramatic difference in plutonic zircons is apparent. Paradoxically, the plutonic data suggest a suture across the shear zone, however the detrital zircon data do not.

(K06-107), and Diamond Creek (K06-228) plutons. Plutons with inherited signatures include the 1.74-1.71 Ga Boucher (K12-96.2L), Tuna Creek (K06-100.5, and 13H-99R), 238-Mile (K05-238), and 245-Mile (K06-245) plutons.

These data describe a uniform metasedimentary basin that was sourced primarily by isotopically evolved 1.8 and 2.5 Ga crust, which was intruded by a suite of plutonic rocks with essentially the same crystallization ages but markedly different zircon populations and Hf isotopic compositions across a structural boundary.

Source of the Vishnu Schist

An important insight gained from these data is the disparity between the juvenile isotopic signature of the Elves Chasm gneiss and the more evolved character of 1.84 Ga detrital grains. My new data show that Paleoproterozoic detrital zircons yield primarily more evolved εHf values than igneous Elves Chasm Gneiss grains, and preclude the Elves Chasm Gneiss from contributing a substantial volume of detrital zircons into the Vishnu basin, as suggested by Shufeldt et al. (2010). The presence of additional Penokean aged crust in central Colorado has been inferred from inherited zircons found in ~1.75 Ga granites and rhyolites (Hill and Bickford, 2001). Subsequent Hf isotopic analysis of many of the same samples discussed by Hill and Bickford (2001) include only one >1800 Ma grain (aged 1877 ± 37), which yielded an $\varepsilon Hf_{(t)}$ value of 1.1. This value is substantially lower than $\varepsilon Hf_{(t)}$ values obtained from the Elves Chasm gneiss, more similar to $\varepsilon Hf_{(t)}$ values from the ~1.85 Ga population of zircons in the Vishnu Schist, and similar to the somewhat evolved Nd isotopic character of 1.88 – 1.84 Ga Penokean plutonic rocks (Barovich et al., 1989). It is possible that Penokean aged crust further to the northeast sourced the ~1.85 Ga population of detrital zircons in the Vishnu schist, however one zircon with similar U-Pb-Hf characteristics is not enough to suggest a central Colorado provenance.

The paucity of juvenile first-cycle 1.75-1.74 Ga detrital zircons also preclude local juvenile Yavapai-type plutons from contributing substantial detritus to the Vishnu Schist. Of course, with the exception of the Elves Chasm gneiss, plutons exposed in the Grand Canyon intrude the Vishnu Schist and could not have contributed detritus to the Vishnu protolith, however my data suggest that very little of the Vishnu Schist was sourced by older juvenile arc terranes such as the 1.78 Ga Green Mountain arc (Jones et al., 2011). In the Gunnison-Salida area, the 1751 Ma Powderhorn Granite yields zircons with slightly evolved $\varepsilon Hf_{(t)}$ values ranging from +2 to +6 (Bickford et al., 2008). 35% of 1.74-1.78 Ga Vishnu grains yielded similar $\varepsilon Hf_{(t)}$ values. In addition, the 1772-1754 Ma Twilight Gneiss of the Needle Mountains is similarly juvenile, and is old enough to have contributed to the Vishnu Schist (Gonzales and Van Schmus, 2007). Therefore, a modest amount of more locally derived detritus could have been sourced from Colorado, however given the much more evolved values of some ~1.85 Ga grains, it is unlikely that any 1.85 Ga crust in Colorado provided the dominant source of Paleoproterozoic detritus to the Vishnu Schist, and even more unlikely that far traveled Penokean crust did so.

The inherited Archean age population and Paleoproterozoic grains with lower εHf values suggest that plutons west of the Crystal shear zone might have interacted with the same type of crust that provided detritus to the Vishnu Schist. Crust that sourced the Vishnu Schist might therefore lie to the west (present coordinates). It is likely that the Paleoproterozoic, and possibly Archean, detrital zircon population is derived from the proximal Mojave province, similar to the model favored by Shufeldt et al. (2010) for the

Archean component of the Vishnu Schist. At present no Elves Chasm gneiss or older aged crust has been identified in the Mojave province, but abundant 1.75-1.78 Ga granitoids with evolved Nd (Bennett and DePaolo, 1987; Ramo and Calzia 1998) and Hf (Wooden et al., 2012) compositions exist (Figure 12). In addition, an Archean component has been recognized in the Nd isotopic composition of the Mojave province in the Death Valley region (Ramo and Calzia, 1998), and detrital zircons of similar ages to the Vishnu Schist have been documented in the Mojave province (Barth et al., 2000; 2009; Strickland et al., 2012).

The source of the >2.4 Ga population of detrital zircons in the Vishnu Schist remains uncertain. Shufeldt et al. (2010) suggested that the Gawler craton of southern Australia had the most similar age spectrum to the Archean population in the Vishnu schist, however recent U-Pb ages obtained from orthogneisses in the Farmington Canyon Complex are similar to the 2.48 Ga age peak in the Vishnu Schist (Mueller et al., 2011). This may provide a potential Laurentian source for the older Vishnu Schist detritus, however the dearth of voluminous Wyoming craton aged detritus in the Vishnu Schist (Shufeldt et al., 2010) still argues against a substantial Laurentian cratonic source. Mueller et al. (2011) recognized this dilemma and suggested that the Mojave province may have evolved independently at 2.5 Ga, which was similarly proposed by Whitmeyer and Karlstrom (2007), and might seem supported by the presence of ~2.5 Ga lithosphere in the Mojave province (Lee et al., 2001) and inherited zircons of the same age in plutons west of Crystal shear zone (see below).

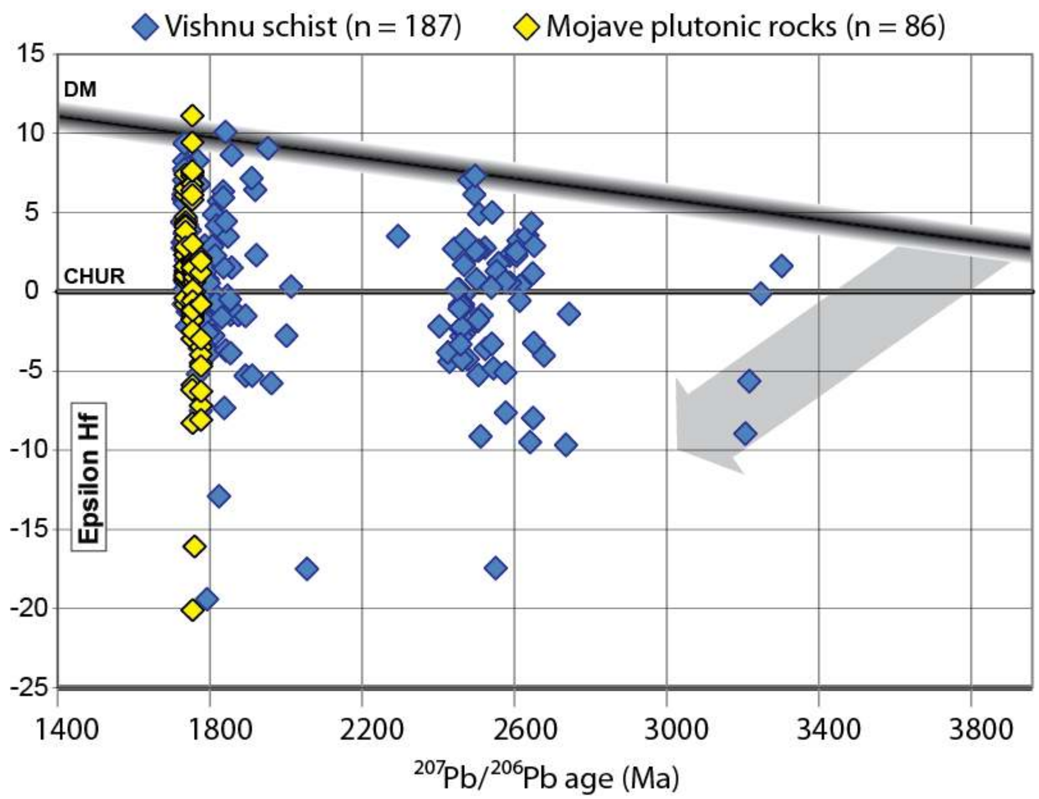

Figure 12. U-Pb-Hf isotopic data from zircons separated from 1.78 - 1.74 Ga Mojave province plutonic rocks shown in yellow (Wooden et al., 2012) compared to the Vishnu Schist.

Source of Inherited Zircons

Understanding the history of the inherited grains in the plutons is of key importance for evaluating crustal evolution models. The refractory nature of zircon gives it the tendency to retain valuable isotopic data through a wide variety of geologic processes and often results in the preservation of distinct zones within a single zircon. These internal heterogeneities can provide information regarding the petrogenesis of the host rock or even protolith. Alternatively, if these zones are not identified or misinterpreted they can obscure the true history of the zircon or provide misleading geochronologic and isotopic information.

The presence or absence of inherited zircons in an igneous rock depends on the temperature and composition of the melt; if the melt is sufficiently saturated in Zr then preexisting zircons may be preserved in the pluton as xenocrystic grains or cores rimed by younger zircon growth. However, if the melt is Zr undersaturated then any preexisting zircons can be dissolved (Watson and Harrison, 1983; Hanchar and Watson, 2003). If inherited xenocrystic zircon grains and cores exist in granodioritic plutons they have two possible sources: (1) they can be assimilated from the partly digested wall-rocks that the pluton intruded; or (2) they can be inherited from the melt-source region of the pluton as incompletely resorbed igneous or metasedimentary grains in the magma.

With the exception of the Elves Chasm basement, the plutons in Grand Canyon intrude the Vishnu Schist such that inherited grains could plausibly be assimilated from Vishnu Schist wall-rocks. The similarity between U-Pb-Hf characteristics of Vishnu detrital zircons and inherited grains in plutons might suggest that this is the case. Alternatively, since granodiorites tend to form from differentiation of basaltic magma in lower crustal magma chambers, inherited grains may reflect the age of older lower crustal igneous material similar to those that were the provenance for the metasedimentary grains. Recent models that emphasize the potential importance of sedimentary recycling via relamination (Hacker et al., 2011) allow for a hybridized possibility whereby xenocrystic grains are inherited from recycled lower crust composed of a relaminated Vishnu-like source.

The origin of zircon inheritance in granitic bodies is difficult to determine without ambiguity (Corfu et al., 2003). However, with the aid of well characterized tectonic histories and field observations, scrutiny of zircon morphology, internal texture, and composition can help elucidate the varied history of complex zircons (Whitehouse et al., 1999; Miller et al. 2000; Cavosie et al., 2004, 2006, 2007; Bea et al., 2007). With detailed structural, geochronological, and thermobarometric studies of the Grand Canyon transect already completed (Ilg et al., 1996; Hawkins et al., 1996; Dumond et al., 2007; Shufeldt et al., 2010), I attempt to interpret the nature of zircon inheritance west of the Crystal shear zone, and the lack of inheritance east of the shear zone, in the context of all available data.

Internal textures of inherited zircons as revealed by CL and BSE imaging primarily show igneous growth zoning, but textures vary even within the same pluton. The inherited cores of the Boucher pluton range from rounded and homogenously CL-dark (K12-96.2L-1C) to almost euhedral with complex igneous zoning (K12-96.2L-17C). Similar to the Boucher pluton, the Tuna Creek pluton yielded an inherited core overgrown by a young rim (K05-100.5-1). In contrast, however, many of the inherited grains in plutons west of Crystal shear zone show no rims and range from euhedral to rounded (Figure 9). Rounded cores or xenocrysts may suggest a detrital origin, however partial resorbtion of igneous grains can yield a similar morphology. In addition, many zircons found in igneous or meta-igneous granulite grade lower crustal xenoliths display rounded morphologies and irregular internal textures (Hanchar and Rudnick, 1995; Corfu et al., 2003; Crowley et al. 2006, 2008; Siebel et al., 2011; Sommer et al., 2013).

The varied morphology and internal texture of xenocrystic grains combined with the similarity in ages between inherited grains and the Vishnu Schist would seem to make a strong case for the assimilation of Vishnu wall-rocks by plutons west of the Crystal shear zone. However, this interpretation begs the question of why there are no inherited zircons in the plutons east of the Crystal shear zone? The Vishnu basin is uniform across the entire Grand Canyon transect, i.e. plutons on either side of the shear zone are intruding the same wall rocks. Why then, do some preserve inherited grains and not others? One explanation is that some plutons crystallized from melts that were initially undersaturated in Zr, and that any zircons assimilated from the Vishnu wall-rocks were dissolved rather than preserved. This explanation is unsatisfactory because resorption of the older and more compositionally evolved Vishnu Schist detrital zircons would substantially lower the $\varepsilon Hf_{(t)}$ values of any zircons that ultimately crystallized from the melt.

In addition, both juvenile plutons and those with inheritance display similar field relations with Vishnu Schist (Figure 13). While many of the plutons across the transect preserve intrusive contacts, the Zoroaster and Tuna plutons in particular are intimately interlayered with Vishnu Schist metaturbidites, yet have completely contrasting U-Pb-Hf systematics.

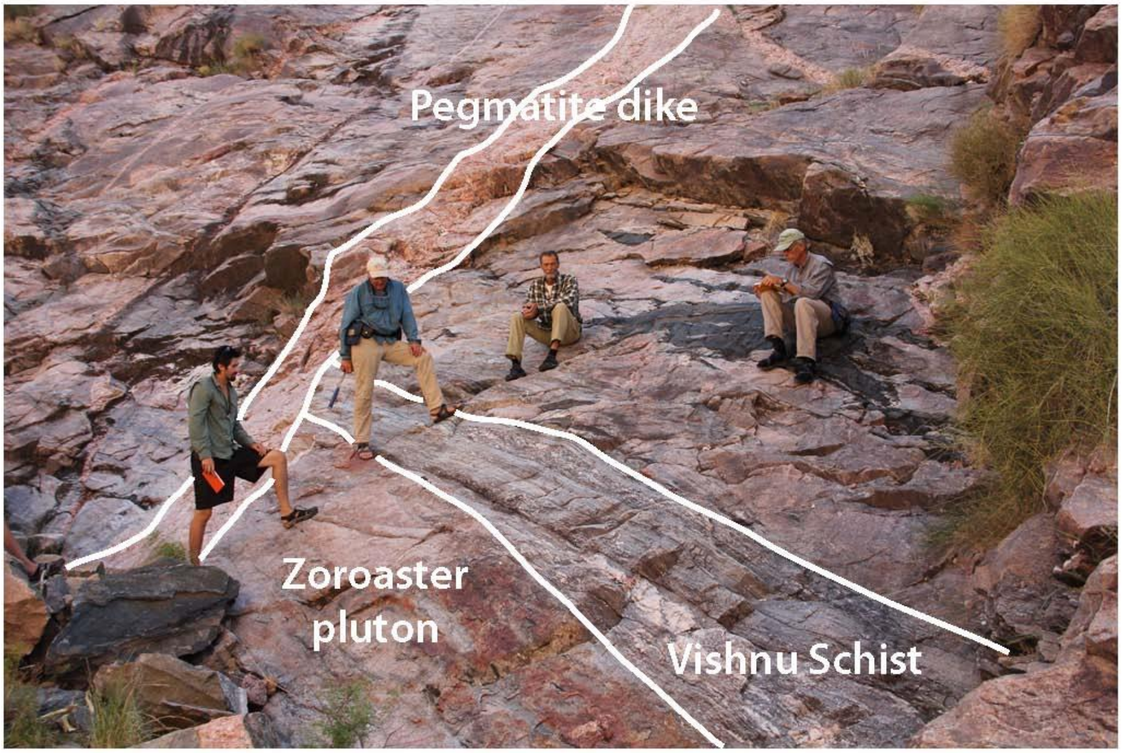

Figure 13. Field photo of the Zoroaster pluton. The pluton is intimately injected into Vishnu Schist and yet shows no evidence for assimilation of Vishnu Schist.

If the xenocrystic population of zircons west of Crystal shear zone is not derived from the Vishnu wall-rocks, then it is likely that they are derived from preexisting lower crust with which juvenile arc magmas interacted. This is my preferred interpretation. The implication of this alternative source for xenocrystic grains is that west of Crystal shear zone there is a lower crustal substrate, perhaps variably distributed, that is substantially older than the crust currently exposed in the Grand Canyon region. The Crystal shear zone has previously been proposed as a suture between the Yavapai and Mojave provinces, and the presence of Archean crust in the Mojave province has been postulated (Wooden et al., 1994; Barth et al., 2000; Whitmeyer and Karlstrom 2007; Shufeldt et al., 2010). These data support the interpretation that the Crystal shear zone represents a discrete crustal boundary between the juvenile Yavapai province and the more evolved Mojave province. Furthermore, it is my interpretation that the Mojave province contains an older lower crustal substrate, and that the boundary between the Mojave and Yavapai provinces can be defined by the presence of older crust to the west of the Crystal shear zone.

Tectonic Model for Crustal Architecture

A long-standing model for the tectonic history of southwestern North America is that of successive accretion of juvenile arc terranes to the cratonic margin (Bennet and DePaolo, 1987; Karlstrom and Bowring, 1988; Whitmeyer and Karlstrom, 2007). The discovery of numerous locations that have evidence for pre-1.8 Ga crust in the orogeny (Hawkins et al., 1996; Hill and Bickford, 2001; Bickford and Hill, 2007; Bickford et al., 2008), as well as substantial Archean detrital zircons in the Vishnu Schist (Shufeldt et al., 2010), lead to the question of the extent and character of older crust involved in the assembly of Proterozoic terranes of Laurentia (Karlstrom et al., 2007). Paired analysis of metasedimentary rocks and the igneous rocks that intrude them provides unique insight into lithospheric formation in the Grand Canyon region.

A summary of our observations and interpretations are presented as a schematic cross section in Figure 14. I envision the Grand Canyon transect as an example of a mid-crustal section of an imbricated accretionary complex. The lithologies exposed in the transect are consistent with an arc setting. Interlayered bimodal metavolcanics and turbidites of the Grand Canyon Metamorphic Suite locally preserve pillow basalts, and Bouma sequences that suggest deposition in a marine environment (Ilg et al., 1996). The present geometry of the transect is characterized by a strong vertical foliation attributed to shortening during the 1.7 Ga Yavapai orogeny. Many plutons are aligned with this fabric, and outcrop as tectonic slivers cut by subvertical shear zones. Thus, I interpret many of these plutons to represent imbricated fragments of arc batholiths rather than the batholiths themselves. High pressure ultramafic cumulates (Low et al., in progress) are also imbricated amongst Vishnu turbidites. These cumulates represent the roots of arc magma chambers that crystallized at ~30 km depths, but are now interleaved with turbidites, suggesting substantial relative transport (minimum 5 km) of ultramafic slivers. The subvertical shear zones across the transect accommodated shortening during the Yavapai orogeny, and minimal vertical offset post 1.7 Ga. However, my view is that the Crystal shear zone (and perhaps others) has an earlier D_1 history and has been transposed into a D_2 orientation. Suturing happened either before or synchronously with deposition of a cratonically sourced Vishnu Schist across both types of crust. The only pluton east of Crystal shear zone to yield xenocrystic zircons is the Boucher pluton, which lies between

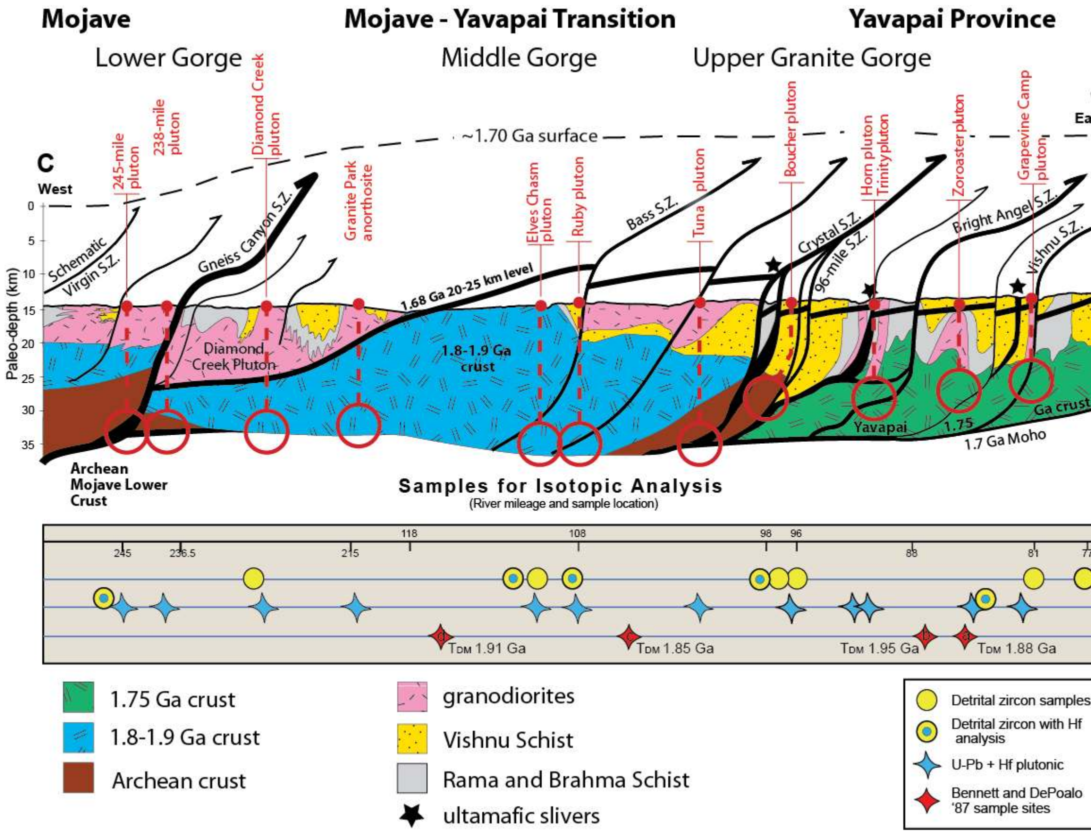

Figure 14. Schematic cross section corresponding to Figure 2A. The Grand Canyon transect is shown here as a mid-crustal imbricated accretionary complex. Red circles show the concept of plutons probing their melt source regions.

the 96-Mile shear zone and the Crystal shear zone. The 96-Mile shear zone is shown as a minor splay of the Crystal shear zone in our cross section (Figure 14).

Karlstrom et al. (2003) proposed that the area between the Crystal and Gneiss Canyon shear zones was an isotopically mixed boundary between the Mojave and Yavapai provinces, analogous to the boundary in western Arizona described by Wooden and DeWitt (1991). Our sample set from the Grand Canyon includes only one pluton west of the Gneiss Canyon shear zone, the 245-Mile pluton (K06-245), which yielded xenocrystic zircons as well as juvenile values in primary grains (Figure 9). Zircons separated from end member Mojave plutons yield substantially evolved $\varepsilon Hf_{(t)}$ values at 1.78-1.75 Ga (Figure 12) (Wooden et al., 2012) that are in contrast to the juvenile values of Paleoproterozoic grains from the 245-Mile pluton. While I interpret the presence of xenocrystic zircons in plutons west of Crystal shear zone to be derived from older crustal fragments that are the source of an isotopically mixed zone, the Gneiss Canyon shear zone is not the western edge of this zone. The presence of the Elves Chasm Gneiss in Mojave crust west of Crystal shear zone provides direct evidence for the presence of older crust in the Mojave province, however our new data suggest that the crustal architecture is even more complex. I propose a heterogeneous crustal architecture west of Crystal shear zone that includes: 1) juvenile 1.74 Ga crust with an inherited Archean component, 2) the juvenile 1840 Ma Elves Chasm Gneiss, and 3) fragments of Archean crust which, combined with juvenile Paleoproterozoic melts, are responsible for the observed isotopically mixed zone. Furthermore, I propose that these older crustal fragments increase in volume to the west, and more extensive mixing of these fragments with Paleoproterozoic melts are the source of the inherited isotopic signature of the

Mojave Province. My interpretations of these data reconcile the model for an isotopically mixed boundary zone between Mojave and Yavapai crust (Wooden and DeWitt, 1991; Karlstrom et al., 2003; Duebendorfer et al., 2006) with the discrete boundary at Crystal shear zone, and provide an explanation for the source of the characteristic evolved isotopic signature of the Mojave province.

Figure 14 shows the current geometry of the transect. I propose two possible tectonic cartoons that explain all observations and might culminate in the present geometry of the transect (Figure 15). Deposition of the Vishnu Schist from 1750-1740 Ma occurred either after or during final suturing between the Mojave and Yavapai provinces. A shallowly dipping tectonic layering (S_1) began to form shortly after deposition, likely facilitated by thrust stacking of turbidites during thickening of arc crust in the early stages of the Yavapai orogeny (Ilg et al., 1996). Near synchronously with the development of S_1, calk-alkaline granodiorite plutons began to intrude the Granite Gorge Metamorphic Suite and become imbricated within thrust sheets. The transect achieved its current configuration by the end of the Yavapai orogeny, and was minimally reactivated during later Mesoproterozoic tectonism (Karlstrom et al., 1997). Deposition of the Vishnu Schist may have occurred in a trench fill sequence during final convergence between the Mojave and Yavapai provinces (Figure 15A). Alternatively, deposition of the Vishnu Schist may have occurred after pre-1750 Ma suturing of the Mojave and Yavapai provinces in a back arc basin subsequently deformed and metamorphosed during the Yavapai orogeny (Figure 15B).

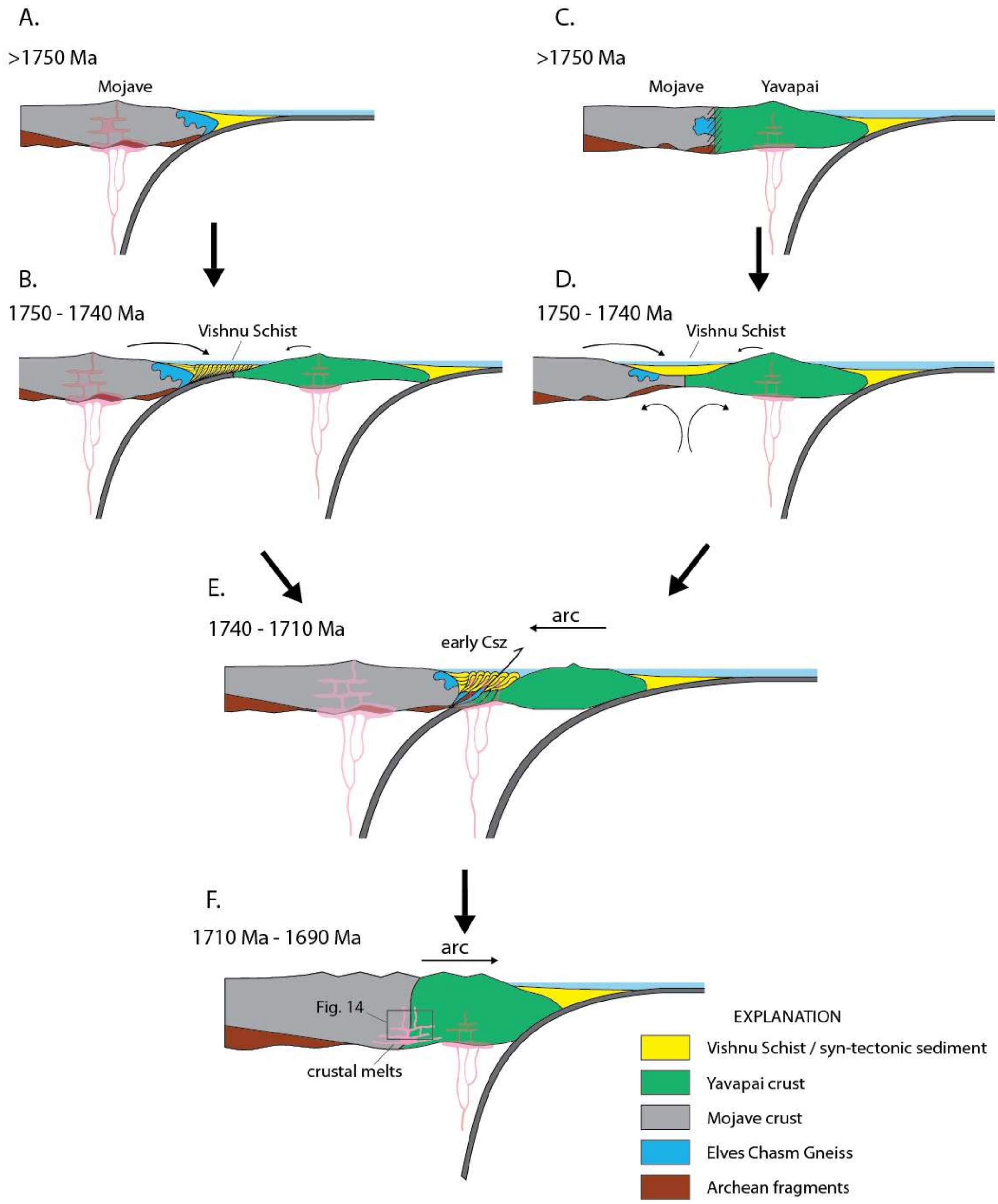

Figure 15. Plate tectonic cartoons illustrating possible scenarios for the depositional setting of the Vishnu Schist and lithospheric formation in the Grand Canyon region. Cartoons are drawn approximately to scale, however crustal thickness is exaggerated. Both models meet at ~1740 Ma (E) when the tectonic history of the Grand Canyon region is well constrained by the work of Ilg et al., 1996, Hawkins et al., 1996, and Dumond et al., 2007. **A:** Pre 1750 Ma there exists no Yavapai type crust in the region. The Mojave arc is evolving as early as 1780 Ma. **B:** Deposition of the Vishnu Schist during final convergence between the newly formed Yavapai arc and Mojave province. Vishnu Schist is depostited across both provinces (and at least in part on the Elves Chasm Gneiss) from 1750 – 1740 Ma in a trench fill sequence receiving most of its sediment from the Mojave province, plus a cratonic source. **C:** Alternatively, pre 1750 Ma the Yavapai and

Mojave provinces are already joined. While no >1750 Ma Yavapai crust exists in the Grand Canyon region, older Yavapai crust exists to the northeast in Colorado. **D:** The Vishnu Schist is deposited across both provinces in a back arc basin after the juxtaposition of older Yavapai crust against Mojave. **E:** By 1740 Ma the arc has migrated such that calk-alkaline plutons begin to intrude the Vishnu Schist. Thrust stacking imbricates Vishnu turbidites with arc plutons, and a shallow S1 foliation develops. The Crystal shear zone manifests as a boundary between Mojave and Yavapai crust. Arc plutons continue to intrude the Vishnu Schist until ~1710 Ma. **F:** From 1710 – 1690 Ma the transect undergoes protracted crustal shortening during the Yavapai orogeny, a penetrative subhorizontal fabric (S2) is developed throughout the transect, and the Crystal shear zone is transposed into this orientation. The transect is intruded by crustal melts, but no longer by calk-alkaline plutons, suggesting that the arc has either migrated or terminated. By 1700 Ma the transect resides at mid crustal levels. The box straddling the Mojave – Yavapai boundary shows the cross section of Figure 14 at 1700 Ma.

CONCLUSIONS

Comparison of metasedimentary rocks with the plutons that intrude them provide unique insight into lithospheric formation. The Grand Canyon transect is underlain by supracrustal rocks that consist of interlayered juvenile arc volcanics, and turbidites sourced in part by evolved Paleoproterozoic crust of the Mojave province, and a yet undertermined Archean craton, but possibly the Gawler craton of Australia. The Vishnu Schist received little of its detritus from local Yavapai type crust, and the Elves Chasm Gneiss did not contribute substantial detritus to the Vishnu Schist. The depositional environment of the Vishnu Schist was certainly an arc setting, however may have been deposited in a back arc basin, or as an accretionary prism in the fore arc.

While the Vishnu Schist was deposited uniformly across both Mojave and Yavapai crust, and does not support the existence of a crustal boundary in Grand Canyon, arc plutons yield markedly different U-Pb-Hf characteristics across the Crystal shear zone. Plutons that intrude the Vishnu Schist and serve as probes of lower crustal melt-source regions across the entire transect are predominantly juvenile, but west of the Crystal shear zone xenocrystic grains suggest the presence of older lower crustal fragments, and more evolved Paleoproterozoic grains support this conclusion.

The Paleoproterozoic rocks of the Grand Canyon are an example of a 100% exposed distributed mid-crustal suture zone between the Mojave and Yavapai crustal provinces. The nature of this boundary is defined by the presence of early Archean (~2.5 Ga) lower crustal fragments in the Mojave province.

Appendix A

Table A 1: U-Pb geochronologic analyses of Vishnu Schist (ALC)

Analysis	U (ppm)	206Pb / 204Pb	U/Th	206Pb* / 207Pb*	± (%)	Isotope ratios 207Pb* / 235U*	± (%)	206Pb* / 238U	± (%)	error corr.	Best age (Ma)	± (Ma)	Conc (%)
OS08842A-1	588	45658	3.3	8.8246	0.2	5.3112	0.8	0.3399	0.8	0.98	1853.3	2.9	101.8
OS08842A-2	595	4986	7.5	9.0902	0.8	4.7549	1.6	0.3135	1.4	0.88	1799.5	13.8	97.7
OS08842A-3	113	13212	1.5	5.5290	0.4	12.7337	1.1	0.5106	1.1	0.94	2660.8	6.6	99.9
OS08842A-4	171	115575	2.1	5.4956	0.3	12.4391	2.6	0.4958	2.6	0.99	2670.9	4.6	97.2
OS08842A-5	205	21671	1.9	8.2260	0.4	5.9110	2.6	0.3527	2.5	0.99	1979.3	7.0	98.4
OS08842A-6	73	320950	2.1	5.7147	0.4	11.9465	1.1	0.4951	1.0	0.93	2605.9	6.7	99.5
OS08842A-8	164	238621	2.3	6.1475	0.2	10.5619	0.7	0.4709	0.6	0.93	2483.6	4.2	100.2
OS08842A-9	152	136824	2.8	9.1746	0.3	4.7772	1.3	0.3179	1.3	0.98	1782.7	5.2	99.8
OS08842A-10	126	2176	2.7	9.0692	1.5	4.6245	7.6	0.3042	7.5	0.98	1803.7	28.1	94.9
OS08842A-11	132	1717	1.7	8.9075	4.4	4.9522	5.8	0.3199	3.8	0.65	1836.4	80.0	97.4
OS08842A-12	427	8353	3.6	5.6475	0.3	11.2544	3.4	0.4610	3.4	1.00	2625.6	5.0	93.1
OS08842A-16	190	7979	1.7	8.7863	1.7	5.2399	3.0	0.3339	2.5	0.83	1861.2	30.4	99.8
OS08842A-17	205	17628	2.5	6.1426	0.2	10.6348	0.8	0.4738	0.7	0.96	2484.9	3.5	100.6
OS08842A-18	319	357901	3.0	8.7838	0.2	5.3482	1.9	0.3407	1.9	1.00	1861.7	3.5	101.5
OS08842A-19	372	1973	4.0	9.0218	2.4	4.5185	3.9	0.2957	3.0	0.78	1813.3	43.5	92.1
OS08842A-20	495	25846	1.9	5.8219	0.9	11.6090	1.1	0.4902	0.6	0.56	2574.9	15.8	99.9
OS08842A-22	249	6719	1.7	9.0031	0.9	4.9700	2.1	0.3245	1.9	0.91	1817.0	15.8	99.7
OS08842A-23	756	3964	0.8	5.4523	4.0	13.4333	7.9	0.5312	6.9	0.87	2683.9	65.5	102.3
OS08842A-24	102	189339	1.4	5.4952	0.4	12.8493	1.2	0.5121	1.1	0.93	2670.9	7.0	99.8
OS08842A-26	142	3647	4.1	8.6077	1.2	5.4435	3.8	0.3398	3.7	0.95	1898.2	21.0	99.4
OS08842A-27	507	18533	1.2	8.8609	0.6	5.2128	1.1	0.3350	0.9	0.84	1845.9	10.8	100.9
OS08842A-28	161	9874	3.1	9.1445	3.1	4.6816	3.2	0.3105	1.0	0.30	1788.7	56.2	97.5
OS08842A-29	123	960	2.5	6.1510	2.5	10.0472	3.1	0.4482	1.8	0.59	2482.6	42.4	96.2
OS08842A-30	874	5227	2.5	9.1396	0.7	3.7842	2.8	0.2508	2.7	0.97	1789.7	12.2	80.6
OS08842A-32	322	56887	1.5	9.2180	0.3	4.7591	1.1	0.3182	1.1	0.97	1774.1	5.1	100.4
OS08842A-33	376	5055	4.6	9.2201	0.8	4.3168	4.9	0.2887	4.8	0.99	1773.7	14.4	92.2
OS08842A-34	463	10216	1.1	5.3927	0.4	12.0593	9.2	0.4717	9.2	1.00	2702.1	6.2	92.2
OS08842A-35	302	1395	1.5	8.2050	1.0	5.9496	1.6	0.3540	1.2	0.76	1983.9	18.4	98.5
OS08842A-36	220	4451	1.2	8.5327	2.4	5.3154	6.4	0.3289	5.9	0.92	1913.9	43.8	95.8
OS08842A-37	256	3866	1.3	8.4832	1.7	5.6248	2.7	0.3461	2.1	0.78	1924.3	30.6	99.6
OS08842A-38	485	23182	2.7	5.9428	0.3	11.5527	2.0	0.4979	2.0	0.99	2540.5	4.6	102.5
OS08842A-39	459	2800	2.4	8.9282	1.0	4.6374	2.6	0.3003	2.4	0.92	1832.2	18.6	92.4
OS08842A-40	335	92264	2.5	9.1600	0.2	4.8312	0.8	0.3210	0.8	0.96	1785.6	4.1	100.5
OS08842A-42	210	37721	1.6	9.2027	0.6	4.7698	1.9	0.3184	1.8	0.95	1777.1	10.6	100.3
OS08842A-43	304	6355	5.1	8.6851	0.7	5.0918	2.0	0.3207	1.8	0.93	1882.0	13.3	95.3

OS08842A-44	218	2317	1.4	8.5799	2.2	5.4938	2.6	0.3419	1.2	0.48	1904.0	40.2	99.6
OS08842A-45	148	10879	1.1	5.8516	1.2	12.0167	2.3	0.5100	2.0	0.85	2566.4	20.5	103.5
OS08842A-47	446	8040	4.9	9.1431	1.1	5.0682	3.6	0.3361	3.5	0.95	1789.0	20.7	104.4
OS08842A-48	412	10414	1.8	8.8327	0.8	5.2740	3.1	0.3379	2.9	0.96	1851.7	14.9	101.3
OS08842A-50	225	4135	2.0	5.8635	0.6	11.0862	3.6	0.4715	3.5	0.99	2563.0	10.0	97.1
OS08842A-53	391	14631	3.1	8.7663	0.3	5.2935	1.0	0.3366	0.9	0.96	1865.3	5.1	100.3
OS08842A-54	418	2786	1.9	7.5257	4.1	7.3605	4.2	0.4017	0.8	0.19	2136.3	72.2	101.9
OS08842A-55	588	29221	1.8	6.1677	0.2	10.4434	1.4	0.4672	1.4	0.99	2478.0	3.0	99.7
OS08842A-56	411	6409	2.0	5.6483	0.7	12.5600	2.7	0.5145	2.6	0.96	2625.4	12.2	101.9
OS08842A-57	271	4701	2.7	9.0831	1.4	4.9715	2.2	0.3275	1.7	0.77	1801.0	25.6	101.4
OS08842A-58	276	12827	1.7	9.1281	0.5	4.9351	1.7	0.3267	1.6	0.95	1791.9	9.8	101.7
OS08842A-59	127	5567	2.5	5.8146	0.4	11.6703	1.9	0.4922	1.9	0.98	2577.0	6.0	100.1
OS08842A-60	124	22780	2.6	6.1817	0.6	10.6211	0.9	0.4762	0.7	0.77	2474.2	10.2	101.5
OS08842A-61	119	33440	2.6	6.2878	0.3	10.0650	1.6	0.4590	1.6	0.98	2445.5	4.8	99.6
OS08842A-62	182	37198	3.0	6.1502	0.2	10.6656	3.5	0.4757	3.5	1.00	2482.8	4.1	101.0
OS08842A-63	328	8938	1.7	7.9447	0.3	6.3771	0.8	0.3675	0.7	0.90	2041.0	6.0	98.8
OS08842A-66	277	3429	3.2	6.3863	1.1	9.2770	2.7	0.4297	2.5	0.92	2419.1	18.0	95.3
OS08842A-67	246	8018	3.3	9.2745	0.6	4.6187	1.7	0.3107	1.6	0.94	1762.9	10.7	98.9
OS08842A-69	652	3796	1.8	9.1186	1.8	4.6743	3.1	0.3091	2.6	0.83	1793.8	32.0	96.8
OS08842A-70	96	12221	2.5	8.8164	0.7	5.3935	1.5	0.3449	1.3	0.87	1855.0	13.2	103.0
OS08842A-71	220	8655	2.5	9.1357	0.6	4.8123	1.1	0.3189	0.9	0.82	1790.4	11.3	99.6
OS08842A-72	182	226170	2.1	6.1487	0.1	10.6908	0.9	0.4768	0.9	0.99	2483.2	2.4	101.2
OS08842A-73	142	3818	1.3	8.7652	0.9	5.2654	1.4	0.3347	1.1	0.77	1865.5	16.3	99.8
OS08842A-74	169	19694	2.6	6.1428	0.4	10.6710	1.0	0.4754	0.9	0.92	2484.9	6.5	100.9
OS08842A-75	184	3156	1.5	6.8117	1.2	8.5391	3.0	0.4219	2.8	0.91	2309.0	21.3	98.3
OS08842A-76	166	34278	3.3	9.1682	0.6	4.9184	1.0	0.3270	0.8	0.83	1784.0	10.1	102.2
OS08842A-78	123	3312	2.6	6.2410	0.3	10.0831	1.8	0.4564	1.7	0.98	2458.1	5.6	98.6
OS08842A-79	557	9847	2.2	9.3724	0.7	4.4744	2.1	0.3041	2.0	0.94	1743.7	13.5	98.2
OS08842A-80	559	10558	1.2	5.4044	0.2	13.2816	1.4	0.5206	1.4	0.99	2698.5	2.9	100.1
OS08842A-81	187	47954	3.1	12.9384	1.2	2.0672	1.7	0.1940	1.2	0.72	1128.7	23.0	101.3
OS08842A-83	462	12841	2.7	9.1968	0.4	4.7891	1.1	0.3194	1.0	0.93	1778.3	7.0	100.5
OS08842A-84	305	5886	2.4	8.0131	1.7	6.4238	1.9	0.3733	0.8	0.42	2025.9	30.7	100.9
OS08842A-88	383	33911	2.2	9.3333	0.3	4.6929	1.5	0.3177	1.5	0.99	1751.4	4.7	101.5
OS08842A-90	134	34178	1.9	9.3499	0.8	4.4766	1.5	0.3036	1.3	0.86	1748.1	14.6	97.8
OS08842A-92	557	33506	7.0	5.6165	0.3	12.2118	1.8	0.4974	1.7	0.99	2634.7	4.3	98.8
OS08842A-93	219	2389	2.2	9.2389	2.4	4.3330	3.7	0.2903	2.8	0.76	1770.0	44.0	92.8
OS08842A-95	509	275465	1.5	9.2259	0.3	4.6985	1.7	0.3144	1.6	0.98	1772.5	6.1	99.4
OS08842A-96	211	73584	2.1	9.1914	0.2	4.7290	1.0	0.3152	1.0	0.97	1779.4	4.3	99.3
OS08842A-97	183	7882	1.0	5.1893	0.9	14.1576	2.5	0.5328	2.4	0.94	2765.4	14.2	99.6
OS08842A-99	179	250810	1.7	5.5043	0.3	12.8994	1.1	0.5150	1.1	0.97	2668.2	4.6	100.4
OS08842A-100	201	57978	2.3	9.2024	0.5	4.8754	1.5	0.3254	1.4	0.95	1777.2	8.3	102.2

K05-986-104-1	830	1381	4.1	9.0766	1.3	2.9416	6.6	0.1936	6.5	0.98	1802.3	23.0	63.3
K05-986-104-4	242	3028	1.3	5.9905	1.8	10.1160	2.7	0.4395	2.0	0.74	2527.1	31.1	92.9
K05-986-104-5	192	22659	2.1	9.3791	0.4	4.6817	1.4	0.3185	1.4	0.97	1742.4	6.8	102.3
K05-986-104-6	258	5032	1.4	6.1769	0.2	10.0099	0.9	0.4484	0.9	0.98	2475.5	2.6	96.5
K05-986-104-7	244	7692	1.0	9.3142	0.7	4.5265	1.2	0.3058	1.0	0.79	1755.1	13.6	98.0
K05-986-104-8	138	12048	1.0	9.3143	0.5	4.5003	0.7	0.3040	0.6	0.78	1755.1	8.4	97.5
K05-986-104-9	313	5834	1.8	9.3542	0.4	4.1122	0.9	0.2790	0.8	0.89	1747.3	7.8	90.8
K05-986-104-10	369	2056	1.3	9.0653	3.5	4.5578	9.8	0.2997	9.1	0.93	1804.5	64.2	93.6
K05-986-104-14	204	8778	1.0	5.6284	0.2	11.9633	0.7	0.4884	0.7	0.96	2631.2	3.3	97.4
K05-986-104-15	293	1408	1.3	8.8712	6.2	4.4617	6.4	0.2871	1.7	0.26	1843.8	111.5	88.2
K05-986-104-16	91	150005	1.5	9.3946	0.6	4.5478	1.2	0.3099	1.0	0.88	1739.4	10.1	100.0
K05-986-104-17	74	102799	2.5	9.3699	0.5	4.5814	1.3	0.3113	1.2	0.91	1744.2	10.0	100.2
K05-986-104-18	128	22996	2.1	6.2827	1.9	11.1220	6.1	0.5068	5.8	0.95	2446.8	32.7	108.0
K05-986-104-20	120	1157	1.1	8.9314	3.6	4.5807	4.7	0.2967	3.0	0.63	1831.5	66.1	91.5
K05-986-104-24	342	4979	1.8	8.0869	0.8	6.0475	4.7	0.3547	4.6	0.98	2009.6	14.7	97.4
K05-986-104-26	170	194538	2.0	8.9960	0.4	5.1036	1.1	0.3330	1.0	0.94	1818.5	6.6	101.9
K05-986-104-28	251	8655	0.9	9.2958	1.1	4.5231	1.2	0.3049	0.5	0.45	1758.7	19.4	97.6
K05-986-104-32	280	314924	2.2	8.1661	0.1	6.1980	0.5	0.3671	0.5	0.99	1992.3	1.2	101.2
K05-986-104-34	397	10724	1.5	9.3691	0.6	4.5634	1.1	0.3101	0.9	0.84	1744.4	10.7	99.8
K05-986-104-35	209	132336	1.6	9.3386	0.4	4.6442	0.8	0.3146	0.7	0.87	1750.3	7.2	100.7
K05-986-104-36	250	1262	1.3	8.8793	4.0	4.6292	4.7	0.2981	2.5	0.53	1842.1	71.7	91.3
K05-986-104-37	111	154798	1.4	9.3703	0.3	4.6279	0.9	0.3145	0.8	0.93	1744.1	6.1	101.1
K05-986-104-38	87	279928	1.4	8.9715	0.6	5.0837	2.0	0.3308	1.9	0.95	1823.4	11.7	101.0
K05-986-104-40	102	201577	0.9	9.4381	0.6	4.5528	0.9	0.3116	0.7	0.74	1730.9	11.0	101.0
K05-986-104-41	215	13494	1.5	9.3215	0.5	4.5830	1.1	0.3098	1.0	0.90	1753.7	8.5	99.2
K05-986-104-42	611	1166	0.9	9.0851	0.6	2.9318	6.0	0.1932	6.0	1.00	1800.6	10.3	63.2
K05-986-104-43	105	14482	1.2	9.2984	0.9	4.6050	1.5	0.3106	1.3	0.81	1758.2	16.5	99.2
K05-986-104-44	123	2799	0.8	9.2008	1.3	4.5540	1.7	0.3039	1.1	0.63	1777.5	23.9	96.2
K05-986-104-47	193	357875	1.6	9.3762	0.2	4.5844	0.7	0.3118	0.7	0.95	1743.0	3.9	100.4
K05-986-104-46	302	3219	1.5	9.3176	0.4	4.3013	4.7	0.2907	4.7	1.00	1754.4	8.0	93.8
K05-986-104-49	188	4038	2.4	9.0598	1.0	4.9456	1.2	0.3250	0.7	0.59	1805.6	18.1	100.5
K05-986-104-50	104	10391	1.4	9.3402	0.7	4.5905	1.3	0.3110	1.2	0.87	1750.0	12.2	99.7
OS081084A-2	318	15764	1.4	9.3770	0.3	4.3287	1.8	0.2944	1.7	0.98	1742.8	6.3	95.4
OS081084A-3	717	99257	3.1	9.1754	0.1	4.8294	0.4	0.3214	0.4	0.95	1782.5	2.3	100.8
OS081084A-4	135	127978	1.6	5.6327	0.3	12.3175	2.4	0.5032	2.3	0.99	2630.0	4.6	99.9
OS081084A-5	230	82242	2.1	9.3230	0.5	4.7122	0.7	0.3186	0.5	0.67	1753.4	9.0	101.7
OS081084A-6	149	64143	1.6	9.3705	0.5	4.6468	1.7	0.3158	1.6	0.96	1744.1	9.1	101.4
OS081084A-7	154	9908	2.3	6.1768	0.4	10.3292	2.5	0.4627	2.5	0.98	2475.5	7.6	99.0
OS081084A-8	218	12998	1.0	9.3711	0.5	4.6244	0.9	0.3143	0.8	0.81	1744.0	9.9	101.0
OS081084A-9	165	121550	1.6	9.3511	0.8	4.5349	1.9	0.3076	1.7	0.91	1747.9	14.1	98.9
OS081084A-10	176	19928	1.7	9.2803	0.9	4.7012	1.7	0.3164	1.5	0.85	1761.8	16.7	100.6

OS081084A-11	191	110670	1.2	9.3625	0.3	4.6376	0.8	0.3149	0.7	0.92	1745.6	5.8	101.1
OS081084A-12	186	135569	2.0	9.3866	0.6	4.6024	1.9	0.3133	1.8	0.95	1740.9	10.4	100.9
OS081084A-13	500	11617	1.9	9.3056	0.3	4.5772	1.4	0.3089	1.4	0.98	1756.8	4.6	98.8
OS081084A-15	148	2770	1.7	9.2668	1.1	3.9392	3.2	0.2648	3.0	0.94	1764.4	20.4	85.8
OS081084A-16	99	253724	2.1	9.1073	0.7	4.9574	2.9	0.3274	2.8	0.97	1796.1	13.3	101.7
OS081084A-17	194	31939	2.5	9.2355	0.4	4.7554	2.5	0.3185	2.5	0.99	1770.6	7.7	100.7
OS081084A-18	500	61432	1.7	9.3695	0.2	4.6620	0.7	0.3168	0.7	0.97	1744.3	3.5	101.7
OS081084A-19	349	28714	2.1	9.3680	0.3	4.5977	0.9	0.3124	0.8	0.94	1744.6	5.4	100.5
OS081084A-20	210	14219	1.1	8.7618	0.4	5.2079	0.8	0.3309	0.8	0.90	1866.2	6.5	98.8
OS081084A-21	268	228678	2.4	9.3428	0.4	4.6342	0.9	0.3140	0.7	0.87	1749.5	7.7	100.6
OS081084A-22	323	4044	1.2	9.2513	1.8	4.4306	2.2	0.2973	1.2	0.54	1767.5	33.0	94.9
OS081084A-23	257	150584	3.0	9.1794	0.3	4.8256	0.9	0.3213	0.9	0.95	1781.7	5.1	100.8
OS081084A-24	193	133971	1.0	9.4194	0.3	4.6109	0.6	0.3150	0.5	0.82	1734.5	6.1	101.8
OS081084A-26	158	67211	1.7	9.4024	0.3	4.7002	1.8	0.3205	1.8	0.98	1737.9	6.0	103.1
OS081084A-27	227	43036	1.7	9.3857	0.2	4.5293	0.6	0.3083	0.6	0.92	1741.1	4.4	99.5
OS081084A-28	342	42528	1.4	9.3725	0.4	4.5490	1.4	0.3092	1.4	0.96	1743.7	7.6	99.6
OS081084A-29	157	86640	1.2	9.3931	0.6	4.5694	1.1	0.3113	0.9	0.86	1739.7	10.2	100.4
OS081084A-30	247	47528	1.4	9.3907	0.3	4.6186	0.8	0.3146	0.7	0.92	1740.1	5.7	101.3
OS081084A-31	140	187648	1.5	9.3851	0.5	4.5498	0.9	0.3097	0.8	0.83	1741.2	9.4	99.9
OS081084A-32	368	92979	1.4	9.3727	0.3	4.5781	0.7	0.3112	0.7	0.92	1743.7	5.2	100.2
OS081084A-33	301	28489	2.4	8.8694	0.3	5.1836	1.1	0.3334	1.0	0.97	1844.2	5.1	100.6
OS081084A-35	221	3968	1.7	6.2203	1.5	9.5372	2.8	0.4303	2.4	0.84	2463.7	26.1	93.6
OS081084A-37	217	53461	0.8	7.8960	0.3	6.4130	1.0	0.3673	1.0	0.94	2051.9	6.1	98.3
OS081084A-38	123	67202	1.4	9.3877	1.0	4.5401	1.2	0.3091	0.7	0.54	1740.7	18.6	99.7
OS081084A-39	183	85874	2.1	9.1249	0.8	4.8650	1.3	0.3220	1.0	0.79	1792.6	14.6	100.4
OS081084A-40	157	27788	1.4	6.0905	1.2	10.8122	8.9	0.4776	8.8	0.99	2499.3	20.3	100.7
OS081084A-41	127	8664	1.6	9.1150	1.2	4.5180	3.1	0.2987	2.9	0.92	1794.6	22.5	93.9
OS081084A-42	115	111104	1.3	9.4312	1.1	4.3916	1.4	0.3004	0.8	0.60	1732.2	19.9	97.7
OS081084A-43	78	87863	0.5	5.8336	0.4	11.5480	0.8	0.4886	0.7	0.86	2571.6	7.1	99.7
OS081084A-44	202	127828	1.9	6.1876	0.2	10.3607	0.7	0.4650	0.6	0.93	2472.6	4.1	99.5
OS081084A-45	77	30571	2.1	8.2306	0.7	5.9967	2.0	0.3580	1.9	0.94	1978.3	12.2	99.7
OS081084A-46	313	51164	2.7	9.1050	0.4	4.7408	1.6	0.3131	1.5	0.97	1796.6	6.7	97.7
OS081084A-47	258	2346	2.9	9.3608	1.4	3.9489	3.0	0.2681	2.7	0.89	1746.0	25.1	87.7
OS081084A-48	487	43009	2.2	9.3240	0.8	4.6450	3.5	0.3141	3.4	0.97	1753.2	14.6	100.4
OS081084A-49	174	20970	2.4	9.0127	0.4	4.8174	1.9	0.3149	1.8	0.97	1815.1	7.8	97.2
OS081084A-50	413	6301	1.6	8.9043	0.6	5.1005	1.9	0.3294	1.8	0.95	1837.0	10.6	99.9
OS081084A-51	275	265308	2.7	6.7867	0.2	8.7576	1.4	0.4311	1.4	0.99	2315.4	3.2	99.8
OS081084A-52	235	22017	2.0	5.1894	0.4	14.7560	8.0	0.5554	8.0	1.00	2765.3	5.9	103.0
OS081084A-53	243	19783	1.5	9.4385	0.9	4.6827	6.3	0.3206	6.3	0.99	1730.8	17.2	103.6
OS081084A-54	475	31217	1.6	9.3914	0.3	4.4573	0.7	0.3036	0.6	0.91	1740.0	5.4	98.2
OS081084A-55	118	28039	0.9	3.9003	0.4	22.1873	1.1	0.6276	1.0	0.94	3224.6	5.7	97.4

OS081084A-57	250	243530	4.6	9.0068	0.2	4.9847	0.6	0.3256	0.5	0.93	1816.3	4.0	100.0
OS081084A-58	205	10869	1.1	9.4491	0.4	4.1978	2.7	0.2877	2.7	0.99	1728.8	8.1	94.3
OS081084A-59	214	38658	1.0	9.3396	1.3	4.7546	3.4	0.3221	3.1	0.93	1750.1	23.3	102.8
OS081084A-60	36	45771	2.1	5.8193	1.0	11.8006	2.0	0.4980	1.7	0.86	2575.7	16.9	101.2
OS081084A-62	274	256305	2.9	9.1619	0.2	4.7781	0.5	0.3175	0.5	0.92	1785.2	3.8	99.6
OS081084A-65	241	21650	1.7	9.4060	0.5	4.5640	1.1	0.3113	0.9	0.87	1737.2	9.5	100.6
OS081084A-68	114	67712	2.7	9.3177	1.2	4.6995	1.5	0.3176	0.8	0.57	1754.4	22.4	101.3
OS081084A-71	187	15202	0.7	9.4297	0.6	4.5665	2.5	0.3123	2.4	0.97	1732.5	11.4	101.1
OS081084A-72	370	10148	2.1	8.8052	1.0	5.2982	5.6	0.3384	5.5	0.98	1857.3	18.9	101.2
OS081084A-74	277	82513	2.2	6.1525	0.2	10.6335	1.1	0.4745	1.1	0.99	2482.2	2.7	100.8
OS081084A-75	179	332331	2.5	6.1642	0.2	10.3847	2.1	0.4643	2.1	1.00	2479.0	3.5	99.2
OS081084A-76	365	6562	1.7	9.2988	1.4	4.7600	2.8	0.3210	2.5	0.87	1758.1	25.7	102.1
OS081084A-77	158	168317	1.1	9.3965	0.6	4.5518	0.9	0.3102	0.7	0.75	1739.0	10.7	100.2
OS081084A-80	365	32625	1.6	9.3441	0.3	4.5746	2.6	0.3100	2.5	0.99	1749.2	6.3	99.5
OS081084A-81	267	33389	3.1	9.1015	0.4	4.7792	1.2	0.3155	1.1	0.94	1797.3	7.3	98.3
OS081084A-82	206	39643	2.1	6.7622	0.3	8.7455	0.8	0.4289	0.8	0.94	2321.5	4.9	99.1
OS081084A-83	222	7560	2.0	9.3087	0.4	4.4304	3.1	0.2991	3.1	0.99	1756.2	7.1	96.1
OS081084A-84	204	100006	1.4	9.3630	0.5	4.5396	1.2	0.3083	1.1	0.89	1745.5	9.9	99.2
OS081084A-86	300	63370	1.7	7.9590	0.3	6.5532	1.1	0.3783	1.0	0.97	2037.9	4.5	101.5
OS081084A-87	503	10371	2.6	8.1935	0.3	5.9866	1.8	0.3558	1.8	0.98	1986.4	6.0	98.8
OS081084A-88	162	140138	1.8	9.3293	1.0	4.6720	1.5	0.3161	1.1	0.76	1752.2	17.4	101.1
OS081084A-89	431	21393	1.9	9.3533	0.3	4.5920	1.2	0.3115	1.2	0.96	1747.5	5.8	100.0
OS081084A-90	531	10537	4.1	6.4613	0.7	8.7020	5.3	0.4078	5.2	0.99	2399.3	12.7	91.9
OS081084A-91	315	54495	2.7	9.0721	0.6	4.9656	1.1	0.3267	0.9	0.85	1803.2	10.2	101.1
OS081084A-92	326	5703	1.9	9.3805	0.9	3.9758	4.5	0.2705	4.4	0.98	1742.1	16.9	88.6
OS081084A-93	525	134423	3.5	9.1451	0.3	4.7804	1.2	0.3171	1.2	0.98	1788.6	4.8	99.3
OS081084A-94	263	72629	1.0	9.3851	0.3	4.6370	1.2	0.3156	1.1	0.95	1741.2	6.4	101.6
OS081084A-95	185	297147	1.2	9.4041	0.4	4.4688	1.3	0.3048	1.2	0.94	1737.5	8.2	98.7
OS081084A-96	232	18951	1.7	9.3451	0.8	4.4869	1.2	0.3041	1.0	0.78	1749.1	13.8	97.9
OS081084A-97	295	30392	2.0	8.9764	0.3	5.1940	1.4	0.3381	1.3	0.97	1822.4	5.8	103.0
OS081084A-98	103	44189	0.8	9.1745	0.5	4.6945	0.8	0.3124	0.7	0.79	1782.7	9.5	98.3
OS081084A-99	93	119123	2.5	5.4863	0.5	13.3492	1.2	0.5312	1.1	0.93	2673.6	7.6	102.7
OS081084A-100	171	18365	1.6	9.0039	0.6	5.2613	4.2	0.3436	4.2	0.99	1816.9	11.3	104.8
K05110-108A-1	168	257185	2.0	5.9584	0.6	11.4868	2.0	0.4964	2.0	0.96	2536.1	9.3	102.5
K05110-108A-2	399	67404	1.4	3.6427	0.2	24.1800	2.6	0.6388	2.6	1.00	3332.0	2.9	95.6
K05110-108A-3	438	238848	1.7	5.9819	0.2	11.4510	3.2	0.4968	3.2	1.00	2529.5	3.8	102.8
K05110-108A-4	241	892575	2.3	8.8699	0.9	5.1960	2.6	0.3343	2.5	0.94	1844.0	16.1	100.8
K05110-108A-6	194	1193113	2.4	6.0115	0.3	10.9488	2.6	0.4774	2.5	0.99	2521.2	5.0	99.8
K05110-108A-7	262	711570	1.5	5.9991	0.7	11.2364	4.1	0.4889	4.0	0.98	2524.7	12.3	101.6
K05110-108A-8	257	338859	2.1	9.0977	1.0	5.0859	2.0	0.3356	1.7	0.86	1798.0	18.6	103.7
K05110-108A-9	334	61241	2.2	5.5104	0.7	12.8636	2.2	0.5141	2.1	0.95	2666.4	10.9	100.3

K05110-108A-10	387	31954	2.0	8.8455	0.5	5.0493	2.5	0.3239	2.5	0.98	1849.0	9.8	97.8
K05110-108A-11	587	284552	1.4	5.7491	0.3	11.9706	2.5	0.4991	2.5	0.99	2595.9	4.8	100.5
K05110-108A-13	29	108843	0.6	7.6644	3.3	7.2844	4.3	0.4049	2.8	0.64	2104.3	58.4	104.2
K05110-108A-14	84	662704	1.2	5.2498	0.6	14.3455	3.5	0.5462	3.5	0.99	2746.3	9.1	102.3
K05110-108A-15	208	801164	0.8	9.1931	0.7	4.7877	3.5	0.3192	3.4	0.98	1779.0	12.7	100.4
K05110-108A-16	163	1533661	1.1	5.4920	1.1	12.7298	2.0	0.5070	1.7	0.84	2671.9	18.2	99.0
K05110-108A-18	824	635018	1.6	6.0530	0.2	11.3382	4.1	0.4978	4.1	1.00	2509.6	3.0	103.8
K05110-108A-19	1031	28086	4.8	8.9880	2.5	5.0196	2.8	0.3272	1.2	0.43	1820.1	45.8	100.3
K05110-108A-20	264	53197	2.2	8.7958	1.3	5.4121	9.7	0.3453	9.6	0.99	1859.2	23.7	102.8
K05110-108A-21	1195	81433	4.4	9.0182	0.3	4.8365	1.6	0.3163	1.6	0.98	1814.0	5.0	97.7
K05110-108A-22	392	1504985	7.0	9.0040	0.4	5.2685	1.8	0.3441	1.8	0.97	1816.9	7.6	104.9
K05110-108A-23	485	475551	3.0	7.9718	0.3	6.6905	3.2	0.3868	3.2	0.99	2035.0	5.9	103.6
K05110-108A-24	550	71622	4.9	6.0990	0.5	10.6767	2.2	0.4723	2.2	0.97	2496.9	9.2	99.9
K05110-108A-25	281	826822	1.1	9.2011	0.6	4.6207	1.6	0.3084	1.5	0.92	1777.4	11.5	97.5
K05110-108A-26	318	988727	3.0	8.9762	0.8	5.2366	2.5	0.3409	2.4	0.95	1822.5	13.8	103.8
K05110-108A-27	786	276100	2.0	5.6072	0.2	12.3762	1.1	0.5033	1.1	0.98	2637.5	3.7	99.6
K05110-108A-28	587	26839	1.8	8.8125	1.1	4.7879	2.8	0.3060	2.6	0.92	1855.8	19.1	92.7
K05110-108A-29	457	87070	2.5	3.8490	0.2	24.2911	2.0	0.6781	2.0	1.00	3245.5	2.9	102.8
K05110-108A-30	259	730485	2.3	6.0422	0.5	10.7038	3.9	0.4691	3.8	0.99	2512.6	8.5	98.7
K05110-108A-31	290	53440	1.9	5.1784	0.7	13.6381	2.3	0.5122	2.2	0.96	2768.8	10.9	96.3
K05110-108A-32	700	23777	3.1	7.8324	1.5	5.9974	3.2	0.3407	2.9	0.89	2066.2	26.1	91.5
K05110-108A-34	154	2326533	1.5	5.8391	0.6	11.2903	1.3	0.4781	1.1	0.87	2570.0	10.5	98.0
K05110-108A-35	759	25343	2.3	6.0588	0.9	9.4128	3.0	0.4136	2.8	0.95	2508.0	15.5	89.0
K05110-108A-36	272	88091	2.0	6.0731	0.5	11.3153	1.2	0.4984	1.1	0.90	2504.1	8.9	104.1
K05110-108A-37	126	511506	2.1	6.0607	0.9	10.8773	1.5	0.4781	1.3	0.83	2507.5	14.6	100.5
K05110-108A-38	147	1654619	3.3	8.6082	0.8	5.4850	1.5	0.3424	1.3	0.85	1898.1	14.3	100.0
K05110-108A-39	190	10289	2.6	5.9306	0.6	8.8708	3.3	0.3816	3.2	0.98	2543.9	10.8	81.9
K05110-108A-40	371	96622	1.8	5.7357	0.4	10.5061	3.0	0.4370	3.0	0.99	2599.8	6.3	89.9
K05110-108A-41	150	1326951	1.7	9.0954	0.9	4.8694	3.5	0.3212	3.4	0.97	1798.5	15.8	99.8
K05110-108A-42	306	469995	1.3	9.1870	0.5	4.7814	2.4	0.3186	2.3	0.98	1780.2	9.4	100.1
K05110-108A-44	299	76811	1.6	8.5867	0.5	5.0521	1.7	0.3146	1.7	0.95	1902.6	9.3	92.7
K05110-108A-45	198	634807	0.7	5.3595	0.4	13.5196	1.9	0.5255	1.9	0.97	2712.3	7.3	100.4
K05110-108A-46	162	360676	1.9	8.6830	1.3	5.4353	4.1	0.3423	3.9	0.95	1882.5	24.2	100.8
K05110-108A-47	216	802479	2.5	8.9695	1.1	4.9632	3.5	0.3229	3.3	0.94	1823.8	20.7	98.9
K05110-108A-48	257	650903	1.9	5.6514	0.7	12.6758	3.7	0.5196	3.6	0.98	2624.4	10.8	102.8
K05110-108A-49	215	231324	1.7	8.2562	2.1	5.9414	4.1	0.3558	3.5	0.86	1972.8	36.7	99.5
K05110-108A-50	489	72799	1.4	8.9982	0.8	4.8188	3.1	0.3145	3.0	0.97	1818.0	13.7	97.0
K05110-108A-51	726	48555	2.2	5.9707	1.0	11.1221	2.8	0.4816	2.6	0.93	2532.6	17.4	100.1
K05110-108A-52	314	20983	2.8	8.4661	0.8	4.9657	2.4	0.3049	2.3	0.95	1927.9	13.7	89.0
K05110-108A-53	984	59575	8.9	8.8744	0.3	5.0126	1.7	0.3226	1.7	0.98	1843.1	5.9	97.8
K05110-108A-55	485	46637	1.8	8.9599	0.3	5.2535	1.3	0.3414	1.2	0.97	1825.7	5.8	103.7

K05110-108A-56	1104	20370	2.2	5.9407	0.8	10.6466	1.9	0.4587	1.7	0.90	2541.1	13.3	95.8
K05110-108A-57	242	1295032	2.1	6.0000	0.2	11.2338	2.7	0.4889	2.7	1.00	2524.4	3.6	101.6
K05110-108A-58	330	1753021	1.5	6.0043	0.4	11.1871	3.1	0.4872	3.1	0.99	2523.2	6.8	101.4
K05110-108A-59	387	1180681	2.2	8.2662	0.4	5.9075	2.1	0.3542	2.0	0.98	1970.6	7.7	99.2
K05110-108A-60	305	817129	1.6	6.0119	0.6	10.3524	3.8	0.4514	3.8	0.99	2521.1	10.8	95.3
K05110-108A-61	411	346525	1.2	9.0811	0.6	4.8019	3.8	0.3163	3.8	0.99	1801.4	10.1	98.3
K05110-108A-62	492	108764	1.5	9.0666	0.3	4.8574	1.6	0.3194	1.6	0.98	1804.3	6.3	99.0
K05110-108A-63	339	1080927	1.9	9.0902	0.3	4.9456	2.1	0.3261	2.1	0.99	1799.5	6.3	101.1
K05110-108A-64	354	675299	0.9	9.1067	0.7	4.8303	1.3	0.3190	1.1	0.83	1796.2	12.7	99.4
K05110-108A-65	471	38246	1.9	8.4533	0.4	5.6523	2.5	0.3465	2.5	0.99	1930.6	7.5	99.3
K05110-108A-66	548	76722	1.9	8.0247	0.5	6.1309	2.1	0.3568	2.0	0.97	2023.3	9.2	97.2
K05110-108A-67	350	58720	2.6	6.2580	1.0	10.1722	3.4	0.4617	3.2	0.96	2453.5	16.9	99.7
K05110-108A-68	986	38550	1.8	5.9404	0.5	10.9015	1.5	0.4697	1.4	0.93	2541.2	8.9	97.7
K05110-108A-69	432	578678	4.1	8.8422	0.9	5.1157	2.1	0.3281	1.9	0.91	1849.7	15.9	98.9
K05110-108A-71	230	107743	1.9	6.0345	0.6	10.6477	1.3	0.4660	1.2	0.90	2514.8	9.4	98.1
K05110-108A-72	486	271964	2.1	6.0363	0.4	11.0754	2.0	0.4849	2.0	0.98	2514.3	6.0	101.4
K05110-108A-73	183	168211	2.4	6.0867	1.4	10.8628	2.1	0.4795	1.5	0.72	2500.3	24.1	101.0
K05110-108A-74	127	692000	2.5	6.0035	0.8	10.4094	2.2	0.4532	2.0	0.92	2523.5	14.3	95.5
K05110-108A-75	409	55680	2.2	8.5104	0.5	5.2793	3.0	0.3259	3.0	0.99	1918.6	9.2	94.8
K05110-108A-76	355	2038199	1.6	6.0226	0.2	11.2478	2.0	0.4913	2.0	0.99	2518.1	3.4	102.3
K05110-108A-77	1537	712999	26.2	8.3047	0.5	5.7029	1.7	0.3435	1.6	0.95	1962.3	9.8	97.0
K05110-108A-79	358	70449	1.4	8.9584	1.8	4.9263	2.6	0.3201	1.9	0.74	1826.1	31.8	98.0
K05110-108A-80	632	56696	1.7	5.4103	0.5	12.1708	2.8	0.4776	2.8	0.99	2696.7	8.0	93.3
K05110-108A-81	1211	36642	2.5	8.6428	2.0	5.0105	3.5	0.3141	2.9	0.82	1890.8	36.8	93.1
K05110-108A-82	257	19759	0.8	8.0816	1.7	5.7119	3.1	0.3348	2.5	0.82	2010.8	30.9	92.6
K05110-108A-83	297	131164	1.7	2.6337	1.3	33.3601	1.9	0.6372	1.4	0.74	3830.6	19.5	83.0
K05110-108A-84	500	173338	1.4	5.8614	1.2	11.0266	1.7	0.4688	1.3	0.73	2563.6	19.7	96.7
K05110-108A-85	330	3788622	1.6	5.3489	0.4	14.0220	2.6	0.5440	2.5	0.99	2715.5	7.3	103.1
K05110-108A-86	620	115076	1.9	7.1644	2.2	7.6376	2.6	0.3969	1.5	0.56	2222.0	37.8	97.0
K05110-108A-87	249	833652	2.2	8.9619	0.5	5.0703	2.7	0.3296	2.6	0.98	1825.3	8.6	100.6
K05110-108A-88	1587	32319	2.9	8.0452	0.5	6.3489	3.2	0.3705	3.2	0.99	2018.8	8.2	100.6
K05110-108A-89	536	51521	2.6	8.9762	0.6	4.7938	3.8	0.3121	3.8	0.99	1822.5	11.8	96.1
K05110-108A-91	389	617773	1.8	9.1807	0.3	4.9873	1.8	0.3321	1.8	0.98	1781.5	5.9	103.8
K05110-108A-92	546	90614	2.0	8.5073	0.6	5.3428	2.9	0.3297	2.9	0.98	1919.2	10.5	95.7
K05110-108A-93	179	654416	0.6	5.7095	0.3	12.1507	2.8	0.5032	2.8	0.99	2607.4	4.8	100.8
K05110-108A-94	312	111982	0.8	5.8422	0.7	11.8822	1.3	0.5035	1.1	0.86	2569.1	11.1	102.3
K05110-108A-95	561	241146	2.3	8.9934	0.4	4.9038	3.0	0.3199	3.0	0.99	1819.0	6.5	98.4
K05110-108A-96	258	476812	1.3	8.8785	1.0	5.4137	2.0	0.3486	1.7	0.87	1842.3	17.4	104.6
K05110-108A-97	204	35676	2.2	8.7130	0.8	5.4415	1.4	0.3439	1.2	0.84	1876.3	14.0	101.5
K05110-108A-99	518	82585	0.6	5.7505	0.8	11.2853	2.1	0.4707	1.9	0.92	2595.5	13.9	95.8
K05110-108A-100	204	238620	2.7	7.1309	1.9	7.7744	2.4	0.4021	1.4	0.58	2230.1	33.8	97.7

K061121A-2	119	65946	0.9	5.8761	0.2	11.1631	1.3	0.4757	1.3	0.99	2559.4	3.1	98.0
K061121A-3	153	318351	1.7	5.7528	0.1	11.6724	1.7	0.4870	1.7	1.00	2594.8	2.2	98.6
K061121A-4	192	31071	1.2	3.7737	0.4	20.1908	4.3	0.5526	4.2	1.00	3276.6	6.3	86.6
K061121A-6	94	445799	1.7	5.5514	0.4	12.5710	1.2	0.5061	1.1	0.95	2654.1	6.1	99.5
K061121A-8	82	32060	1.2	8.8998	0.4	4.6009	3.0	0.2970	3.0	0.99	1838.0	7.4	91.2
K061121A-9	137	15048	1.7	6.3002	0.7	8.8815	5.5	0.4058	5.5	0.99	2442.1	11.3	89.9
K061121A-10	170	18652	1.9	8.9818	0.2	4.7284	3.5	0.3080	3.5	1.00	1821.3	4.0	95.0
K061121A-13	79	109057	0.6	9.2117	0.6	4.7450	1.3	0.3170	1.1	0.89	1775.3	10.5	100.0
K061121A-15	190	9898	1.0	6.1047	0.7	9.7762	8.1	0.4328	8.1	1.00	2495.3	11.1	92.9
K061121A-16	155	68242	0.8	5.8807	0.3	11.2486	0.9	0.4798	0.9	0.95	2558.1	5.1	98.8
K061121A-17	166	98306	1.6	6.1634	0.2	10.4686	0.7	0.4680	0.6	0.93	2479.2	4.2	99.8
K061121A-18	88	183949	1.0	5.4909	0.4	12.6604	0.6	0.5042	0.4	0.68	2672.2	7.2	98.5
K061121A-19	138	287293	1.6	8.8409	0.5	5.2733	0.8	0.3381	0.6	0.74	1850.0	9.2	101.5
K061121A-20	119	351988	2.0	6.1598	0.3	10.6880	0.5	0.4775	0.4	0.76	2480.2	5.4	101.5
K061121A-21	146	273112	1.8	6.1608	0.3	10.6714	0.8	0.4768	0.7	0.93	2479.9	4.6	101.4
K061121A-22	122	62098	2.2	8.7815	0.5	5.0495	1.2	0.3216	1.1	0.92	1862.2	8.2	96.5
K06246-1A-1	275	119362	2.3	9.4230	0.3	4.5007	2.8	0.3076	2.7	0.99	1733.9	5.7	99.7
K06246-1A-2	734	5358	7.2	4.2634	1.2	14.4105	2.9	0.4456	2.7	0.92	3083.4	18.5	77.0
K06246-1A-3	656	3087	2.3	9.5061	1.8	3.9540	3.7	0.2726	3.3	0.88	1717.7	32.9	90.5
K06246-1A-5	140	116347	2.5	6.1753	0.2	10.4418	0.6	0.4677	0.6	0.93	2475.9	3.9	99.9
K06246-1A-6	250	44193	2.6	9.3995	0.4	4.5276	0.8	0.3087	0.6	0.83	1738.4	7.9	99.8
K06246-1A-7	236	261923	2.9	9.4087	0.4	4.4931	1.1	0.3066	1.0	0.95	1736.6	6.5	99.3
K06246-1A-8	274	1409383	1.1	3.8727	0.1	23.2149	0.9	0.6520	0.9	0.99	3235.9	2.2	100.0
K06246-1A-9	401	6160	1.2	5.7906	4.1	10.3891	10.3	0.4363	9.4	0.92	2583.9	68.0	90.3
K06246-1A-10	235	141645	2.9	9.4209	0.5	4.4994	0.8	0.3074	0.6	0.77	1734.3	9.6	99.6
K06246-1A-11	241	254904	2.9	9.4203	0.4	4.5568	1.0	0.3113	0.9	0.93	1734.4	6.7	100.7
K06246-1A-12	270	59398	2.7	9.3871	0.3	4.5520	1.1	0.3099	1.0	0.97	1740.8	5.0	100.0
K06246-1A-13	266	113569	2.9	9.4011	0.4	4.6878	4.4	0.3196	4.4	1.00	1738.1	7.0	102.9
K06246-1A-14	343	200038	2.5	9.4329	0.4	4.4205	4.9	0.3024	4.9	1.00	1731.9	6.5	98.3
K06246-1A-15	347	9130	2.6	9.3956	0.3	4.3109	1.4	0.2938	1.3	0.97	1739.2	6.2	95.5
K06246-1A-17	544	22230	1.1	5.5022	4.0	10.5337	7.0	0.4204	5.7	0.82	2668.9	66.3	84.8
K06246-1A-18	226	45261	2.7	9.4198	0.4	4.5677	0.5	0.3121	0.4	0.72	1734.5	6.6	100.9
K06246-1A-19	131	134109	3.5	6.2273	0.4	10.5243	1.0	0.4753	0.9	0.89	2461.8	7.3	101.8
K06246-1A-20	368	32427	2.3	9.4064	0.1	4.4932	0.6	0.3065	0.6	0.97	1737.1	2.7	99.2
K06246-1A-21	280	279398	2.6	5.4001	0.3	13.4078	1.2	0.5251	1.2	0.98	2699.8	4.4	100.8
K06246-1A-22	210	481861	2.2	5.1164	0.2	14.6815	0.9	0.5448	0.9	0.98	2788.6	2.9	100.5
K06246-1A-23	192	220996	2.7	6.1750	0.3	10.5045	0.5	0.4704	0.5	0.87	2476.0	4.3	100.4
K06246-1A-24	143	114394	3.0	6.1895	0.2	10.5498	0.8	0.4736	0.8	0.98	2472.1	2.5	101.1
K06246-1A-26	112	164263	3.3	6.2056	0.4	10.6589	1.4	0.4797	1.3	0.95	2467.7	7.2	102.4
K06246-1A-27	188	49554	0.7	5.8788	0.3	11.6006	1.1	0.4946	1.1	0.97	2558.6	4.9	101.3
K06246-1A-28	265	130083	2.6	9.0944	0.4	4.9591	0.8	0.3271	0.7	0.88	1798.7	6.6	101.4

K06246-1A-29	958	4819	1.6	8.7869	0.3	4.3855	2.8	0.2795	2.7	0.99	1861.0	5.9	85.4
K06246-1A-30	113	21152	1.5	8.9643	0.8	5.1216	1.5	0.3330	1.3	0.85	1824.9	14.0	101.5
K06246-1A-31	466	6470	1.0	5.6217	0.5	11.8205	1.9	0.4819	1.8	0.97	2633.2	7.7	96.3
K06246-1A-32	258	102984	2.6	9.4107	0.4	4.5576	0.8	0.3111	0.7	0.90	1736.2	6.5	100.6
K06246-1A-33	279	29192	1.9	8.5900	0.4	5.5428	0.7	0.3453	0.6	0.87	1901.9	6.5	100.5
K06246-1A-34	306	50100	2.6	9.4033	0.3	4.6688	0.7	0.3184	0.6	0.90	1737.7	5.4	102.5
K06246-1A-35	208	61163	2.1	9.3828	0.4	4.5000	0.8	0.3062	0.7	0.86	1741.7	7.2	98.9
K06246-1A-36	260	4337	3.0	8.9443	7.6	4.8755	10.1	0.3163	6.7	0.66	1828.9	137.3	96.9
K06246-1A-37	134	81178	2.9	6.1882	0.6	10.5227	3.2	0.4723	3.2	0.98	2472.4	10.5	100.9
K06246-1A-38	156	318372	2.3	6.1640	0.3	10.5057	1.1	0.4697	1.0	0.96	2479.0	5.2	100.1
K06246-1A-39	263	69938	2.5	9.3834	0.2	4.5262	0.7	0.3080	0.7	0.96	1741.6	3.7	99.4
K06246-1A-41	517	32318	4.5	9.5294	0.3	4.3428	2.0	0.3001	2.0	0.99	1713.2	5.8	98.8
K06246-1A-42	260	167042	2.6	9.3893	0.4	4.5711	0.8	0.3113	0.7	0.88	1740.4	6.7	100.4
K06246-1A-43	362	6899	0.7	8.8773	0.4	5.2079	2.0	0.3353	2.0	0.98	1842.5	7.8	101.2
K06246-1A-44	453	13128	1.7	9.3854	0.4	4.4061	2.3	0.2999	2.3	0.98	1741.2	8.0	97.1
K06246-1A-46	417	60996	1.8	9.4041	0.2	4.5466	1.3	0.3101	1.3	0.99	1737.5	3.0	100.2
K06246-1A-47	399	4876	4.1	9.4071	0.7	4.1246	2.7	0.2814	2.6	0.96	1736.9	13.5	92.0
K06246-1A-49	250	13048	2.6	9.3921	0.4	4.6460	1.3	0.3165	1.3	0.96	1739.9	6.6	101.9
K06246-1A-50	344	5910	2.3	9.3665	0.6	4.5102	1.1	0.3064	0.9	0.82	1744.9	11.9	98.7
K06246-1A-51	286	31916	2.4	9.4270	0.3	4.5991	0.6	0.3144	0.6	0.89	1733.1	5.3	101.7
K06246-1A-52	296	35160	2.5	6.3544	0.2	9.6824	1.0	0.4462	1.0	0.98	2427.6	3.5	98.0
K06246-1A-53	138	54169	0.6	5.5137	0.3	12.8861	2.7	0.5153	2.7	0.99	2665.4	4.5	100.5
K06246-1A-54	361	7184	2.5	9.4517	0.5	4.3502	1.3	0.2982	1.2	0.92	1728.3	9.0	97.3
K06246-1A-55	432	3846	3.7	9.4696	1.6	4.4097	2.9	0.3029	2.5	0.84	1724.8	29.0	98.9
K06246-1A-56	398	4298	2.2	9.4120	0.6	4.2341	1.0	0.2890	0.8	0.82	1736.0	10.5	94.3
K06246-1A-57	463	6672	2.2	9.4143	0.8	4.5491	5.2	0.3106	5.2	0.99	1735.5	15.4	100.5
K06246-1A-59	257	13589	2.7	9.3844	0.4	4.6033	1.2	0.3133	1.1	0.93	1741.4	7.7	100.9
K06246-1A-60	440	34335	2.1	9.3863	0.4	4.5240	2.2	0.3080	2.1	0.98	1741.0	7.4	99.4
K06246-1A-61	536	5137	1.7	9.3885	0.7	4.5365	1.6	0.3089	1.5	0.91	1740.6	12.4	99.7
K06246-1A-63	273	14812	1.3	5.8755	1.2	11.0348	3.4	0.4702	3.2	0.93	2559.6	20.1	97.1
K06246-1A-64	418	14003	1.9	9.4074	0.4	4.3779	0.9	0.2987	0.8	0.91	1736.9	6.9	97.0
K06246-1A-65	289	11794	2.6	9.3989	0.5	4.4842	1.6	0.3057	1.5	0.95	1738.5	9.5	98.9
K06246-1A-66	259	71530	2.5	9.4184	0.4	4.5656	0.9	0.3119	0.9	0.91	1734.7	7.1	100.9
K06246-1A-67	218	32459	2.8	9.4123	0.3	4.6215	1.3	0.3155	1.3	0.98	1735.9	5.2	101.8
K06246-1A-69	286	168423	2.6	9.4324	0.3	4.4996	1.6	0.3078	1.5	0.98	1732.0	6.3	99.9
K06246-1A-70	530	18323	1.6	9.4227	0.3	4.5031	1.7	0.3077	1.6	0.99	1733.9	4.9	99.7
K06246-1A-71	284	2823	2.9	9.3712	0.2	4.0413	1.0	0.2747	1.0	0.97	1744.0	4.6	89.7
K06246-1A-74	336	7328	1.3	9.4550	0.7	4.3185	1.7	0.2961	1.5	0.90	1727.6	13.2	96.8
K06246-1A-75	248	31795	2.9	9.4096	0.5	4.5728	1.5	0.3121	1.4	0.94	1736.4	9.3	100.8
K06246-1A-77	353	38988	2.2	9.4231	0.3	4.5343	1.1	0.3099	1.1	0.96	1733.8	5.6	100.4
K06246-1A-78	242	90372	3.3	9.4217	0.5	4.5099	2.2	0.3082	2.2	0.97	1734.1	9.2	99.9

K06246-1A-79	110	3159	1.7	6.1288	0.5	8.9566	1.2	0.3981	1.1	0.90	2488.7	9.2	86.8
K06246-1A-81	253	46135	2.3	9.4291	0.4	4.5357	1.8	0.3102	1.7	0.98	1732.7	7.1	100.5
K06246-1A-82	388	6648	2.3	9.3578	0.5	4.4239	1.2	0.3002	1.1	0.92	1746.6	8.5	96.9
K06246-1A-83	323	19485	2.5	9.4036	0.6	4.5415	1.2	0.3097	1.0	0.85	1737.6	11.6	100.1
K06246-1A-86	342	158585	2.4	9.3931	0.2	4.6764	0.9	0.3186	0.9	0.98	1739.7	3.7	102.5
K06246-1A-88	365	70655	2.1	9.4020	0.2	4.5157	0.8	0.3079	0.7	0.96	1737.9	4.1	99.6
K06246-1A-89	391	15711	2.5	9.4135	0.3	4.3955	1.0	0.3001	0.9	0.95	1735.7	5.9	97.5
K06246-1A-90	323	4852	2.0	9.3729	0.8	4.1890	1.2	0.2848	0.9	0.77	1743.6	14.2	92.6
K06246-1A-91	195	75545	2.5	9.3936	0.7	4.6267	1.0	0.3152	0.7	0.70	1739.6	12.8	101.5
K06246-1A-92	330	184751	1.9	9.3925	0.4	4.6771	0.8	0.3186	0.7	0.84	1739.8	7.9	102.5
K06246-1A-93	487	205451	2.0	9.3878	0.3	4.5375	1.0	0.3089	1.0	0.96	1740.7	5.0	99.7
K06246-1A-94	246	121810	3.3	9.3935	0.5	4.5305	0.8	0.3087	0.7	0.82	1739.6	8.5	99.7
K06246-1A-95	373	23183	2.6	8.7657	0.7	5.1765	1.2	0.3291	1.0	0.84	1865.4	12.2	98.3
K06246-1A-96	330	13331	2.3	9.3982	0.5	4.4245	0.9	0.3016	0.7	0.86	1738.7	8.3	97.7
K06246-1A-97	536	11859	1.0	5.2180	0.4	12.9523	2.3	0.4902	2.3	0.99	2756.3	6.1	93.3
K06246-1A-98	245	499348	2.6	9.4188	0.2	4.4880	0.9	0.3066	0.9	0.97	1734.7	4.1	99.4
K06246-1A-100	294	5392	1.9	9.3902	0.7	4.6344	2.3	0.3156	2.1	0.95	1740.2	13.5	101.6

Notes:
Analyses with >10% uncertainty (1-sigma) in 206Pb/238U age are not included.
Analyses with >10% uncertainty (1-sigma) in 206Pb/207Pb age are not included, unless 206Pb/238U age is <500 Ma.
Best age is determined from 206Pb/238U age for analyses with 206Pb/238U age < 900 Ma and from 206Pb/207Pb age for analyses with 206Pb/238Uage > 900 Ma.
Concordance is based on 206Pb/238U age / 206Pb/207Pb age. Value is not reported for 206Pb/238U ages <500 Ma because of large uncertainty in 206Pb/207Pb age.
Analyses with 206Pb/238U age > 500 Ma and with >20% discordance (<80% concordance) are not included.
Analyses with 206Pb/238U age > 500 Ma and with >5% reverse discordance (<105% concordance) are not included.
All uncertainties are reported at the 1-sigma level, and include only measurement errors.
Systematic errors are shown as 206Pb/238U uncertainty, 206Pb/207Pb uncertainty to the right of each sample (at 2-sigma level).
U concentration and U/Th are calibrated relative to Sri Lanka zircon and are accurate to ~20%.
Common Pb correction is from 204Pb, with composition interpreted from Stacey and Kramers (1975).
Uncertainties of 1.5 for 206Pb/ 204Pb, 0.3 for 207Pb/ 204Pb, and 2.0 for 208Pb/ 204Pb are applied to common Pb composition.
U/Pb and 206Pb/207Pb fractionation is calibrated relative to fragments of a large Sri Lanka zircon of 563.5 ± 3.2 Ma (2-sigma).
U decay constants and composition as follows: 238U = 9.8485 x 10-10, 235U = 1.55125 x 10-10, 238U/235U = 137.88
Analytical methods as described by Gehrels et al. (2008).

Table A 2: Hf isotopic data for Vishnu Schist (ALC)

Sample	$^{176}Hf/^{177}Hf$	± (1s)	$^{176}Lu/^{177}Hf$	$^{176}Hf/^{177}Hf$ (T)	E-Hf (0)	E-Hf (0) ± (1s)	E-Hf (T)	Age (Ma)
OS0884-2-1	0.281644	0.000035	0.001396	0.281594	-40.4	1.2	-0.3	1853
OS0884-2-2	0.281638	0.000037	0.001754	0.281578	-40.6	1.3	-2.1	1800
OS0884-2-3	0.280834	0.000034	0.000555	0.280806	-69.0	1.2	-9.5	2661
OS0884-2-4	0.281022	0.000040	0.000912	0.280975	-62.4	1.4	-3.3	2671
OS0884-2-6	0.281196	0.000041	0.000462	0.281173	-56.2	1.5	2.2	2606
OS0884-2-8	0.281217	0.000032	0.000690	0.281184	-55.5	1.1	-0.2	2484
OS0884-2-9	0.281457	0.000039	0.000629	0.281436	-47.0	1.4	-7.5	1783
OS0884-2-17	0.281145	0.000036	0.000649	0.281114	-58.0	1.3	-2.7	2485
OS0884-2-18	0.281590	0.000028	0.000998	0.281554	-42.3	1.0	-1.5	1862
OS0884-2-22	0.281581	0.000025	0.001013	0.281546	-42.6	0.9	-2.8	1817
OS0884-2-27	0.281445	0.000036	0.001316	0.281399	-47.4	1.3	-7.4	1846
OS0884-2-30	0.281632	0.000034	0.000931	0.281601	-40.8	1.2	-1.5	1790
OS0884-2-32	0.281924	0.000050	0.001155	0.281885	-30.4	1.8	8.2	1774
OS0884-2-38	0.281275	0.000042	0.000919	0.281230	-53.4	1.5	2.7	2541
OS0884-2-40	0.281711	0.000033	0.001944	0.281645	-38.0	1.2	0.0	1786
OS0884-2-41	0.281318	0.000048	0.001904	0.281252	-51.9	1.7	-12.9	1831
OS0884-2-50	0.281193	0.000050	0.000866	0.281151	-56.3	1.8	0.5	2563
OS0884-2-100	0.281648	0.000038	0.000832	0.281620	-40.2	1.3	-1.1	1777
OS0884-2-53	0.281667	0.000044	0.000856	0.281636	-39.5	1.5	1.5	1865
OS0884-2-55	0.281189	0.000048	0.001586	0.281114	-56.4	1.7	-2.9	2478
OS0884-2-56	0.281209	0.000038	0.000969	0.281160	-55.7	1.3	2.2	2625
OS0884-2-57	0.281688	0.000042	0.000911	0.281657	-38.8	1.5	0.7	1801
OS0884-2-58	0.281659	0.000041	0.001052	0.281623	-39.8	1.5	-0.7	1792
OS0884-2-59	0.281229	0.000035	0.001033	0.281178	-55.0	1.2	1.8	2577
OS0884-2-60	0.281212	0.000033	0.000863	0.281171	-55.6	1.2	-0.9	2474
OS0884-2-61	0.281122	0.000037	0.000694	0.281090	-58.8	1.3	-4.5	2445
OS0884-2-62	0.281199	0.000035	0.000663	0.281167	-56.1	1.2	-0.8	2483
OS0884-2-66	0.281223	0.000045	0.001134	0.281170	-55.2	1.6	-2.2	2419
OS0884-2-67	0.281778	0.000043	0.001862	0.281716	-35.6	1.5	2.0	1763
OS0884-2-69	0.281746	0.000044	0.001003	0.281712	-36.7	1.5	2.5	1794
OS0884-2-70	0.281718	0.000040	0.000545	0.281698	-37.7	1.4	3.5	1855
OS0884-2-71	0.281747	0.000036	0.001348	0.281701	-36.7	1.3	2.1	1790
OS0884-2-72	0.281215	0.000044	0.001143	0.281161	-55.5	1.5	-1.0	2483
OS0884-2-74	0.281267	0.000036	0.000660	0.281236	-53.7	1.3	1.7	2485
OS0884-2-75	0.281467	0.000039	0.001468	0.281403	-46.6	1.4	3.5	2309
OS0884-2-76	0.281581	0.000038	0.000555	0.281562	-42.6	1.4	-3.0	1784
OS0884-2-78	0.281322	0.000030	0.000843	0.281282	-51.7	1.1	2.7	2458
OS0884-2-79	0.281912	0.000032	0.001573	0.281860	-30.9	1.1	6.6	1744
OS0884-2-80	0.281002	0.000035	0.001299	0.280935	-63.1	1.3	-4.1	2699
OS0884-2-83	0.281705	0.000093	0.001011	0.281671	-38.2	3.3	0.7	1778
OS0884-2-88	0.281883	0.000032	0.001114	0.281846	-31.9	1.1	6.3	1751
OS0884-2-90	0.281736	0.000056	0.001254	0.281695	-37.1	2.0	0.9	1748
OS0884-2-92	0.281157	0.000045	0.001108	0.281101	-57.6	1.6	0.3	2635
OS0884-2-93	0.281787	0.000043	0.001753	0.281728	-35.3	1.5	2.6	1770
OS0884-2-95	0.281753	0.000061	0.002621	0.281665	-36.5	2.2	0.4	1773
OS0884-2-96	0.281571	0.000037	0.000672	0.281549	-42.9	1.3	-3.6	1779
OS0884-2-97	0.281017	0.000050	0.000993	0.280964	-62.5	1.8	-1.4	2765
OS0884-2-99	0.281191	0.000049	0.001772	0.281100	-56.4	1.7	1.1	2668
K0598.6-104-1	0.281637	0.000040	0.003100	0.281531	-40.6	1.4	-3.7	1802
K0598.6-104-5	0.281757	0.000035	0.000834	0.281730	-36.3	1.2	2.0	1742
K0598.6-104-9	0.281704	0.000041	0.002097	0.281634	-38.2	1.5	-1.3	1747

K0598.6-104-10	0.281722	0.000065	0.001356	0.281675	-37.6	2.3	1.5	1805
K0598.6-104-17	0.281815	0.000038	0.000770	0.281790	-34.3	1.4	4.1	1744
K0598.6-104-20	0.281821	0.000050	0.001304	0.281776	-34.1	1.8	5.7	1832
K0598.6-104-26	0.281657	0.000024	0.001065	0.281620	-39.9	0.8	-0.2	1819
K0598.6-104-28	0.281749	0.000035	0.001700	0.281692	-36.6	1.2	1.0	1759
K0598.6-104-34	0.281779	0.000046	0.002534	0.281695	-35.6	1.6	0.8	1744
K0598.6-104-35	0.281744	0.000042	0.001256	0.281702	-36.8	1.5	1.2	1750
K0598.6-104-36	0.281813	0.000034	0.000764	0.281786	-34.4	1.2	6.3	1842
K0598.6-104-37	0.281912	0.000046	0.001247	0.281871	-30.9	1.6	7.0	1744
K0598.6-104-41	0.281808	0.000036	0.000984	0.281775	-34.6	1.3	3.8	1754
K0598.6-104-47	0.281753	0.000039	0.001459	0.281704	-36.5	1.4	1.1	1743
K0598.6-104-49	0.281558	0.000037	0.001014	0.281523	-43.4	1.3	-3.9	1806
K0598.6-104-50	0.281773	0.000037	0.001261	0.281731	-35.8	1.3	2.2	1750
OS08108-4-2	0.281777	0.000049	0.001782	0.281718	-35.6	1.7	1.6	1743
OS08108-4-3	0.281626	0.000057	0.000798	0.281599	-41.0	2.0	-1.7	1783
OS08108-4-4	0.281234	0.000048	0.000996	0.281184	-54.8	1.7	3.2	2630
OS08108-4-6	0.281808	0.000041	0.001627	0.281754	-34.5	1.5	2.9	1744
OS08108-4-7	0.281173	0.000045	0.000926	0.281130	-57.0	1.6	-2.3	2476
OS08108-4-8	0.281789	0.000042	0.001315	0.281745	-35.2	1.5	2.6	1744
OS08108-4-11	0.281661	0.000048	0.001552	0.281609	-39.8	1.7	-2.2	1746
OS08108-4-13	0.281702	0.000030	0.001009	0.281668	-38.3	1.1	0.1	1757
OS08108-4-17	0.281751	0.000033	0.001248	0.281709	-36.6	1.2	1.9	1771
OS08108-4-21	0.281740	0.000050	0.001247	0.281698	-37.0	1.8	1.0	1750
OS08108-4-27	0.281738	0.000037	0.001421	0.281691	-37.0	1.3	0.6	1741
OS08108-4-28	0.281803	0.000040	0.001957	0.281738	-34.7	1.4	2.3	1744
OS08108-4-30	0.281887	0.000036	0.001497	0.281837	-31.8	1.3	5.8	1740
OS08108-4-32	0.281736	0.000029	0.001010	0.281703	-37.1	1.0	1.0	1744
OS081084-1-39	0.281775	0.000041	0.001547	0.281722	-35.7	1.4	2.9	1793
OS081084-1-40	0.281437	0.000072	0.001242	0.281377	-47.7	2.6	7.0	2499
OS081084-1-43	0.281210	0.000041	0.000842	0.281168	-55.7	1.4	1.3	2572
OS081084-1-44	0.281308	0.000094	0.002268	0.281201	-52.2	3.3	0.1	2473
OS081084-1-47	0.281843	0.000044	0.001595	0.281790	-33.3	1.6	4.2	1746
OS081084-1-48	0.281756	0.000045	0.001497	0.281706	-36.4	1.6	1.4	1753
OS081084-1-57	0.281702	0.000034	0.002855	0.281603	-38.3	1.2	-0.8	1816
K051108-108A-2	0.280736	0.000053	0.000992	0.280673	-72.4	1.9	1.6	3332
K051108-108A-3	0.280989	0.000058	0.001797	0.280903	-63.5	2.0	-9.2	2529
K051108-108A-6	0.281140	0.000046	0.000575	0.281112	-58.2	1.6	-1.9	2521
K051108-108A-7	0.281376	0.000016	0.001563	0.281300	-49.8	0.6	4.9	2525
K051108-108A-10	0.281930	0.000047	0.001207	0.281888	-30.2	1.7	10.0	1849
K051108-108A-11	0.280942	0.000056	0.000827	0.280901	-65.2	2.0	-7.7	2596
K051108-108A-15	0.281929	0.000056	0.002623	0.281840	-30.3	2.0	6.7	1779
K051108-108A-21	0.281750	0.000043	0.001250	0.281707	-36.6	1.5	2.8	1814
K051108-108A-28	0.281665	0.000039	0.002695	0.281570	-39.6	1.4	-1.1	1856
K051108-108A-29	0.280596	0.000036	0.001104	0.280527	-77.4	1.3	-5.7	3246
K051108-108A-30	0.281386	0.000037	0.000900	0.281343	-49.5	1.3	6.1	2513
K051108-108A-32	0.281008	0.000054	0.000971	0.280970	-62.8	1.9	-17.5	2066
K051108-108A-44	0.281476	0.000059	0.001567	0.281420	-46.3	2.1	-5.3	1903
K051108-108A-46	0.281566	0.000041	0.000711	0.281540	-43.1	1.4	-1.5	1882
K051108-108A-48	0.281201	0.000039	0.000656	0.281168	-56.0	1.4	2.5	2624
K051108-108A-50	0.281820	0.000045	0.001694	0.281761	-34.1	1.6	4.8	1818
K051108-108A-51	0.281152	0.000052	0.000737	0.281116	-57.8	1.8	-1.5	2533
K051108-108A-52	0.281802	0.000044	0.001854	0.281734	-34.8	1.6	6.4	1928
K051108-108A-53	0.281694	0.000043	0.001210	0.281651	-38.6	1.5	1.5	1843
K051108-108A-57	0.281264	0.000040	0.000586	0.281236	-53.8	1.4	2.6	2524
K051108-108A-58	0.281051	0.000040	0.000732	0.281016	-61.3	1.4	-5.3	2523

K051108-108A-59	0.281389	0.000053	0.000709	0.281362	-49.4	1.9	-5.8	1971
K051108-108A-61	0.281641	0.000048	0.002329	0.281562	-40.4	1.7	-2.6	1801
K051108-108A-62	0.281685	0.000056	0.001075	0.281648	-38.9	2.0	0.5	1804
K051108-108A-63	0.281646	0.000043	0.000880	0.281616	-40.3	1.5	-0.7	1800
K051108-108A-64	0.281682	0.000039	0.001818	0.281620	-39.0	1.4	-0.7	1796
K051108-108A-65	0.281624	0.000049	0.000228	0.281615	-41.1	1.7	2.3	1931
K051108-108A-66	0.281558	0.000033	0.001520	0.281500	-43.4	1.2	0.3	2023
K051108-108A-68	0.281117	0.000048	0.001394	0.281050	-59.0	1.7	-3.7	2541
K051108-108A-69	0.281551	0.000041	0.001483	0.281499	-43.6	1.5	-3.7	1850
K051108-108A-71	0.281298	0.000043	0.001171	0.281242	-52.6	1.5	2.6	2515
K051108-108A-72	0.281430	0.000045	0.001145	0.281375	-47.9	1.6	7.3	2514
K051108-108A-74	0.281135	0.000044	0.000455	0.281113	-58.3	1.6	-1.8	2523
K051108-108A-75	0.281788	0.000031	0.000755	0.281760	-35.3	1.1	7.1	1919
K051108-108A-76	0.281236	0.000046	0.000973	0.281189	-54.8	1.6	0.8	2518
K051108-108A-77	0.281813	0.000045	0.000753	0.281785	-34.4	1.6	9.0	1962
K051108-108A-82	0.281466	0.000046	0.001174	0.281421	-46.7	1.6	-2.8	2011
K051108-108A-84	0.281044	0.000041	0.000867	0.281001	-61.6	1.4	-4.9	2564
K051108-108A-87	0.281783	0.000043	0.001332	0.281737	-35.4	1.5	4.1	1825
K051108-108A-89	0.281647	0.000036	0.001323	0.281601	-40.2	1.3	-0.7	1822
K051108-108A-92	0.281478	0.000019	0.001907	0.281409	-46.2	0.7	-5.3	1919
K051108-108A-93	0.281189	0.000035	0.001314	0.281123	-56.4	1.2	0.5	2607
K051108-108A-94	0.280728	0.000038	0.001725	0.280643	-72.7	1.3	-17.5	2569
K051108-108A-99	0.281010	0.000041	0.000771	0.280972	-62.8	1.4	-5.2	2596
K06-112-1-2	0.281092	0.000042	0.000914	0.281047	-59.9	1.5	-3.3	2559
K06-112-1-3	0.281184	0.000040	0.001008	0.281134	-56.6	1.4	0.6	2595
K06-112-1-4	0.280690	0.000030	0.000460	0.280661	-74.1	1.0	-0.1	3277
K06-112-1-6	0.281214	0.000031	0.000715	0.281177	-55.6	1.1	3.5	2654
K06-112-1-8	0.281581	0.000039	0.000436	0.281566	-42.6	1.4	-1.6	1838
K06-112-1-9	0.281165	0.000040	0.001215	0.281109	-57.3	1.4	-3.9	2442
K06-112-1-10	0.281722	0.000030	0.001049	0.281686	-37.6	1.0	2.2	1821
K06-112-1-13	0.281522	0.000054	0.000495	0.281505	-44.7	1.9	-5.2	1775
K06-112-1-15	0.281110	0.000039	0.000993	0.281062	-59.2	1.4	-4.3	2495
K06-112-1-16	0.281202	0.000034	0.001105	0.281148	-56.0	1.2	0.2	2558
K06-112-1-17	0.281179	0.000037	0.001039	0.281130	-56.8	1.3	-2.3	2479
K06-112-1-18	0.281165	0.000030	0.000364	0.281146	-57.3	1.1	2.9	2672
K06-112-1-19	0.281777	0.000044	0.001392	0.281728	-35.6	1.6	4.4	1850
K06-112-1-20	0.281198	0.000044	0.000613	0.281169	-56.1	1.5	-0.8	2480
K06-112-1-21	0.281109	0.000039	0.000794	0.281071	-59.3	1.4	-4.3	2480
K06-112-1-22	0.281519	0.000049	0.000937	0.281486	-44.8	1.7	-3.9	1862
K06-246-2-1	0.281806	0.000050	0.001527	0.281756	-34.6	1.8	2.7	1734
K06-246-2-5	0.281200	0.000035	0.000597	0.281172	-56.0	1.2	-0.8	2476
K06-246-2-6	0.281846	0.000033	0.001337	0.281802	-33.2	1.2	4.5	1738
K06-246-2-7	0.281880	0.000036	0.000931	0.281849	-32.0	1.3	6.1	1737
K06-246-2-8	0.280557	0.000036	0.001872	0.280440	-78.8	1.3	-9.0	3236
K06-246-2-12	0.281874	0.000041	0.001174	0.281835	-32.2	1.4	5.7	1741
K06-246-2-13	0.281970	0.000042	0.001898	0.281908	-28.8	1.5	8.2	1738
K06-246-2-14	0.281863	0.000046	0.001825	0.281803	-32.6	1.6	4.3	1732
K06-246-2-15	0.281837	0.000034	0.001743	0.281780	-33.5	1.2	3.7	1739
K06-246-2-17	0.280905	0.000034	0.001211	0.280843	-66.5	1.2	-8.0	2669
K06-246-2-18	0.281806	0.000040	0.001224	0.281766	-34.6	1.4	3.1	1735
K06-246-2-20	0.281897	0.000040	0.001684	0.281842	-31.4	1.4	5.8	1737
K06-246-2-23	0.281127	0.000038	0.000544	0.281101	-58.6	1.3	-3.3	2476
K06-246-2-24	0.281193	0.000047	0.000557	0.281167	-56.3	1.6	-1.1	2472
K06-246-2-26	0.281227	0.000030	0.000498	0.281204	-55.1	1.1	0.1	2468
K06-246-2-28	0.281151	0.000053	0.001787	0.281090	-57.8	1.9	-19.4	1799

K06-246-2-29	0.281626	0.000064	0.001227	0.281582	-41.0	2.3	-0.5	1861
K06-246-2-31	0.281148	0.000047	0.001440	0.281075	-57.9	1.7	-0.6	2633
K06-246-2-32	0.281881	0.000057	0.001181	0.281842	-32.0	2.0	5.8	1736
K06-246-2-33	0.281560	0.000041	0.000926	0.281527	-43.3	1.5	-1.6	1902
K06-246-2-34	0.281886	0.000046	0.001347	0.281842	-31.8	1.6	5.8	1738
K06-246-2-42	0.281887	0.000043	0.001304	0.281844	-31.8	1.5	6.0	1740
K06-246-2-43	0.281833	0.000041	0.001657	0.281775	-33.7	1.4	5.9	1843
K06-246-2-46	0.281732	0.000080	0.002376	0.281654	-37.2	2.8	-0.8	1738
K06-246-1-100	0.281949	0.000037	0.001830	0.281889	-29.6	1.3	7.6	1740
K06-246-1-53	0.281307	0.000097	0.002276	0.281191	-52.3	3.4	4.3	2665
K06-246-1-59	0.281918	0.000052	0.001461	0.281870	-30.7	1.8	6.9	1741
K06-246-1-60	0.281915	0.000061	0.002560	0.281831	-30.7	2.2	5.5	1741
K06-246-1-61	0.281958	0.000065	0.003116	0.281855	-29.2	2.3	6.4	1741
K06-246-1-63	0.281323	0.000044	0.000878	0.281280	-51.7	1.6	5.0	2560
K06-246-1-65	0.281920	0.000032	0.001402	0.281874	-30.6	1.1	7.0	1739
K06-246-1-71	0.281853	0.000033	0.001713	0.281797	-32.9	1.2	4.4	1744
K06-246-1-79	0.281362	0.000048	0.001759	0.281278	-50.3	1.7	3.2	2489
K06-246-1-82	0.281956	0.000057	0.001983	0.281890	-29.3	2.0	7.8	1747
K06-246-1-90	0.281876	0.000038	0.002300	0.281800	-32.1	1.3	4.5	1744
K06-246-1-91	0.281733	0.000045	0.001636	0.281679	-37.2	1.6	0.1	1740
K06-246-1-92	0.281881	0.000049	0.002339	0.281804	-32.0	1.7	4.5	1740
K06-246-1-93	0.281840	0.000050	0.002360	0.281762	-33.4	1.8	3.1	1741
K06-246-1-94	0.281980	0.000038	0.001262	0.281938	-28.5	1.3	9.3	1740
K06-246-1-95	0.281879	0.000039	0.001198	0.281837	-32.0	1.4	8.6	1865
K06-246-1-96	0.281963	0.000039	0.002109	0.281893	-29.1	1.4	7.7	1739
K06-246-1-97	0.280806	0.000033	0.001284	0.280738	-70.0	1.2	-9.7	2756

Notes:

Hf fractionation is corrected by comparing measured 179Hf/177Hf against known 179/177 (line by line). Beta Hf is applied as a power law. Yb fractionation is corrected by comparing measured 173Yb/171Yb against known 173/171 (line by line) if 171Yb intensity is more than ~1 mv. Beta Yb is applied as a power law.

Data are filtered by intensity of Hf (removed if below cutoff value determined by monitoring the average offset of the standards from their known values, which is set at the minimum offset)

Data are filtered by removing 1 max and 1 min value (out of 60).

Data are aflso filtered by 95% filter (rejected if outside of 2-sigma std dev of full set)

Uncertainties are standard error of the mean, expressed at 1-sigma

Table A 3: U-Pb geochronologic analyses of Grand Canyon plutons (ALC)

						Isotope ratios							
Analysis	U	206Pb	U/Th	206Pb*	±	207Pb*	±	206Pb*	±	error	Best age	±	Conc
	(ppm)	204Pb		207Pb*	(%)	235U*	(%)	238U	(%)	corr.	(Ma)	(Ma)	(%)
K12-81L-3	380	13227	2.9	9.3282	0.3	4.3766	1.6	0.2961	1.5	0.98	1752.4	5.8	95.4
K12-81L-4	326	31750	2.6	9.2709	0.4	4.6048	1.3	0.3096	1.2	0.94	1763.6	8.1	98.6
K12-81L-5	461	13045	2.1	9.2852	0.5	4.7474	1.0	0.3197	0.8	0.86	1760.8	9.2	101.6
K12-81L-7	613	32924	2.2	9.3032	0.3	4.7505	1.1	0.3205	1.0	0.96	1757.3	5.4	102.0
K12-81L-8	535	717972	2.3	9.3100	0.1	4.7798	0.6	0.3227	0.6	0.98	1755.9	2.4	102.7
K12-81L-11	331	25079	2.1	9.3239	0.4	4.5433	1.8	0.3072	1.8	0.98	1753.2	7.3	98.5
K12-85-3L-1	431	799646	2.5	9.2997	0.2	4.7879	1.0	0.3229	1.0	0.99	1758.0	3.3	102.6
K12-85-3L-2	355	463479	2.4	9.3229	0.2	4.6172	0.9	0.3122	0.9	0.98	1753.4	3.1	99.9
K12-85-3L-3	337	203658	2.1	9.3185	0.2	4.6001	1.8	0.3109	1.8	1.00	1754.3	3.3	99.5
K12-85-3L-4	207	130576	2.7	9.3132	0.3	4.5137	1.4	0.3049	1.4	0.98	1755.3	5.2	97.7
K12-85-3L-6	439	506467	2.6	9.3141	0.1	4.7203	0.7	0.3189	0.7	0.99	1755.1	1.7	101.7
K12-85-3L-7	420	64044	2.6	9.3325	0.2	4.6445	0.9	0.3144	0.8	0.98	1751.5	3.1	100.6
K12-85-3L-8	584	315929	2.0	9.3141	0.2	4.6076	0.6	0.3113	0.6	0.93	1755.1	4.4	99.5
K12-85-3L-8	400	426493	2.1	9.2974	0.1	4.6399	1.2	0.3129	1.2	0.99	1758.4	2.2	99.8
K12-85-3L-9	429	98216	2.1	9.3035	0.1	4.6497	3.0	0.3137	3.0	1.00	1757.2	2.3	100.1
K12-85-3L-10	548	75545	2.1	9.3054	0.2	4.5951	1.1	0.3101	1.0	0.98	1756.9	3.9	99.1
K12-85-3L-11	377	527926	2.3	9.3240	0.3	4.5178	2.3	0.3055	2.3	0.99	1753.2	4.6	98.0
K12-85-3L-12	482	140658	2.1	9.2977	0.2	4.7447	2.7	0.3199	2.7	1.00	1758.4	3.0	101.8
K12-85-3L-13	246	351595	2.7	9.3070	0.3	4.8653	2.5	0.3284	2.5	0.99	1756.5	5.6	104.2
K12-85-3L-14	291	709520	2.5	9.3189	0.2	4.7576	0.6	0.3215	0.6	0.92	1754.2	4.4	102.5
K12-85-3L-15	254	208016	2.6	9.3676	0.4	4.6381	1.5	0.3151	1.4	0.97	1744.7	6.9	101.2
K12-85-3L-16	594	20945	2.4	9.3229	0.3	4.4926	1.6	0.3038	1.6	0.98	1753.4	5.2	97.5
K12-85-3L-17	405	33649	2.9	9.4042	0.3	4.3643	6.6	0.2977	6.6	1.00	1737.5	5.6	96.7
K12-85-3L-18	417	824257	2.5	9.3182	0.2	4.8390	1.1	0.3270	1.1	0.98	1754.3	4.1	104.0
K12-85-3L-19	150	135133	2.8	9.3566	0.5	4.1866	1.7	0.2841	1.6	0.95	1746.8	9.9	92.3
K12-85-3L-20	464	381133	2.6	9.3217	0.1	4.6711	0.8	0.3158	0.8	0.99	1753.6	2.3	100.9
K12-85-3L-23	681	15378	2.1	9.3178	0.5	3.8783	3.0	0.2621	2.9	0.99	1754.4	8.5	85.5
K12-85-3L-24	467	7421	2.5	9.4001	0.4	3.9772	2.8	0.2712	2.7	0.99	1738.3	6.8	89.0
K12-90-5R-1C	115	33405	1.0	9.4239	1.0	4.4444	1.5	0.3038	1.2	0.76	1733.7	18.6	98.6
K12-90-5R-1M	119	37574	1.3	9.4634	0.8	4.4370	1.5	0.3045	1.3	0.87	1726.0	13.8	99.3
K12-90-5R-2	251	211913	1.0	9.5060	0.3	4.4226	1.1	0.3049	1.0	0.95	1717.7	6.2	99.9
K12-90-5R-3	141	15553	1.1	9.4735	0.8	4.4505	1.0	0.3058	0.6	0.64	1724.0	14.3	99.8
K12-90-5R-4	136	32743	1.0	9.4269	0.8	4.4577	1.3	0.3048	1.0	0.80	1733.1	14.1	99.0
K12-90-5R-5	207	141355	1.1	9.5034	0.4	4.4539	0.7	0.3070	0.6	0.86	1718.2	6.8	100.4
K12-90-5R-6	208	70867	1.0	9.5112	0.6	4.4272	0.7	0.3054	0.4	0.57	1716.7	10.6	100.1
K12-90-5R-7	189	178549	1.0	9.5204	0.4	4.4147	1.6	0.3048	1.6	0.97	1715.0	7.2	100.0
K12-90-5R-8	181	91224	1.0	9.4794	0.7	4.4312	1.1	0.3046	0.8	0.73	1722.9	13.2	99.5
K12-90-5R-9	441	378955	1.1	9.4358	0.9	4.6737	5.5	0.3198	5.4	0.99	1731.4	16.2	103.3
K12-90-5R-10	154	99876	1.1	9.4618	0.5	4.4630	1.2	0.3063	1.1	0.92	1726.3	8.4	99.8
K12-90-5R-11	167	117174	1.0	9.5222	0.5	4.4192	1.2	0.3052	1.1	0.92	1714.6	8.8	100.1
K12-90-5R-12	117	19173	1.2	9.2963	3.2	4.5555	3.8	0.3071	2.0	0.52	1758.6	59.0	98.2
K12-90-5R-13C	138	25690	1.1	9.3503	2.9	4.5458	3.3	0.3083	1.7	0.51	1748.0	52.7	99.1
K12-90-5R-13M	110	121576	1.0	9.3826	1.3	4.4767	2.3	0.3046	1.9	0.83	1741.7	23.7	98.4
K12-90-5R-14	193	92830	1.2	9.4921	0.7	4.4856	0.9	0.3088	0.5	0.61	1720.4	12.6	100.8
K12-90-5R-15	169	117329	1.0	9.4638	0.5	4.4635	1.2	0.3064	1.1	0.89	1725.9	10.1	99.8
K12-90-5R-16	324	30961	1.0	9.5005	0.5	4.4532	1.3	0.3068	1.2	0.94	1718.8	8.4	100.4
K12-90-5R-17	515	326735	1.7	9.5112	0.1	4.4376	1.2	0.3061	1.2	1.00	1716.7	2.1	100.3
K12-90-5R-18	258	343994	1.1	9.5194	0.4	4.4434	0.8	0.3068	0.7	0.88	1715.1	6.6	100.6
K12-90-5R-19	141	156619	1.1	9.4506	0.4	4.4431	1.1	0.3045	1.0	0.93	1728.5	7.6	99.1

K12-90-5R-20	180	48838	1.0	9.5083	0.4	4.4371	1.1	0.3060	1.0	0.93	1717.3	7.1	100.2
K12-90-5R-21	196	147613	1.0	9.5292	0.4	4.4239	0.8	0.3057	0.7	0.84	1713.3	7.8	100.4
K12-90-5R-22	219	37869	0.9	9.5326	0.4	4.4496	1.0	0.3076	0.9	0.89	1712.6	8.3	101.0
K12-90-5R-23	170	83577	1.1	9.4930	0.5	4.4653	1.1	0.3074	1.0	0.90	1720.3	8.7	100.5
K12-90-5R-24	99	57895	1.1	9.4984	0.9	4.4522	1.3	0.3067	1.0	0.74	1719.2	16.4	100.3
K12-90-5R-25	74	89557	1.2	9.5656	1.3	4.4562	1.7	0.3092	1.0	0.61	1706.2	24.6	101.8
K12-90-5R-26	273	96485	0.9	9.5024	0.2	4.4849	0.7	0.3091	0.7	0.97	1718.4	3.0	101.0
K12-90-5R-27	154	81917	1.4	9.4674	0.9	4.4940	3.0	0.3086	2.9	0.95	1725.2	16.7	100.5
K12-90-5R-28	78	83153	1.2	9.5267	0.6	4.4115	1.2	0.3048	1.0	0.86	1713.7	10.9	100.1
K12-90-5R-29	212	262351	1.1	9.5087	0.3	4.4222	1.1	0.3050	1.1	0.96	1717.2	6.0	99.9
K12-90-5R-30	143	138158	1.0	9.4820	0.5	4.3788	1.3	0.3011	1.2	0.93	1722.4	8.6	98.5
K12-91-5R-1C	96	77959	3.0	9.3640	0.6	4.6967	1.8	0.3190	1.6	0.93	1745.4	11.8	102.3
K12-91-5R-1M	138	8020	3.1	9.3817	0.6	4.4841	1.4	0.3051	1.3	0.90	1741.9	11.4	98.5
K12-91-5R-3C	72	84597	3.3	9.3512	0.8	4.6271	1.9	0.3138	1.7	0.90	1747.9	14.9	100.7
K12-91-5R-4	138	110976	3.5	9.2780	0.4	4.6955	1.9	0.3160	1.8	0.98	1762.2	7.6	100.4
K12-91-5R-5	77	92938	4.4	9.2800	0.8	4.7534	2.0	0.3199	1.9	0.93	1761.8	13.8	101.6
K12-91-5R-6	55	9627	4.3	9.2835	1.0	4.6528	1.5	0.3133	1.2	0.75	1761.2	18.7	99.8
K12-91-5R-7C	99	13047	3.5	9.3867	0.6	4.7587	3.4	0.3240	3.4	0.98	1740.9	11.6	103.9
K12-91-5R-7M	73	91492	4.1	9.2886	0.6	4.7030	0.9	0.3168	0.7	0.76	1760.2	11.0	100.8
K12-91-5R-8C	114	94340	3.6	9.2979	0.6	4.8008	1.6	0.3237	1.4	0.93	1758.3	10.4	102.8
K12-91-5R-9M	150	8283	3.5	9.2875	0.7	4.6691	1.1	0.3145	0.8	0.75	1760.4	13.2	100.1
K12-91-5R-11C	68	68023	3.1	9.2391	0.8	4.6654	1.5	0.3126	1.2	0.83	1769.9	14.8	99.1
K12-91-5R-11M	183	7464	2.5	9.3039	0.6	4.5070	1.4	0.3041	1.3	0.91	1757.1	10.9	97.4
K12-91-5R-12C	251	4096	2.7	9.2960	1.6	4.0832	5.8	0.2753	5.6	0.96	1758.7	28.8	89.1
K12-91-5R-12M	173	1831	3.2	9.2921	1.5	4.4807	2.1	0.3020	1.4	0.68	1759.5	28.2	96.7
K12-91-5R-13C	164	7345	2.7	9.3155	0.8	4.6572	2.0	0.3147	1.8	0.91	1754.9	15.1	100.5
K12-91-5R-14M	105	68791	2.5	9.2795	0.8	4.6847	1.9	0.3153	1.7	0.91	1761.9	14.5	100.3
K12-91-5R-15C	232	118209	2.2	9.2958	0.3	4.5305	1.1	0.3054	1.1	0.97	1758.7	5.2	97.7
K12-91-5R-15M	182	4316	2.6	9.3209	0.7	4.1898	2.1	0.2832	2.0	0.94	1753.8	12.6	91.7
K12-91-5R-16C	88	23766	3.7	9.3794	0.8	4.6177	1.8	0.3141	1.6	0.90	1742.3	14.2	101.1
K12-91-5R-16M	128	3630	4.2	9.3646	0.7	4.4041	1.7	0.2991	1.6	0.92	1745.2	12.1	96.7
K12-91-5R-17C	160	242434	2.7	9.2920	0.6	4.7905	0.9	0.3228	0.7	0.77	1759.5	10.6	102.5
K12-91-5R-17M	95	97255	4.7	9.3484	0.7	4.7828	2.1	0.3243	2.0	0.94	1748.4	13.0	103.6
K12-91-5R-18C	174	49787	2.4	9.3289	0.3	4.8721	1.7	0.3296	1.6	0.98	1752.2	5.4	104.8
K12-91-5R-18M	73	85222	3.7	9.3621	0.7	4.6703	1.2	0.3171	0.9	0.80	1745.7	12.9	101.7
K12-91-5R-19C	130	86977	2.8	9.3324	0.6	4.5787	3.1	0.3099	3.0	0.98	1751.5	10.9	99.4
K12-91-5R-19M	156	14648	2.4	9.2814	0.6	4.4832	2.6	0.3018	2.5	0.97	1761.6	11.6	96.5
K12-91-5R-20C	216	176130	2.3	9.3241	0.4	4.7960	0.7	0.3243	0.5	0.75	1753.2	8.1	103.3
K12-91-5R-20M	324	5231	2.0	9.5152	1.2	3.7112	6.0	0.2561	5.9	0.98	1716.0	22.8	85.7
K12-96-2L-1C	299	433373	4.7	8.8942	0.3	5.3051	1.2	0.3422	1.1	0.96	1839.1	6.1	103.2
K12-96-2L-1M	159	12082	2.5	9.2863	2.7	4.2832	8.9	0.2885	8.5	0.95	1760.6	49.8	92.8
K12-96-2L-3C	137	66872	2.1	5.7429	0.2	11.8153	1.1	0.4921	1.0	0.98	2597.7	3.8	99.3
K12-96-2L-3M	296	2373	3.3	9.4565	0.9	4.0201	2.3	0.2757	2.1	0.92	1727.3	17.2	90.9
K12-96-2L-4C	109	38120	3.1	9.4614	2.0	4.2090	3.4	0.2888	2.8	0.81	1726.4	37.0	94.7
K12-96-2L-4M	353	6561	2.5	9.4284	1.0	3.9456	6.5	0.2698	6.4	0.99	1732.8	19.2	88.9
K12-96-2L-6C	143	7423	2.4	9.4053	0.8	4.2221	1.9	0.2880	1.7	0.89	1737.3	15.6	93.9
K12-96-2L-8C	247	7513	1.5	9.1461	5.0	4.6895	7.8	0.3111	6.1	0.77	1788.4	90.8	97.6
K12-96-2L-8M	393	12965	2.4	9.4255	0.4	4.4963	1.3	0.3074	1.3	0.96	1733.4	6.9	99.7
K12-96-2L-10C	245	21268	1.9	9.4165	0.6	4.5690	1.0	0.3120	0.7	0.78	1735.1	11.0	100.9
K12-96-2L-10M	303	29155	2.3	9.4425	0.3	4.4238	0.9	0.3030	0.9	0.96	1730.1	4.7	98.6
K12-96-2L-11C	370	11399	2.1	9.4134	1.0	4.4912	3.2	0.3066	3.0	0.95	1735.7	18.6	99.3
K12-96-2L-13C	190	20888	2.7	9.4546	0.8	4.6071	2.3	0.3159	2.2	0.95	1727.7	14.1	102.4
K12-96-2L-15M	289	12891	2.6	9.4467	0.9	4.0431	2.3	0.2770	2.1	0.92	1729.2	17.1	91.2
K12-96-2L-16M	292	5085	3.3	9.4271	1.1	4.3433	1.9	0.2970	1.5	0.79	1733.0	21.1	96.7
K12-96-2L-17C	119	128553	1.5	6.1481	0.4	10.3573	1.3	0.4618	1.2	0.95	2483.4	6.4	98.6

K12-96-2L-20C	270	8362	1.6	9.4455	0.9	4.5058	1.4	0.3087	1.1	0.76	1729.5	16.8	100.3
K12-96-2L-20M	281	8304	2.5	9.4712	0.7	4.3726	1.7	0.3004	1.6	0.92	1724.5	12.4	98.2
K12-96-2L-21C	288	4029	1.8	9.4417	1.0	3.9402	5.7	0.2698	5.6	0.99	1730.2	17.8	89.0
K12-96-2L-21M	289	15520	2.2	9.4660	0.4	4.3755	2.7	0.3004	2.7	0.99	1725.5	8.1	98.1
K12-96-2L-22C	385	12063	3.7	8.3873	0.4	5.5761	1.3	0.3392	1.2	0.94	1944.7	7.5	96.8
K12-96-2L-23C	170	40636	2.9	9.4925	0.5	3.9623	4.1	0.2728	4.1	0.99	1720.4	8.5	90.4
K12-96-2L-23M	305	4225	2.2	9.3194	2.1	4.2628	3.3	0.2881	2.6	0.78	1754.1	38.4	93.0
K12-96-2L-24M	235	2515	2.7	9.4278	0.7	4.0426	2.5	0.2764	2.4	0.96	1732.9	12.2	90.8
K12-96-2L-25C	156	4941	2.8	9.0883	1.6	4.8628	5.4	0.3205	5.2	0.96	1799.9	29.1	99.6
13H99R-1	182	26688	1.5	6.1151	0.3	9.9157	2.8	0.4398	2.8	0.99	2492.5	5.1	94.3
13H99R-2	594	3043	1.5	8.8354	0.9	4.3208	7.6	0.2769	7.5	0.99	1851.1	17.1	85.1
13H99R-3	284	7617	1.8	9.1764	0.8	4.6818	5.8	0.3116	5.8	0.99	1782.3	14.2	98.1
13H99R-5	236	8397	3.8	9.0816	0.5	4.5334	1.7	0.2986	1.6	0.95	1801.3	9.6	93.5
13H99R-6	488	31647	1.5	9.3239	0.5	4.3688	2.6	0.2954	2.5	0.98	1753.2	9.3	95.2
13H99R-7	210	2547	3.2	6.4635	1.1	7.4739	5.1	0.3504	4.9	0.98	2398.7	18.7	80.7
13H99R-8	104	8643	1.4	9.1875	0.9	4.5280	2.0	0.3017	1.8	0.91	1780.1	15.6	95.5
13H99R-9	273	376297	1.9	5.8047	0.7	11.0905	1.6	0.4669	1.5	0.89	2579.8	12.5	95.7
13H99R-10	87	52781	1.4	9.2677	1.0	4.6966	2.1	0.3157	1.8	0.87	1764.3	18.6	100.2
13H99R-11	171	27888	1.8	9.2666	0.4	4.5933	1.9	0.3087	1.8	0.97	1764.5	8.2	98.3
13H99R-14	292	21578	1.5	9.3921	0.3	4.4287	3.8	0.3017	3.8	1.00	1739.9	6.3	97.7
13H99R-16	96	112110	0.6	9.3901	1.1	4.6451	1.9	0.3164	1.5	0.81	1740.3	20.1	101.8
13H99R-17	311	13117	2.2	8.8841	0.4	4.8707	2.1	0.3138	2.1	0.98	1841.2	7.0	95.6
13H99R-18	393	502265	1.2	9.4576	0.3	4.4806	1.3	0.3073	1.2	0.98	1727.1	4.6	100.0
13H99R-21	229	5245	1.9	8.8350	0.5	4.4312	7.1	0.2839	7.1	1.00	1851.2	9.8	87.0
13H99R-22	275	125193	1.2	9.3497	0.5	4.6308	1.9	0.3140	1.8	0.96	1748.1	9.8	100.7
13H99R-25	120	1888	2.6	8.4678	2.2	5.4297	2.8	0.3335	1.7	0.62	1927.6	39.4	96.2
13H99R-26	251	6101	1.8	9.3748	0.4	4.1993	4.3	0.2855	4.2	1.00	1743.2	7.8	92.9
13H99R-27	297	17385	1.5	9.3579	1.1	4.2727	4.0	0.2900	3.8	0.96	1746.6	20.5	94.0
13H99R-29	404	2622	2.2	9.3227	1.5	3.6403	7.2	0.2461	7.0	0.98	1753.4	27.7	80.9
13H99R-31	88	44061	1.5	9.4100	1.1	4.6444	2.3	0.3170	2.0	0.88	1736.4	20.1	102.2
13H99R-32	78	41883	1.3	9.3974	1.0	4.5706	2.6	0.3115	2.4	0.93	1738.8	17.6	100.5
13H99R-34	457	1639	2.3	9.0079	1.4	4.0491	4.5	0.2645	4.3	0.95	1816.1	26.1	83.3
13H99R-35	497	14746	1.5	9.4478	0.4	4.5454	4.9	0.3115	4.9	1.00	1729.0	6.8	101.1
13H99R-36	221	2153	1.4	8.8360	3.4	4.9510	3.9	0.3173	1.9	0.48	1851.0	62.2	96.0
13H99R-37	430	5151	18.3	8.9898	1.4	4.6823	2.4	0.3053	1.9	0.81	1819.7	25.4	94.4
13H99R-38	87	11535	1.5	9.2538	1.0	4.4421	3.4	0.2981	3.3	0.96	1767.0	18.2	95.2
13H99R-40	163	1680	1.5	4.4711	1.9	14.8802	4.6	0.4825	4.2	0.91	3007.2	30.4	84.4
13H99R-41	509	17898	1.2	9.3356	0.6	4.7559	2.6	0.3220	2.5	0.97	1750.9	11.1	102.8
13H99R-44	149	633	1.3	8.7013	3.4	4.1948	8.8	0.2647	8.1	0.92	1878.7	60.9	80.6
13H99R-45	373	2183	4.3	8.4715	1.1	4.5690	3.9	0.2807	3.7	0.96	1926.8	19.7	82.8
13H99R-46	393	1727	1.7	9.1488	1.6	3.7464	7.3	0.2486	7.2	0.98	1787.8	28.7	80.1
13H99R-47	212	199649	1.4	6.1362	0.1	10.7699	1.6	0.4793	1.6	1.00	2486.7	2.5	101.5
13H99R-48	300	2111	1.7	9.3204	2.6	3.8341	3.4	0.2592	2.1	0.62	1753.9	47.9	84.7
13H99R-49	295	2911	3.7	8.5752	1.2	5.5863	2.1	0.3474	1.8	0.83	1905.0	21.5	100.9
13H99R-50	250	3809	3.5	8.7385	0.9	4.3227	2.3	0.2740	2.1	0.91	1871.0	17.1	83.4
13H99R-51	217	8454	1.4	9.3373	0.4	4.3790	3.1	0.2965	3.0	0.99	1750.6	8.1	95.6
13H99R-52	203	154052	1.4	5.1664	0.2	14.0706	2.3	0.5272	2.3	1.00	2772.6	3.5	98.5
13H99R-53	268	85058	1.4	9.4682	0.3	4.3289	1.1	0.2973	1.1	0.97	1725.1	4.8	97.3
13H99R-54	153	349886	1.6	9.0904	0.5	5.0225	2.2	0.3311	2.2	0.98	1799.5	8.3	102.5
K12-115L-1	139	8526	5.2	8.8216	0.8	5.1334	2.1	0.3284	1.9	0.93	1853.9	14.3	98.8
K12-115L-2	223	9227	3.5	8.7873	0.7	5.0700	1.9	0.3231	1.8	0.93	1860.9	12.4	97.0
K12-115L-3	235	73680	4.2	8.8243	0.6	5.3889	5.9	0.3449	5.9	0.99	1853.4	10.8	103.1
K12-115L-4C	305	33153	3.2	8.6783	1.9	5.5604	3.4	0.3500	2.8	0.82	1883.5	34.5	102.7
K12-115L-7	403	5072	2.4	8.8436	0.5	4.7426	2.0	0.3042	1.9	0.97	1849.4	8.5	92.6
K12-115L-9	121	62444	4.2	8.8486	0.6	5.2156	0.9	0.3347	0.7	0.77	1848.4	11.0	100.7

K12-115L-12	172	152547	5.4	8.7540	1.4	5.5466	4.0	0.3522	3.7	0.94	1867.8	24.5	104.1
K12-115L-15	446	27207	3.4	8.8187	0.5	5.3982	1.8	0.3453	1.7	0.96	1854.5	9.2	103.1
K12-115L-18	583	8327	2.0	8.8279	0.7	5.0921	2.8	0.3260	2.7	0.97	1852.6	13.1	98.2
K12-115L-19C	393	8479	2.5	8.8105	0.5	5.2372	1.5	0.3347	1.4	0.93	1856.2	9.9	100.3
K12-115L-22	335	15181	4.1	8.9769	0.4	4.8055	2.7	0.3129	2.7	0.99	1822.3	7.8	96.3
K12-115L-25	279	12954	3.2	8.7714	0.8	5.2038	2.7	0.3310	2.6	0.96	1864.2	14.2	98.9
K12-115L-26	335	11325	4.1	8.7958	0.7	5.2784	3.5	0.3367	3.4	0.98	1859.2	11.9	100.6
K12-115L-27	441	47257	3.1	8.8096	0.6	5.2132	2.6	0.3331	2.5	0.97	1856.4	10.8	99.8

Notes:

Analyses with >10% uncertainty (1-sigma) in 206Pb/238U age are not included.

Analyses with >10% uncertainty (1-sigma) in 206Pb/207Pb age are not included, unless 206Pb/238U age is <500 Ma.

Best age is determined from 206Pb/238U age for analyses with 206Pb/238U age < 900 Ma and from 206Pb/207Pb age for analyses with 206Pb/238Uage > 900 Ma.

Concordance is based on 206Pb/238U age / 206Pb/207Pb age. Value is not reported for 206Pb/238U ages <500 Ma because of large uncertainty in 206Pb/207Pb age.

Analyses with 206Pb/238U age > 500 Ma and with >20% discordance (<80% concordance) are not included.

Analyses with 206Pb/238U age > 500 Ma and with >5% reverse discordance (<105% concordance) are not included.

All uncertainties are reported at the 1-sigma level, and include only measurement errors.

Systematic errors are shown as 206Pb/238U uncertainty, 206Pb/207Pb uncertainty to the right of each sample (at 2-sigma level).

U concentration and U/Th are calibrated relative to Sri Lanka zircon and are accurate to ~20%.

Common Pb correction is from 204Pb, with composition interpreted from Stacey and Kramers (1975).

Uncertainties of 1.5 for 206Pb/ 204Pb, 0.3 for 207Pb/ 204Pb, and 2.0 for 208Pb/ 204Pb are applied to common Pb composition.

U/Pb and 206Pb/207Pb fractionation is calibrated relative to fragments of a large Sri Lanka zircon of 563.5 ± 3.2 Ma (2-sigma).

U decay constants and composition as follows: 238U = 9.8485 x 10-10, 235U = 1.55125 x 10-10, 238U/235U = 137.88

Analytical methods as described by Gehrels et al. (2008).

Table A 4: Hf isotopic data for Grand Canyon plutons (ALC)

Sample	$^{176}Hf/^{177}Hf$	± (1s)	$^{176}Lu/^{177}Hf$	$^{176}Hf/^{177}Hf$ (T)	E-Hf (0)	E-Hf (0) ± (1s)	E-Hf (T)	Age (Ma)
K12-81L-3	0.281931	0.000036	0.002576	0.281846	-30.2	1.3	6.3	1752
K12-81L-5	0.282024	0.000041	0.003186	0.281918	-26.9	1.5	9.1	1761
K12-81L-7	0.282124	0.000051	0.004981	0.281957	-23.4	1.8	10.4	1757
K12-81L-8	0.282152	0.000050	0.003547	0.282034	-22.4	1.8	13.1	1756
K12-81L-11	0.282006	0.000048	0.002820	0.281912	-27.5	1.7	8.7	1753
K12-85.3L-1	0.281997	0.000056	0.004510	0.281847	-27.9	2.0	6.5	1758
K12-85.3L-2	0.282141	0.000045	0.003789	0.282015	-22.8	1.6	12.3	1753
K12-85.3L-3	0.282081	0.000049	0.003088	0.281978	-24.9	1.7	11.1	1754
K12-85.3L-4	0.282002	0.000048	0.001816	0.281941	-27.7	1.7	9.8	1755
K12-85.3L-6	0.282064	0.000053	0.002334	0.281986	-25.5	1.9	11.4	1755
K12-85.3L-7	0.282039	0.000055	0.004704	0.281883	-26.4	1.9	7.6	1751
K12-85.3L-8	0.281937	0.000040	0.003132	0.281833	-30.0	1.4	5.9	1755
K12-85.3L-9	0.282112	0.000058	0.003778	0.281986	-23.8	2.1	11.4	1757
K12-85.3L-10	0.281998	0.000075	0.003973	0.281865	-27.8	2.7	7.1	1757
K12-85.3L-11	0.282058	0.000044	0.003757	0.281933	-25.7	1.5	9.4	1753
K12-85.3L-12	0.282036	0.000052	0.003929	0.281905	-26.5	1.9	8.5	1758
K12-85.3L-13	0.282065	0.000046	0.003384	0.281952	-25.5	1.6	10.2	1756
K12-85.3L-14	0.282003	0.000048	0.002453	0.281921	-27.6	1.7	9.1	1754
K12-85.3L-15	0.282042	0.000043	0.002178	0.281970	-26.3	1.5	10.6	1745
K12-85.3L-16	0.282187	0.000055	0.004845	0.282025	-21.2	2.0	12.7	1753
K12-85.3L-17	0.282003	0.000046	0.003463	0.281889	-27.6	1.6	7.5	1737
K12-85.3L-18	0.282062	0.000050	0.004324	0.281918	-25.6	1.8	8.9	1754
K12-85.3L-19	0.282019	0.000058	0.003019	0.281919	-27.1	2.0	8.8	1747
K12-85.3L-20	0.282035	0.000036	0.003011	0.281935	-26.5	1.3	9.5	1754
K12-85.3L-23	0.282058	0.000046	0.004162	0.281920	-25.7	1.6	9.0	1754
K12-85.3L-24	0.282087	0.000061	0.004303	0.281945	-24.7	2.2	9.5	1738
K12-90.5R-1C	0.281923	0.000069	0.000422	0.281909	-30.5	2.4	8.2	1734
K12-90.5R-1M	0.281952	0.000046	0.000308	0.281942	-29.4	1.6	9.1	1726
K12-90.5R-2	0.281900	0.000057	0.000946	0.281869	-31.3	2.0	6.5	1724
K12-90.5R-3	0.281941	0.000043	0.000455	0.281926	-29.8	1.5	8.4	1718
K12-90.5R-4	0.282016	0.000048	0.000672	0.281994	-27.2	1.7	11.1	1733
K12-90.5R-5	0.281906	0.000041	0.000639	0.281885	-31.1	1.4	6.9	1718
K12-90.5R-6	0.281894	0.000044	0.000909	0.281864	-31.5	1.6	6.2	1717
K12-90.5R-7	0.282050	0.000048	0.000899	0.282020	-26.0	1.7	11.7	1715
K12-90.5R-8	0.281903	0.000037	0.000762	0.281878	-31.2	1.3	6.8	1723
K12-90.5R-9	0.281860	0.000050	0.000737	0.281836	-32.7	1.8	5.5	1731
K12-90.5R-10	0.281895	0.000049	0.000675	0.281873	-31.5	1.7	6.7	1726
K12-90.5R-11	0.281931	0.000050	0.000819	0.281904	-30.2	1.8	7.5	1715

K12-90.5R-14	0.281995	0.000051	0.000765	0.281970	-27.9	1.8	10.0	1720
K12-90.5R-15	0.281862	0.000038	0.000659	0.281841	-32.6	1.3	5.5	1726
K12-90.5R-16	0.281895	0.000031	0.000968	0.281863	-31.5	1.1	6.2	1719
K12-90.5R-17	0.281988	0.000033	0.000990	0.281956	-28.2	1.2	9.4	1717
K12-90.5R-18	0.281923	0.000046	0.000635	0.281902	-30.5	1.6	7.5	1715
K12-90.5R-19	0.281938	0.000050	0.000618	0.281918	-29.9	1.8	8.3	1728
K12-90.5R-20	0.282068	0.000042	0.000871	0.282039	-25.4	1.5	12.4	1717
K12-90.5R-21	0.281981	0.000045	0.000878	0.281953	-28.4	1.6	9.2	1713
K12-90.5R-22	0.281937	0.000042	0.001057	0.281903	-30.0	1.5	7.5	1713
K12-90.5R-23	0.282026	0.000048	0.000726	0.282002	-26.8	1.7	11.1	1720
K12-90.5R-24	0.282021	0.000038	0.000789	0.281996	-27.0	1.3	10.9	1719
K12-90.5R-26	0.281942	0.000040	0.001108	0.281906	-29.8	1.4	7.7	1718
K12-90.5R-27	0.281900	0.000032	0.000372	0.281887	-31.3	1.1	7.2	1725
K12-90.5R-28	0.281957	0.000038	0.000527	0.281940	-29.3	1.4	8.8	1714
K12-90.5R-29	0.281923	0.000040	0.000762	0.281898	-30.5	1.4	7.4	1717
K12-90.5R-30	0.281958	0.000039	0.000605	0.281938	-29.2	1.4	8.9	1722
K12-91.5R-1C	0.282031	0.000041	0.001308	0.281988	-26.7	1.5	11.2	1745
K12-91.5R-1M	0.281959	0.000038	0.001341	0.281914	-29.2	1.3	8.5	1742
K12-91.5R-3C	0.281997	0.000043	0.001336	0.281953	-27.9	1.5	10.0	1748
K12-91.5R-4	0.281937	0.000030	0.000943	0.281905	-30.0	1.1	8.7	1762
K12-91.5R-5	0.281978	0.000049	0.000894	0.281948	-28.5	1.7	10.2	1762
K12-91.5R-6	0.281988	0.000041	0.000778	0.281962	-28.2	1.4	10.7	1761
K12-91.5R-7C	0.282034	0.000034	0.001137	0.281996	-26.6	1.2	11.4	1741
K12-91.5R-7M	0.281859	0.000032	0.000753	0.281834	-32.7	1.1	6.1	1760
K12-91.5R-8C	0.281981	0.000035	0.001137	0.281943	-28.4	1.2	9.9	1758
K12-91.5R-14M	0.281941	0.000038	0.001543	0.281889	-29.9	1.3	8.1	1762
K12-91.5R-13C	0.281980	0.000042	0.002134	0.281909	-28.5	1.5	8.6	1755
K12-91.5R-15C	0.282030	0.000046	0.002696	0.281940	-26.7	1.6	9.8	1759
K12-91.5R-15M	0.282010	0.000043	0.001286	0.281967	-27.4	1.5	10.7	1754
K12-91.5R-16C	0.281934	0.000039	0.001204	0.281894	-30.1	1.4	7.8	1742
K12-91.5R-16M	0.281961	0.000045	0.001336	0.281917	-29.1	1.6	8.7	1745
K12-91.5R-17C	0.281969	0.000043	0.001268	0.281927	-28.8	1.5	9.4	1759
K12-91.5R-17M	0.281962	0.000038	0.001021	0.281928	-29.1	1.4	9.2	1748
K12-91.5R-18M	0.281958	0.000046	0.000686	0.281935	-29.3	1.6	9.3	1746
K12-91.5R-18C	0.281890	0.000039	0.001869	0.281828	-31.7	1.4	5.7	1752
K12-91.5R-19C	0.281904	0.000044	0.001600	0.281850	-31.2	1.6	6.5	1751
K12-91.5R-19M	0.281892	0.000040	0.001373	0.281847	-31.6	1.4	6.6	1762
K12-91.5R-20C	0.282012	0.000050	0.002182	0.281939	-27.3	1.8	9.7	1753
K12-91.5R-20M	0.281989	0.000037	0.002581	0.281905	-28.1	1.3	7.6	1716
K12-96.2L-1C	0.281889	0.000035	0.000929	0.281856	-31.7	1.2	8.7	1839
K12-96.2L-3M	0.281986	0.000033	0.002053	0.281918	-28.3	1.2	8.3	1727

K12-96.2L-4M	0.281995	0.000063	0.001817	0.281935	-28.0	2.2	9.0	1733
K12-96.2L-8M	0.281910	0.000040	0.001212	0.281870	-30.9	1.4	6.6	1726
K12-96.2L-6C	0.282045	0.000044	0.001055	0.282010	-26.2	1.6	11.8	1737
K12-96.2L-11C	0.281910	0.000045	0.000925	0.281879	-31.0	1.6	7.1	1736
K12-96.2L-10C	0.281974	0.000040	0.001080	0.281938	-28.7	1.4	9.2	1735
K12-96.2L-10M	0.281927	0.000052	0.001242	0.281886	-30.3	1.8	7.2	1730
K12-96.2L-13C	0.281884	0.000045	0.000972	0.281852	-31.9	1.6	6.0	1728
K12-96.2L-15M	0.281927	0.000044	0.000795	0.281901	-30.3	1.6	7.7	1729
K12-96.2L-16M	0.281877	0.000039	0.000706	0.281854	-32.1	1.4	6.2	1733
K12-96.2L-17C	0.281156	0.000029	0.000960	0.281110	-57.6	1.0	-2.9	2483
K12-96.2L-20C	0.281947	0.000039	0.001250	0.281906	-29.6	1.4	7.9	1729
K12-96.2L-20M	0.281901	0.000039	0.000892	0.281872	-31.2	1.4	6.6	1724
K12-96.2L-21M	0.282034	0.000042	0.001848	0.281973	-26.6	1.5	10.2	1725
K12-96.2L-21C	0.282024	0.000037	0.001022	0.281990	-26.9	1.3	10.9	1730
K12-96.2L-22C	0.281412	0.000033	0.000360	0.281399	-48.5	1.2	-5.1	1945
K12-96.2L-23C	0.281933	0.000048	0.001024	0.281900	-30.1	1.7	7.5	1720
K12-96.2L-23M	0.282071	0.000043	0.002679	0.281982	-25.3	1.5	11.2	1754
K12-96.2L-24M	0.281872	0.000033	0.000939	0.281841	-32.3	1.2	5.7	1733
13H-099R-1	0.281262	0.000050	0.001186	0.281205	-53.9	1.8	0.7	2492
13H-099R-11	0.281907	0.000043	0.001571	0.281854	-31.0	1.5	6.9	1764
13H-099R-14	0.281987	0.000052	0.001426	0.281940	-28.2	1.8	9.4	1740
13H-099R-17	0.281918	0.000054	0.002224	0.281840	-30.7	1.9	8.2	1841
13H-099R-18	0.282021	0.000040	0.000794	0.281995	-27.0	1.4	11.1	1727
13H-099R-2	0.281524	0.000034	0.001427	0.281474	-44.6	1.2	-4.6	1851
13H-099R-21	0.281836	0.000039	0.001598	0.281780	-33.5	1.4	6.3	1851
13H-099R-22	0.281787	0.000038	0.001631	0.281733	-35.3	1.3	2.2	1748
13H-099R-26	0.281863	0.000046	0.000145	0.281858	-32.6	1.6	6.6	1743
13H-099R-35	0.281913	0.000045	0.001775	0.281855	-30.8	1.6	6.1	1729
13H-099R-47	0.281349	0.000050	0.001619	0.281272	-50.8	1.8	3.0	2487
13H-099R-52	0.281087	0.000043	0.000528	0.281059	-60.0	1.5	2.1	2773
13H-099R-6	0.281808	0.000041	0.002253	0.281733	-34.6	1.5	2.3	1753
13H-099R-7	0.281319	0.000030	0.000543	0.281294	-51.8	1.1	1.7	2399
K12-115L-1	0.281891	0.000048	0.001511	0.281838	-31.6	1.7	8.4	1854
K12-115L-3	0.281896	0.000049	0.002146	0.281820	-31.4	1.7	7.7	1853
K12-115L-2	0.281993	0.000039	0.002361	0.281910	-28.0	1.4	11.1	1861
K12-115L-7	0.281954	0.000042	0.002559	0.281864	-29.4	1.5	9.2	1849
K12-115L-9	0.281921	0.000041	0.001254	0.281877	-30.5	1.4	9.7	1848
K12-115L-15	0.281916	0.000059	0.003148	0.281805	-30.7	2.1	7.2	1854
K12-115L-18	0.281920	0.000066	0.003738	0.281788	-30.6	2.3	6.6	1853
K12-115L-19C	0.281941	0.000042	0.003042	0.281834	-29.9	1.5	8.3	1856
K12-115L-22	0.281943	0.000043	0.002153	0.281869	-29.8	1.5	8.7	1822

K12-115L-25	0.282010	0.000043	0.002696	0.281914	-27.4	1.5	11.3	1864
K12-115L-26	0.281908	0.000055	0.001978	0.281838	-31.0	1.9	8.5	1859
K12-115L-27	0.281882	0.000051	0.003121	0.281772	-31.9	1.8	6.1	1856

Notes:
Hf fractionation is corrected by comparing measured 179Hf/177Hf against known 179/177 (line by line). Beta Hf is applied as a power law.
Yb fractionation is corrected by comparing measured 173Yb/171Yb against known 173/171 (line by line) if 171Yb intensity is more than ~1 mv. Beta Yb is applied as a power law.
Data are filtered by intensity of Hf (removed if below cutoff value determined by monitoring the average offset of the standards from their known values, which is set at the minimum offset)
Data are filtered by removing 1 max and 1 min value (out of 60).
Data are aflso filtered by 95% filter (rejected if outside of 2-sigma std dev of full set)
Uncertainties are standard error of the mean, expressed at 1-sigma

Table A 5: U-Pb geochronologic data from Grand Canyon plutons (GEMOC)

				AGES (common-Pb corrected, Ma)								
Analysis No.	Th	U	Th/U	$^{207}Pb/^{206}Pb$	± 1σ	$^{207}Pb/^{235}U$	± 1σ	$^{206}Pb/^{238}U$	± 1σ	$^{208}Pb/^{232}Th$	± 1σ	Disc.
	(ppm)	(ppm)										%
K05-100.5-1Rim	106	137	0.78	1739	8	1740	8	1740	16	1798	17	0.0
K05-100.5-2Core	130	129	1.01	2547	8	2547	9	2547	22	2729	25	0.0
K05-100.5-3	68	149	0.46	2475	7	2474	9	2472	20	2588	23	0.1
K05-100.5-4	91	124	0.74	2936	7	2936	9	2936	22	3047	26	0.0
K05-100.5-5	86	146	0.59	2476	8	2476	9	2475	21	2596	23	0.0
K05-100.5-6	67	123	0.55	1732	8	1716	8	1703	14	1770	17	1.9
K05-100.5-7	199	286	0.69	1749	8	1747	8	1746	15	1825	16	0.2
K05-100.5-8	129	218	0.59	2469	9	2465	11	2461	24	2693	30	0.4
K05-100.5-9	106	209	0.51	2470	8	2471	9	2472	21	2575	23	-0.1
K05-100.5-12	90	166	0.54	2498	8	2497	9	2496	21	2829	26	0.1
K05-100.5-19	78	555	0.14	2756	7	2754	9	2751	23	2872	26	0.2
K05-100.5-39	175	194	0.90	1734	10	1731	10	1729	18	1870	21	0.3
K05-100.5-54	103	205	0.51	1731	9	1731	8	1731	16	1817	18	0.0
K05-100.5-57	220	497	0.44	2487	8	2487	10	2487	22	2785	26	0.0
K05-100.5-58	280	1625	0.17	2397	9	2396	10	2394	23	3742	36	0.2
K05-100.5-71	162	132	1.22	1778	8	1777	8	1776	15	1877	17	0.2
K05-100.5-75	90	168	0.54	2504	8	2503	10	2502	22	2762	26	0.1
K05-100.5-82	109	212	0.52	2468	7	2467	9	2465	20	2640	24	0.1
K05-100.5-89	261	706	0.37	1758	34	1770	12	1780	18	1782	20	-1.5
K05-100.5-95	66	144	0.46	2417	30	2399	13	2378	21	2373	24	1.9
K05-100.5-97	42	101	0.42	1731	8	1727	8	1723	15	2606	28	0.6
K05-100.5-100	408	754	0.54	2473	8	2473	9	2472	20	2626	23	0.0
K05-100.5-101	241	247	0.98	1853	8	1853	8	1853	16	1933	17	0.0
K05-100.5-110	1403	1278	1.10	2373	30	1866	12	1446	13	1375	13	43.5
K05-100.5-113	362	652	0.56	2472	35	2424	14	2367	26	2353	29	5.1
K06-107-2	161	192	0.84	1721	23	1727	10	1732	16	1749	44	-0.8
K06-107-3	155	226	0.69	1723	20	1724	8	1725	14	1766	30	-0.2
K06-107-4	104	147	0.70	1739	31	1738	14	1737	19	1651	66	0.1
K06-107-5	126	133	0.95	1720	20	1713	8	1709	14	1742	32	0.7
K06-107-6	101	129	0.78	1741	24	1733	11	1726	17	1740	45	1
K06-107-7	149	135	1.10	1722	29	1624	11	1550	12	1626	64	11.3
K06-107-8	177	185	0.96	1735	23	1723	10	1714	15	1754	47	1.4
K06-107-9	167	197	0.85	1724	23	1724	10	1723	16	1732	46	0.1
K06-107-10	180	223	0.81	1725	25	1726	11	1727	17	1698	53	-0.2

K06-107-12	153	182	0.84	1721	21	1689	8	1663	14	1659	33	3.8
K05-113-01	208	673	0.31	1843	9	1842	9	1841	17	1925	36	0.1
K05-113-02	145	616	0.24	1853	10	1849	11	1846	18	1836	49	0.4
K05-113-03	126	429	0.29	1847	12	1803	12	1766	16	1791	67	5.0
K05-113-05	147	551	0.27	1811	14	1777	14	1748	20	1762	74	4.0
K05-113-06	91	307	0.29	1834	9	1833	9	1832	16	1841	36	0.1
K05-113-07	145	474	0.31	1842	10	1802	11	1768	18	1783	51	4.6
K05-113-08	223	627	0.35	1847	11	1839	11	1832	18	1861	57	1.0
K05-113-09	67	328	0.20	1832	9	1831	10	1831	15	1845	52	0.0
K05-113-10	58	285	0.20	1791	26	1753	22	1722	23	1816	150	4.4
K05-113-11	191	692	0.28	1836	11	1836	11	1836	17	1852	63	0.0
K05-113-15	84	336	0.25	1828	14	1828	14	1829	20	1763	77	0.0
K05-113-16	64	344	0.19	1821	39	1760	14	1709	18	1699	19	7.0
K05-113-17	292	864	0.34	1845	12	1774	11	1715	16	1789	65	8.0
K05-113-18	91	369	0.25	1839	27	1818	9	1799	15	1795	16	2.5
K05-113-19	205	617	0.33	1847	20	1742	18	1656	21	1772	116	11.7
K05-113-20	74	280	0.26	1840	9	1836	9	1833	16	1785	40	0.5
K05-113-21	118	502	0.23	1866	14	1790	14	1726	19	1771	76	8.5
K05-113-38	94	351	0.27	1867	18	1865	17	1863	22	1776	97	0.2
K05-113-41	148	571	0.26	1841	10	1840	10	1839	17	1796	50	0.1
K05-113-43	150	578	0.26	1848	9	1847	9	1847	15	1834	48	0.0
K05-113-45	163	599	0.27	1846	10	1845	10	1844	17	1884	46	0.1
K05-113-46	54	247	0.22	1850	11	1847	11	1844	18	2025	59	0.3
K05-113-47	91	361	0.25	1840	10	1827	10	1815	16	1807	51	1.6
K05-113-48	46	219	0.21	1853	17	1853	15	1853	19	2125	108	0.0
K06-228.3-1-1	414	558	0.74	1737	21	1730	9	1724	15	1850	31	0.9
K06-228.3-1-5	122	191	0.64	1726	21	1720	10	1715	16	1792	29	0.7
K06-228.3-1-7	159	200	0.79	1757	21	1741	9	1728	16	1829	27	1.8
K06-228.3-1-8	596	649	0.92	1733	20	1733	9	1732	15	1798	23	0.1
K06-228.3-1-12	427	447	0.96	1820	25	1776	12	1738	19	1808	48	5.1
K06-228.3-1-13	544	491	1.11	1740	20	1746	9	1751	15	1803	24	-0.7
K06-228.3-1-15	1023	883	1.16	1738	20	1742	9	1745	15	1792	24	-0.4
K06-228.3-1-16	1092	895	1.22	1735	21	1720	9	1707	16	1735	28	1.9
K06-228.3-1-18	348	352	0.99	1742	25	1736	10	1732	15	1789	47	0.6
K06-228.3-1-22	992	846	1.17	1738	21	1728	10	1720	16	1761	32	1.2
K06-238-1	26	77	0.34	1724	23	1722	10	1719	16	1762	36	0.3
K06-238-2	42	144	0.29	2275	45	2183	19	2086	24	2064	27	9.7
K06-238-5	22	70	0.31	1737	25	1717	11	1701	16	1754	42	2.3
K06-238-6	203	871	0.23	1721	23	1714	10	1709	15	1769	40	0.8

K06-238-9	65	141	0.46	1739	22	1733	9	1729	14	1903	40	0.7
K06-238-10	103	713	0.14	1730	28	1744	12	1755	17	1857	64	-1.6
K06-238-12	68	183	0.37	1728	23	1716	10	1705	15	1787	42	1.5
K06-238-13Core	51	253	0.20	1724	33	1722	12	1721	15	1720	18	0.2
K06-238-13Rim	85	729	0.12	1731	30	1581	13	1472	16	1474	60	16.7
K06-238-16	141	278	0.51	1801	20	1802	9	1803	15	2033	34	-0.1
K06-238-17	131	301	0.43	1731	21	1752	9	1769	15	1859	33	-2.5
K06-238-18	111	240	0.46	1739	28	1740	13	1740	19	1818	57	-0.1
K06-238-19	233	419	0.56	1849	26	1872	12	1894	19	1941	58	-2.8
K06-238-22	53	179	0.30	1859	23	1848	11	1838	17	1861	44	1.3
K06-238-24	453	730	0.62	1740	35	1746	16	1752	21	1937	93	-0.8
K06-238-26	260	450	0.58	1730	22	1733	10	1735	16	1835	36	-0.3
K06-238-30	170	444	0.38	2453	25	2472	13	2496	21	2618	83	-2.1
K06-238-31	83	268	0.31	1761	23	1765	10	1769	16	1848	43	-0.6
K06-238-32	195	433	0.45	1760	29	1776	13	1789	18	1871	68	-1.9
K06-238-35	208	463	0.45	1749	24	1753	11	1757	17	1925	49	-0.5
K06-238-36	156	413	0.38	1733	39	1734	18	1735	21	2044	115	-0.1
K06-245-2-3	100	421	0.24	2658	36	2537	16	2388	25	2353	30	12.1
K06-245-2-4	103	383	0.27	1731	21	1721	8	1713	13	1771	33	1.2
K06-245-2-6	202	531	0.38	1768	28	1580	11	1443	11	1513	51	20.5
K06-245-2-7	269	862	0.31	1734	27	1689	12	1653	18	1705	53	5.3
K06-245-2-11	241	822	0.29	1730	26	1628	11	1550	15	1617	47	11.7
K06-245-2-13	403	876	0.46	1778	24	1738	11	1705	17	1780	43	4.6
K06-245-2-14	237	644	0.37	1733	22	1596	8	1495	11	1477	32	15.4
K06-245-2-15	391	1004	0.39	1737	27	1723	13	1712	19	1803	57	1.6
K06-245-2-16	84	434	0.19	1744	31	1736	14	1729	20	1773	70	1
K06-245-2-17	373	847	0.44	1748	23	1602	9	1494	13	1519	36	16.3
K06-245-2-19	144	124	1.16	2645	20	2613	11	2571	21	3031	60	3.4
K06-245-2-20	71	623	0.11	1680	33	1666	11	1655	16	1653	18	1.7
K06-245-2-24	125	948	0.13	1741	21	1568	8	1443	12	1063	19	19.1
K06-245-2-26	157	395	0.40	1738	27	1685	10	1642	12	1638	51	6.3
K06-245-2-31	189	580	0.33	1747	22	1639	9	1556	13	1546	31	12.2
K06-245-2-34	117	368	0.32	1731	29	1558	11	1433	12	1324	48	19.2
K06-245-2-36	158	345	0.46	2454	21	2449	12	2443	24	2534	56	0.6
K06-245-2-38	85	237	0.36	1750	27	1644	10	1563	12	1438	43	12

Table A 6: Hf isotopic data for Grand Canyon plutons (GEMOC)

Analysis No.	$^{176}Hf/^{177}Hf$	1 se	$^{176}Lu/^{177}Hf$	$^{176}Hf/^{177}Hf$ (T)	E Hf (0)	Epsilon Hf (T)	1 sigma	Age
K05-100.5-1Rim	0.281768	0.000008	0.000519	0.281751	-36.0	2.6	0.6	1739
K05-100.5-2Core	0.281134	0.000009	0.000679	0.281101	-58.4	-1.8	0.6	2547
K05-100.5-3	0.281192	0.000009	0.000666	0.281161	-56.3	-1.3	0.6	2475
K05-100.5-4	0.280895	0.000009	0.000843	0.280848	-66.8	-1.7	0.7	2936
K05-100.5-5	0.281187	0.000011	0.000640	0.281157	-56.5	-1.4	0.8	2476
K05-100.5-6	0.281806	0.000009	0.001013	0.281773	-34.6	3.2	0.7	1732
K05-100.5-7	0.281767	0.000008	0.000704	0.281744	-36.0	2.6	0.6	1749
K05-100.5-8	0.281196	0.000010	0.000563	0.281169	-56.2	-1.1	0.7	2469
K05-100.5-9	0.281195	0.000009	0.000723	0.281161	-56.2	-1.4	0.7	2470
K05-100.5-12	0.281168	0.000008	0.000576	0.281141	-57.2	-1.5	0.6	2498
K05-100.5-19	0.280887	0.000009	0.000744	0.280848	-67.1	-5.9	0.6	2756
K05-100.5-39	0.281802	0.000010	0.002025	0.281735	-34.8	1.9	0.8	1734
K05-100.5-54	0.281799	0.000006	0.001065	0.281764	-34.9	2.9	0.5	1731
K05-100.5-57	0.281209	0.000007	0.000493	0.281186	-55.7	-0.2	0.5	2487
K05-100.5-58	0.281257	0.000010	0.001673	0.281180	-54.0	-2.4	0.8	2397
K05-100.5-71	0.281601	0.000007	0.000834	0.281573	-41.9	-2.8	0.5	1778
K05-100.5-75	0.281188	0.000011	0.000580	0.281160	-56.5	-0.7	0.8	2504
K05-100.5-82	0.281191	0.000009	0.000698	0.281158	-56.4	-1.6	0.6	2468
K05-100.5-89	0.281821	0.000009	0.001555	0.281769	-34.1	3.7	0.7	1758
K05-100.5-95	0.281383	0.000012	0.002979	0.281246	-49.6	0.4	0.8	2417
K05-100.5-97	0.281900	0.000010	0.002843	0.281807	-31.3	4.4	0.7	1731
K05-100.5-100	0.281225	0.000009	0.000711	0.281191	-55.2	-0.3	0.6	2473
K05-100.5-101	0.281303	0.000008	0.000465	0.281287	-52.4	-11.3	0.6	1853
K05-100.5-110	0.281275	0.000010	0.001983	0.281185	-53.4	-2.8	0.7	2373
K05-100.5-113	0.281314	0.000009	0.002261	0.281207	-52.0	0.3	0.7	2472
K06-107-2	0.281942	0.000016	0.000547	0.281924	-29.8	8.3	0.9	1721
K06-107-3	0.281915	0.000011	0.000729	0.281891	-30.8	7.2	0.6	1723
K06-107-4	0.281969	0.000014	0.000443	0.281955	-28.9	9.8	0.8	1739
K06-107-5	0.281948	0.000010	0.000437	0.281934	-29.6	8.7	0.6	1720
K06-107-6	0.281941	0.000011	0.000482	0.281925	-29.8	8.8	0.6	1741
K06-107-7	0.281980	0.000014	0.000663	0.281958	-28.5	9.6	0.8	1722
K06-107-8	0.281966	0.000011	0.000554	0.281948	-29.0	9.5	0.6	1735
K06-107-9	0.281940	0.000013	0.000512	0.281923	-29.9	8.4	0.7	1724
K06-107-10	0.281958	0.000019	0.000567	0.281939	-29.2	9.0	0.9	1725
K06-107-12	0.281942	0.000011	0.000459	0.281927	-29.8	8.4	0.6	1721
K05-113-1	0.281954	0.000012	0.001725	0.281894	-29.4	10.1	0.8	1843
K05-113-2	0.281969	0.000008	0.002175	0.281893	-28.9	10.3	0.5	1853
K05-113-3	0.282057	0.000017	0.003080	0.281949	-25.7	12.1	1.2	1847

K05-113-5	0.281965	0.000015	0.002119	0.281892	-29.0	9.3	1.3	1811
K05-113-6	0.281967	0.000009	0.002032	0.281896	-28.9	10.0	0.6	1834
K05-113-7	0.282011	0.000008	0.003342	0.281894	-27.4	10.1	0.6	1842
K05-113-8	0.282113	0.000016	0.003846	0.281978	-23.8	13.2	1.2	1847
K05-113-9	0.281964	0.000009	0.002251	0.281886	-29.0	9.5	0.6	1832
K05-113-10	0.282005	0.000009	0.002145	0.281932	-27.6	10.2	0.7	1791
K05-113-11	0.282000	0.000010	0.002302	0.281920	-27.8	10.8	0.7	1836
K05-113-15	0.281982	0.000008	0.002253	0.281904	-28.4	10.1	0.6	1828
K05-113-16	0.281911	0.000012	0.001224	0.281869	-30.9	8.7	1.0	1821
K05-113-17	0.282067	0.000015	0.003010	0.281962	-25.4	12.5	1.2	1845
K05-113-18	0.281959	0.000011	0.002051	0.281887	-29.2	9.8	0.7	1839
K05-113-19	0.282080	0.000018	0.003978	0.281941	-24.9	11.8	1.2	1847
K05-113-20	0.281946	0.000012	0.001960	0.281878	-29.7	9.4	0.7	1840
K05-113-21	0.281947	0.000011	0.001724	0.281886	-29.6	10.3	0.8	1866
K05-113-38	0.282002	0.000012	0.003217	0.281888	-27.7	10.4	0.9	1867
K05-113-41	0.281969	0.000011	0.002407	0.281885	-28.9	9.7	0.8	1841
K05-113-43	0.282013	0.000011	0.003169	0.281902	-27.3	10.5	0.7	1848
K05-113-45	0.281992	0.000015	0.002161	0.281916	-28.0	10.9	0.9	1846
K05-113-46	0.281994	0.000016	0.002302	0.281913	-28.0	10.9	1.1	1850
K05-113-47	0.282033	0.000014	0.002679	0.281939	-26.6	11.6	1.0	1840
K05-113-48	0.282022	0.000017	0.003883	0.281885	-27.0	10.0	1.2	1853
K06-228.3-1-01	0.281968	0.000011	0.001576	0.281916	-28.9	8.4	0.6	1737
K06-228.3-1-05	0.281985	0.000020	0.001399	0.281939	-28.3	9.0	1.0	1726
K06-228.3-1-07	0.281958	0.000012	0.001299	0.281915	-29.2	8.8	0.6	1757
K06-228.3-1-08	0.281875	0.000011	0.001430	0.281828	-32.2	5.2	0.6	1733
K06-228.3-1-12	0.282013	0.000016	0.002845	0.281915	-27.3	10.3	0.8	1820
K06-228.3-1-13	0.282008	0.000015	0.003196	0.281902	-27.5	8.0	0.8	1740
K06-228.3-1-15	0.282035	0.000018	0.002188	0.281963	-26.5	10.1	0.9	1738
K06-228.3-1-16	0.281900	0.000013	0.001310	0.281857	-31.3	6.3	0.7	1735
K06-228.3-1-18	0.281869	0.000019	0.001574	0.281817	-32.4	5.0	1.0	1742
K06-228.3-1-22	0.282060	0.000014	0.003377	0.281948	-25.6	9.6	0.8	1738
K06-238-01	0.282010	0.000012	0.001099	0.281974	-27.4	10.2	0.4	1724
K06-238-02	0.281262	0.000010	0.000665	0.281233	-53.9	-3.4	0.4	2275
K06-238-05	0.282020	0.000014	0.001346	0.281976	-27.1	10.5	0.5	1737
K06-238-06	0.281768	0.000013	0.000232	0.281760	-36.0	2.5	0.5	1721
K06-238-09	0.282022	0.000012	0.002446	0.281941	-27.0	9.4	0.4	1739
K06-238-10	0.281740	0.000011	0.000110	0.281736	-37.0	1.9	0.4	1730
K06-238-12	0.281961	0.000013	0.000929	0.281931	-29.1	8.7	0.5	1728
K06-238-13Core	0.281898	0.000020	0.001382	0.281851	-31.4	5.8	0.7	1724
K06-238-13Rim	0.281873	0.000020	0.001229	0.281833	-32.3	5.3	0.7	1731
K06-238-16	0.281979	0.000015	0.001634	0.281923	-28.5	10.2	0.5	1801

K06-238-17	0.281974	0.000011	0.001627	0.281921	-28.7	8.5	0.4	1731
K06-238-18	0.281925	0.000013	0.001209	0.281885	-30.4	7.4	0.5	1739
K06-238-19	0.281645	0.000010	0.000717	0.281620	-40.3	0.5	0.4	1849
K06-238-22	0.281571	0.000022	0.000269	0.281562	-42.9	-1.4	0.8	1859
K06-238-24	0.282025	0.000022	0.002995	0.281925	-26.9	8.8	0.8	1740
K06-238-26	0.281916	0.000013	0.001002	0.281883	-30.7	7.1	0.5	1730
K06-238-30	0.281216	0.000011	0.000637	0.281186	-55.5	-0.9	0.4	2453
K06-238-31	0.281671	0.000010	0.000977	0.281638	-39.4	-0.9	0.4	1761
K06-238-32	0.281629	0.000015	0.001321	0.281584	-40.9	-2.8	0.5	1760
K06-238-35	0.281890	0.000017	0.001538	0.281839	-31.6	6.0	0.6	1749
K06-238-36	0.281890	0.000017	0.001191	0.281851	-31.6	6.0	0.6	1733
K06-245-2-3	0.281106	0.000015	0.001992	0.281005	-59.4	-2.6	0.5	2658
K06-245-2-4	0.281893	0.000013	0.000966	0.281861	-31.5	6.3	0.5	1731
K06-245-2-6	0.281890	0.000009	0.000871	0.281861	-31.6	7.2	0.3	1768
K06-245-2-7	0.281849	0.000011	0.000980	0.281817	-33.1	4.8	0.4	1734
K06-245-2-11	0.281907	0.000010	0.000690	0.281884	-31.0	7.1	0.4	1730
K06-245-2-13	0.281739	0.000013	0.000966	0.281707	-37.0	2.0	0.5	1778
K06-245-2-14	0.281864	0.000014	0.001410	0.281818	-32.6	4.8	0.5	1733
K06-245-2-15	0.281907	0.000014	0.000779	0.281881	-31.0	7.2	0.5	1737
K06-245-2-16	0.281845	0.000014	0.000466	0.281830	-33.2	5.5	0.5	1744
K06-245-2-17	0.281894	0.000012	0.001113	0.281857	-31.5	6.6	0.4	1748
K06-245-2-19	0.281368	0.000018	0.000429	0.281337	-50.1	8.9	0.6	2645
K06-245-2-20	0.281876	0.000011	0.000604	0.281850	-32.1	4.8	0.4	1680
K06-245-2-24	0.281824	0.000009	0.000390	0.281811	-34.0	4.8	0.3	1741
K06-245-2-26	0.281887	0.000016	0.000936	0.281856	-31.8	6.3	0.6	1738
K06-245-2-31	0.281891	0.000009	0.000852	0.281863	-31.6	6.8	0.3	1747
K06-245-2-34	0.281821	0.000014	0.000897	0.281791	-34.1	3.9	0.5	1731
K06-245-2-36	0.281257	0.000013	0.000859	0.281217	-54.0	0.2	0.5	2454
K06-245-2-38	0.281830	0.000011	0.000396	0.281817	-33.8	5.2	0.4	1750

APPENDIX B

Geochemical Evolution and Metallogeny of Continents (GEMOC) Key Centre Methods

U-Pb Geochronology

U-Pb geochronology at the GEMOC Key Centre was conducted *in-situ* using an HP 4500 inductively coupled plasma quadrupole mass spectrometer (ICP-MS) paired with a custom-made UV laser ablation microprobe (LAM) that incorporates a petrographic microscope for detailed sample scrutiny (Norman et al., 1996). Samples and standards were ablated also in a custom-made chamber and transported to the ICP-MS with He carrier gas in order to minimize U/Pb fractionation. In addition, the laser was focused above the sample in order to further minimize fractionation effects; laser conditions were rigorously maintained throughout the duration of sample analysis.

Samples were compared to the zircon standard 02123, with four standard analyses completed before and after every 12 unknowns. The 02123 standard is a gem quality zircon from a Norwegian syenite that yields a perfectly concordant ID-TIMS age of 295 ± 1 Ma (Ketchum et al., 2001). Isotope ratios for both standards and unknowns are determined from background-subtracted signals; the uncertainties in both the background and signal are added in quadrature.

Masses 206, 207, 208, 232, and 238 were measured, and all isotopic ratios were calculated using the in-house on-line data reduction software GLITTER. Mass 204 was not measured due to large isobaric interference from Hg. Common Pb correction was therefore conducted after Andersen (2002), using $^{206}Pb/^{238}U$, $^{207}Pb/^{235}U$, and $^{208}Pb/^{232}Th$

ratios to solve mass-balance equations and correct the data in three-dimensional concordia space.

For additional details regarding analytical methods see Belousova et al. (2001), Griffin et al. (2004), and Jackson et al. (2004).

Hf Isotopes

Hf-isotope analyses at GEMOC were carried out in-situ using a New Wave/Merchantek UP-213 laser-ablation microprobe, attached to a Nu Plasma multi-collector ICPMS. The analyses were carried out with a beam diameter of ca 55 μm and a 5 Hz repetition rate. This resulted in total Hf signals of 1-6 × 10^{-11} A, depending on conditions and the Hf contents. Typical ablation times were 100-120 seconds, resulting in pits 40-60 μm deep. He carrier gas transported the ablated sample from the laser-ablation cell via a mixing chamber to the ICPMS torch.

Interference of ^{176}Lu on ^{176}Hf is corrected by measuring the intensity of the interference-free ^{175}Lu isotope and using ^{176}Lu/^{175}Lu = 0.02669 (DeBievre & Taylor 1993) to calculate ^{176}Lu/^{177}Hf. Similarly, the interference of ^{176}Yb on ^{176}Hf has been corrected by measuring the interference-free ^{172}Yb isotope and using ^{176}Yb/^{172}Yb to calculate ^{176}Yb/^{177}Hf. The appropriate value of ^{176}Yb/^{172}Yb was determined by spiking the JMC475 Hf standard with Yb, and finding the value of ^{176}Yb/^{172}Yb (0.58669) required to yield the value of 176Hf/177Hf obtained on the pure Hf solution. Detailed discussions regarding the overlap corrections for ^{176}Lu and ^{176}Yb are provided in Pearson et al. (2008). Analyses of standard zircons (Griffin et al., 2000; Pearson et al., 2008) illustrate the precision and accuracy obtainable on the ^{176}Hf/^{177}Hf ratio, despite the severe corrections on ^{176}Hf. The typical 2 SE precision on the $^{176}Hf/^{177}Hf$ ratios presented here is ± 0.00002, equivalent to ± 0.7 εHf unit.

The Mud Tank and 91500 zircon standards, analyzed together with the samples, were used as independent control on reproducibility and instrument stability. Average $^{176}Hf/^{177}Hf$ values obtained for the Mud Tank (0.282523 ± 0.000066) and 91500 (0.282299 ± 0.000042) during this study are similar to the long-term averages, which in turn are similar to the TIMS values (Griffin et al., 2006, 2007).

For the calculation of εHf values, we have adopted the chondritic values of Bouvier et al. (2008): $^{176}Lu/^{177}Hf$ (CHUR, today) = 0.0336 and $^{176}Hf/^{177}Hf$ (CHUR, today) = 0.282785. For the calculation of εHf values, we have adopted the decay constant (1.867 × 10-11 yr^{-1}) for ^{176}Lu proposed by Scherer et al. (2001) because it gives the best fit for terrestrial rocks (Amelin and Davis, 2005; Albarède et al., 2006).

For additional details regarding analytical methods see Griffin et al. (2000, 2002, 2004).

Arizona Laserchron Center (ALC) Methods

U-Pb Geochronology

U-Pb geochronology of zircons is conducted *in-situ* by laser ablation multicollector inductively coupled plasma mass spectrometry (LA-MC-ICPMS). The analyses involve ablation of zircon with a New Wave UP193HE Excimer laser prior to May 2011, and afterwards a Photon Machines Analyte G2 excimer laser using a spot diameter of 30 microns. The ablated material is carried in helium into the plasma source of a Nu HR ICPMS, which is equipped with a flight tube of sufficient width that U, Th, and Pb isotopes are measured simultaneously. All measurements are made in static mode, using Faraday detectors with 3×10^{11} ohm resistors for ^{238}U, ^{232}Th, ^{208}Pb-^{206}Pb, and discrete dynode ion counters for ^{204}Pb and ^{202}Hg. Ion yields are ~0.8 mv per ppm. Each analysis consists of one 15-second integration on peaks with the laser off (for backgrounds), 15 one-second integrations with the laser firing, and a 30 second delay to purge the previous sample and prepare for the next analysis. The resulting ablation pit is ~15 microns in depth.

For each analysis, the errors in determining ^{206}Pb/238U and $^{206}Pb/^{204}Pb$ result in a measurement error of ~1-2% (at 2-sigma level) in the $^{206}Pb/^{238}U$ age. The errors in measurement of $^{206}Pb/^{207}Pb$ and $^{206}Pb/^{204}Pb$ also result in ~1-2% (at 2-sigma level) uncertainty in age for grains that are >1.0 Ga, but are substantially larger for younger grains due to low intensity of the ^{207}Pb signal. For most analyses, the cross-over in precision of $^{206}Pb/^{238}U$ and $^{206}Pb/^{207}Pb$ ages occurs at ~1.0 Ga.

^{204}Hg interference with ^{204}Pb is accounted for measurement of ^{202}Hg during laser ablation and subtraction of ^{204}Hg according to the natural $^{202}Hg/^{204}Hg$ of 4.35. This Hg is correction is not significant for most analyses because our Hg backgrounds are low (generally ~150 cps at mass 204).

Common Pb correction is accomplished by using the Hg-corrected ^{204}Pb and assuming an initial Pb composition from Stacey and Kramers (1975). Uncertainties of 1.5 for $^{206}Pb/^{204}Pb$ and 0.3 for $^{207}Pb/^{204}Pb$ are applied to these compositional values based on the variation in Pb isotopic composition in modern crystal rocks.

Inter-element fractionation of Pb/U is generally ~5%, whereas apparent fractionation of Pb isotopes is generally <0.2%. In-run analysis of fragments of a large zircon crystal (generally every fifth measurement) with known age of 563.5 ± 3.2 Ma (2-

sigma error) is used to correct for this fractionation. The uncertainty resulting from the calibration correction is generally 1-2% (2-sigma) for both $^{206}Pb/^{207}Pb$ and $^{206}Pb/^{238}U$ ages.

For additional details regarding analytical methods see Gehrels et al. (2006, 2008), and Gehrels and Pecha (2014).

Hf Isotopes

Hf isotope analyses are conducted with a Nu HR ICPMS connected to a New Wave UP193HE laser (2009-2010) or a Photon Machines Analyte G2 excimer laser (2011). Instrument settings are established first by analysis of 10 ppb solutions of JMC475 and a Spex Hf solution, and then by analysis of 10 ppb solutions containing Spex Hf, Yb, and Lu. The mixtures range in concentration of Yb and Lu, with ^{176}(Yb+Lu) up to 70% of the ^{176}Hf. When all solutions yield $^{176}Hf/^{177}Hf$ of ~0.28216, instrument settings are optimized for laser ablation analyses and seven different standard zircons (Mud Tank, 91500, Temora, R33, FC52, Plesovice, and Sri Lanka) are analyzed. These standards are included with unknowns on the same epoxy mounts. When precision and accuracy are acceptable, unknowns are analyzed using exactly the same acquisition parameters.

Laser ablation analyses are conducted with a laser beam diameter of 40 microns, with the ablation pits located on top of the U-Pb analysis pits. CL images are used to ensure that the ablation pits do not overlap multiple age domains or inclusions. Each acquisition consists of one 40-second integration on backgrounds (on peaks with no laser firing) followed by 60 one-second integrations with the laser firing. Using a typical laser fluence of ~5 J/cm2 and pulse rate of 7 hz, the ablation rate is ~0.8 microns per second. Each standard is analyzed once for every ~20 unknowns.

Isotope fractionation is accounted for using the method of Woodhead et al. (2004): βHf is determined from the measured $^{179}Hf/^{177}Hf$; βYb is determined from the measured $^{173}Yb/^{171}Yb$ (except for very low Yb signals); βLu is assumed to be the same as βYb; and an exponential formula is used for fractionation correction. Yb and Lu interferences are corrected by measurement of $^{176}Yb/^{171}Yb$ and $^{176}Lu/^{175}Lu$ (respectively), as advocated by Woodhead et al. (2004). Critical isotope ratios are $^{179}Hf/^{177}Hf$ =0.73250 (Patchett & Tatsumoto, 1980); $^{173}Yb/^{171}Yb$ = 1.132338 (Vervoort et al. 2004); $^{176}Yb/^{171}Yb$ =0.901691 (Vervoort et al., 2004; Amelin and Davis, 2005); $^{176}Lu/^{175}Lu$ = 0.02653 (Patchett, 1983). All corrections are done line-by-line. For very low Yb signals, βHf is used for fractionation of Yb isotopes. The corrected $^{176}Hf/^{177}Hf$ values are filtered for outliers (2-sigma filter), and the average and standard error are calculated from the resulting ~58 integrations. There is no capability to use only a portion of the acquired data.

All solutions, standards, and unknowns analyzed during a session are reduced together such that unknown values are calibrated based on the standards analyzed during the same session. The most weight is put on the following standards: Temore2, 91500, Mud Tank, FC1, and Plesovice, with less reliance placed on R33. The cutoff for using βHf versus βYb is determined by monitoring the average offset of the standards from their known values, and the cutoff is set at the minimum offset. For most data sets, this is achieved at ~6 mv of ^{171}Yb. For sessions in which the standards yield $^{176}Hf/^{177}Hf$ values that are shifted consistently from the know values, a correction factor is applied to the

$^{176}Hf/^{177}Hf$ of all standards and unknowns. This correction factor is generally less than 1 epsilon unit. For example: all values were increased by 1.0 epsilon units for samples analyzed in August 2012, all values increased by 0.3 epsilon units for samples analyzed in May 2013, all values were decreased by 0.2 epsilon units for samples analyzed in May 2014.

The $^{176}Hf/^{177}Hf$ at time of crystallization is calculated from measurement of present-day $^{176}Hf/^{177}Hf$ and $^{176}Lu/^{177}Hf$, using the decay constant of ^{176}Lu ($\lambda = 1.867 \times 10^{-11}$) from Scherer et al. (2001) and Söderlund et al. (2004). No capability is provided for calculating Hf Depleted Mantle model ages because the $^{176}Hf/^{177}Hf$ and $^{176}Lu/^{177}Hf$ of the source material(s) from which the zircon crystallized is not known.

For additional details regarding analytical methods see Cecil et al. (2011), and Gehrels and Pecha (2014).

APPENDIX C

Pluton Descriptions by Sample

Grapevine Camp Pluton (K12-81L):

The 1737 ± 1 Ma Grapevine camp pluton is a medium grained, biotite granite exposed at river mile 81 as a narrow body aligned with S_2 foliation (Hawkins et al., 1996). Truncated on its western margin by the Vishnu fault zone, the Grapevine Camp pluton is marks the edge of the Mineral Canyon block. The Vishnu fault zone is the first of several thermal boundaries juxtaposing blocks with peak temperatures that vary up to 200 °C, but remarkably constant pressures of 0.6 – 0.7 GPa (Ilg et al., 1996; Dumond et al., 2007). The Mineral Canyon block is characterized by peak temperatures of 735 ± 135 °C (Dumond et al., 2007). The pluton preserves an annealed mylonitic fabric defined by ribbons of quartz and feldspar rich layers (S_1) that is cut by the Phanerozoic Vishnu fault (Huntoon et al., 1980), but the last ductile motion on the shear zone is inferred to be between 1.68 – 1.3 Ga (Ilg et al., 1996). The eastern edge of the pluton displays clear intrusive relations to the Vishnu schist on its eastern side (Hawkins et al., 1996; Ilg et al., 1996). The age of the pluton and the presence of early gneissic layering suggests that the Grapevine Camp pluton is part of the 1.74 – 1.71 Ga suite of arc-plutons, however it is compositionally similar to the younger granite-pegmatite anatectic suite.

Hawkins et al. (1996) described the external morphology an appearance of zircons separated from the Grapevine Camp pluton as slightly rounded and colorless, with pitted crystal faces and ubiquitous fractures and dusty inclusions. Our observations show similar features; zircons from the Grapevine Camp pluton range in size from long axes of approximately 70 – 200 μm with aspect ratios from 1:1 to 2:1. Grains are predominantly rounded and subhedral. Internal textures revealed by CL imaging show many blotchy CL-dark regions disrupting, and in some cases completely obliterating, igneous growth zoning.

A total of 18 grains from the Grapevine Camp pluton were analyzed, with 21 total analyses conducted; 3 attempts were made to analyses distinct zircon domains, but those analyses did not pass the data reduction process. Of the 21 analyses, only 6 yielded satisfactory results. Most of the analyses were discarded due to high common Pb. Several grains yielded high U and Th concentrations (>1000 ppm), but all analyses yielded U/Th ratios between 0.8 – 2.6. No systematic variation was observed between age, U concentration, U/Th ratios, or concordance.

Hawkins et al. (1996) interpreted the external features of these zircons to mean that they were partially resorbed during magmatism, recrystallization, or deformation. The internal textures revealed by our CL provide additional evidence for the alteration of Grapevine Camp pluton zircons. Quenching of CL is an effect of radiation damage (Geisler et al., 2001; Nasdala et al., 2002, 2003), thus the morphology, internal texture, and U and Th concentrations of these grains are consistent with extensive metamictization. The lack of reliable ages obtained from these zircons and common Pb contamination is therefore not surprising. Nevertheless, 6 grains yielded >95% concordant ages with a weighted mean of 1756 ± 16 Ma (MSWD = 0.3). This age is in contrast with the age of 1737 ± 1 Ma reported by Hawkins et al. (1996), and the depositional constraints of 1750 – 1740 Ma for the Grand Canyon Metamorphic Suite, but is within uncertainty of the latter. Given the high degree of metamictization of these grains, it is likely that some open-system behavior is influencing the age determination.

While the Hf data presented herein is linked to these ages, we defer to the 1737 ± 1 Ma reported by Hawkins et al. (1996) for the true crystallization age of the Grapevine Camp pluton.

Of the 6 Grapevine Camp pluton zircons that yielded reliable U-Pb ages, we obtained Hf isotopic data from 4 of them. $\varepsilon Hf_{(t)}$ values ranged from 6.3 to 10.4. The εHf of the depleted mantle at 1756 Ma is 10.1. Three of the four analyses are indistinguishable from the depleted mantle $\varepsilon Hf_{(t)}$, and the fourth is still juvenile at 3.8 epsilon units below depleted mantle (Bahlburg et al., 2011).

Zoroaster Pluton (K12-85.3L):

The 1740 ± 2 Ma Zoroaster pluton is a medium grained biotite granite to granodiorite orthogneiss (Hawkins et al., 1996). Well-documented intrusive relationships into the Grand Canyon Metamorphic Suite include screens of Vishnu schist that are entrained in the pluton (Figure 12). Localized mafic domains suggest some degree of mamga mixing (Figure 12). The compositional layering of the pluton and adjacent schists define a kilometer-scale F_2 plunging 44° towards 226° (Lingley, 1973; Ilg et al., 1996). The Zoroaster pluton lies in the Clear Creek metamorphic block, which is characterized by temperatures from 518 – 552 ± 110 °C.

The morphology of Zoroaster pluton zircons as described by Hawkins et al. (1996) are doubly terminated and prismatic. Our observations consist of predominantly rounded and subhedral, with a few euhedral grains. Zircons range in size from long axes of approximately 50 – 250 µm with aspect ratios from 1:1 to 2:1. Internal textures revealed by CL imaging show many blotchy CL-dark regions disrupting, and in some cases completely obliterating, igneous growth zoning. Some grains preserve pristine igneous growth zoning.

A total of 25 grains from the Zoroaster pluton were analyzed, with 22 grains passing the data reduction process. 2 analyses were discarded due to high ^{204}Pb counts, and 1 was discarded due to reverse discordance. No attempts were made to analyze distinct crystal domains based on CL texture. The two grains excluded for high ^{204}Pb yielded high U concentrations. Finally, 2 ages were manually removed from the population based on filtering of age, concordance, U concentration, and U/Th ratios using the AgePick program (Gehrels, 2009). The Remaining 20 grains yielded a weighted mean age of 1755 ± 14 Ma (MSWD = 0.6). This is within uncertainty of the 1740 ± 2 Ma reported by Hawkins et al. (1996).

We obtained Hf isotopic data from 21 zircons separated from the Zoroaster pluton. $\varepsilon Hf_{(t)}$ values range from 5.9 to 12.7. The εHf value of the depleted mantle at 1755 Ma is 10.1, and of the 21 Zoroaster pluton zircons, 19 of them yielded $\varepsilon Hf_{(t)}$ values that are indistinguishable from the depleted mantle at the 2σ level. All analyses are juvenile after Bahlburg et al. (2011).

Horn Creek Pluton (K12-90.5R):

The 1713 ± 2 Ma Horn pluton is a medium grained hornblende quartz diorite to tonalite (Hawkins et al., 1996). The pluton outcrops as a long sliver oriented parallel to the S_2 foliation, but displays intrusive relations with the Grand Canyon Metamorphic suite (Ilg et al., 1996). A strong northwest striking magmatic foliation (S_1) is transposed by the S_2 foliation. Peak temperatures for the Trinity Creek metamorphic block, in which the Horn pluton lies, are 722 ± 83 °C (Dumond et al., 2007).

Hawkins et al. (1996) described the external morphology of zircons from the Horn pluton as clear grains ranging from prismatic to equant. Our observations show that zircons range in size from long axes of approximately 100 – 400 µm with aspect ratios from 1:1 to 2:1. Grains are predominantly subhedral, with many broken and some showing signs of resorption. Internal textures revealed by CL imaging show igneous growth zoning; most grains shows fairly pristine concentric zoning, but some show irregular sector zoning and some appear nearly homogenous. Blotchy, CL-dark sections are minimal any typically restricted to the edges of grains.

A total of 30 grains from the Horn Creek pluton were analyzed, and every analysis passed the data reduction process. Two attempts were made to date distinct crystal domains, however both attempted resulted in overlapping ages. Three analyses were excluded after manual filtering using the AgePick program revealed much higher U concentrations than all other grains. The remaining 29 analyses yielded a weighted mean age of 1719 ± 14 Ma (MSWD = 0.3), in good agreement with the 1713 ± 1 Ma age of Hawkins et al. (1996). Interestingly, Hawkins et al. (1996) reported a single grains that plotted to the right of their best chord. They interpreted this result as a mixture of a 1713 Ma overgrowth and an inherited core that they were unable to identify by transmitted light observation (Hanchar and Rudnick, 1995). However, our CL images show no evidence for inherited cores in Horn pluton zircons, and our attempts to identify distinct age domains failed.

We obtained 28 Hf isotopic analyses from the Horn pluton. $\varepsilon Hf_{(t)}$ values ranged from 5.5 to 12.4. Of the 28 analyses, 18 were indistinguishable from the εHf value of the depleted mantle at 1719 Ma, and all were within 5 epsilon units of the depleted mantle value of 10.2.

Trinity Pluton (K12-91.5R):

The 1730 ± 3 Trinity pluton is a medium to coarse grained granodiorite to granitic biotite orthogneiss (Hawkins et al., 1996). In the past it has been speculated that the Trinity gneiss was basement to the supracrustal Grand Canyon Metamorphic Suite (Noble and Hunter, 1916), however its age and field relations clearly show that it is intrusive to the Brahma schist (Ilg et al., 1996). The pluton preserves a strong gneissic layering (S_1) and outcrops as an isoclinally folded (F_2) sheet (Ilg et al., 1996). Trinity pluton is naturally underlain by the Trinity Creek metamorphic block.

Hawkins et al. (1996) described the zircons of the Trinity pluton as clear, colorless, doubly terminated and euhedral. Our observations show that zircons from the Trinity pluton range in size from long axes of approximately 100 – 300 µm with aspect ratios from 1:1 to 3:1. Grains are predominantly elongate and subhedral to euhedral. Internal textures revealed by CL imaging show concentric igneous growth zoning and many grains with CL-dark rims that were avoided during analysis. Several apparently distinct cores were identified in CL images, and attempts were made to date discrete crystal domains (see below).

A total of 20 grains from the Trinity pluton were analyzed with 17 core-mantle pair analyses conducted yielding 37 total analyses. Of the 37, 28 analyses passed the data reduction process. 7 analyses were discarded due to high ^{204}Pb counts, 1 due to unacceptable $^{206}Pb/^{238}U$ age uncertainty, and 1 due to discordance. Many analyses discarded for high ^{204}Pb counts were conducted quite near to CL-dark rims and likely included some metamict material. Finally, 1 age was removed during manual filtering using AgePick.

Although there appeared to be many CL-distinct crystal domains, all analyses attempting to discern cores from mantles yielded overlapping ages. Furthermore, no systematic variation was observed between U concentration, U/Th, or concordance for cores and mantles. A weighted mean age of 1755 ± 16 Ma (MSWD = 0.4) was determined from 27 analyses. This age is in contrast with Hawkins et al. (1996) age of 1730 ± 3 Ma, but within uncertainty of the depositional age of the Granite Gorge Metamorphic Suite into which it intrudes.

We obtained 23 Hf isotopic analyses from the Trinity pluton. $\varepsilon Hf_{(t)}$ values range from 5.7 to 11.4 and of the 23 total grains 18 are indistinguishable from the 10.1 $\varepsilon Hf_{(t)}$ of the depleted mantle. All grains are within five epsilon units of the depleted mantle.

Boucher Pluton (K12-96.2L):

The Boucher pluton is a granodiorite to tonalitic pluton that outcrops at river mile 96.2 and is bounded on its eastern side by the 96 Mile shear zone (Ilg et al., 1996). The pluton is weakly foliated with strain localization on its western margin related to motion on the 96 Mile shear zone (Hawkins et al., 199; Ilg et al., 1996). The 96 Mile shear zone marks the boundary between the Trinity Creek block and the Topaz Canyon block, which at greenshist to lower amphibolite grade preserves the lowest grade metamorphism in the Upper Granite Gorge (Ilg et al., 1996; Dumond et al., 1996). An identical age of 1714 ± 1 Ma was determined from both Pb-Pb and U-Pb analysis of titanite (Hawkins, 1996), indicating that peak temperatures in the Topaz Canyon block were below the closure temperature of titanite (~590 °C). In this paper, we present 25 new U-Pb zircon ages from the Boucher pluton.

Zircons from the Boucher pluton range in size from long axes of approximately 100 – 300 μm with aspect ratios from 1:1 to 3:1. Grains are predominantly elongate and subhedral to euhedral. Internal textures revealed by CL imaging show concentric igneous growth zoning and many grains with CL-dark rims that were avoided during analysis. Several apparently distinct cores were identified in CL images, and attempts were made to date discrete crystal domains on every grain (see below).

A total of 25 grains from the Trinity pluton were analyzed with 25 core-mantle pair analyses conducted yielding 50 total analyses. Of the 50, 25 analyses passed the data reduction process. 20 analyses were discarded due to high ^{204}Pb counts, 1 due to unacceptable ^{206}Pb/^{238}U age uncertainty, 2 due to reverse discordance, and 2 due to discordance.

In total, 8 core-mantle pair analyses passed the data reduction process, however only 2 core-mantle pairs yielded non-overlapping ages. 20 of the 25 analyses were used to calculate a weighted mean age of 1730 ± 15 Ma (MSWD = 0.5). This age includes 6 core-mantle pairs that yielded overlapping ages. This age is barely within uncertainty of the titanite ages of Hawkins (1996); however, with the higher closure temperature of zircon, it is likely that our new age of 1730 Ma is a more accurate crystallization age for the Boucher pluton.

No systematic variation was observed between U concentration, U/Th, or concordance in these core-mantle pairs. The remaining 4 analyses came from core analyses and yield a variety of ages. Grain K12-96.2L-1C yielded an age of 1839 ± 19 Ma, which corresponds to the 1840 ± 1 Ma age of the Elves Chasm gneiss (Hawkins et al., 1996). Grain K12-96.2L-22C yielded an age of 1945 ± 22 Ma. Grain K12-96.2L-17C yielded an age of 2483 ± 24 Ma, corresponding quite closely to the 2481 Ma age peak defined in the Vishnu schist (Shufeldt et al., 2010). Finally, grain K12-96.2L-3C yielded an age of 2598 ± 22 Ma. Grains K12-96.2L-1C and 22C did not yield mantle analyses that passed the data reduction process, however grains K12-96.2L-1C and 3C yielded mantle analyses that contributed to the 1730 Ma weighted mean age.

The morphology of these inherited cores varies, however all mantles display concentric igneous growth zoning. K12-96.2L-1C is a homogenous CL-dark care with an irregular shape. K12-96.2L-3C is slightly rounded with igneous growth zoning evident in CL-texture. Between the core and mantle is a thin CL-dark rim. K12-96.2L-17C is nearly euhedral with complex igneous zoning. K12-96.2L-22C is also nearly euhedral, with faint igneous growth zoning and a generally CL-dark texture.

We obtained 20 Hf isotopic analyses from Boucher pluton zircons. 17 Analyses from the 1730 Ma population yield $\varepsilon Hf_{(t)}$ values that range from 5.7 to 11.8. All grains from this population yielded $\varepsilon Hf_{(t)}$ values within five epsilon units of the depleted mantle, and 15 analyses were indistinguishable from the depleted mantle $\varepsilon Hf_{(t)}$ value of 10.1 at 1730 Ma. Grain K12-96.2L-1C yielded an epsilon Hf value of 8.7, which suggests the involvement of Elves Chasm gneiss like crust. Grain K12-96.2L-17C yielded an evolved $\varepsilon Hf_{(t)}$ value of -2.9, and grain K12-96.2L-17C yielded an intermediate value of -2.9.

Tuna Creek Pluton (13H-99R; K05-100.5):

Zircons from the Tuna Creek pluton range in size from long axes of approximately 50 – 200 µm, though most grains are ≤100 µm, with aspect ratios from 1:1 to 1:3. Grains are predominantly subhedral to euhedral. Internal textures revealed by CL imaging show concentric igneous growth zoning, and many have CL-dark rims. Distinct core and rim textures were identified in some cases, but were unable to be resolved by a 30 µm beam.

A total of 54 grains from the Tuna Creek pluton were analyzed at the ALC, with 40 grains passing the data reduction process. Manual filtering of ages via AgePick yielded interesting results; 34 grains show a near continuum of ages from 1725 – 1928 Ma. An additional 6 grains yield ages ranging from 2399 – 3007 Ma. 17 grains of similar U/Th ratios, U concentration, and concordance yielded a weighted mean age of 1751 ± 15 Ma (MSWD = 1.1). Similarly, 25 grains analyzed at the GEMOC Key Centre yield ages ranging from 1732 – 2936 Ma, with 7 grains defining a weighted mean age of 1737 ± 7 Ma (MSWD = 0.7). In total, 65 ages from the Tuna Creek pluton range from 1725 ± 10 Ma to 3007 ± 60 Ma. 24 grains contribute to a peak age of 1740 ± 14 Ma (MSWD = 1.5) which we take to be the crystallization age of the Tuna Creek pluton. The inherited population defines an age peak of 2.48 Ga that is identical to that of the Vishnu Schist. The morphology and CL-texture of inherited grains is varied, but all together indistinguishable the younger population.

Inheritance was identified in the Tuna pluton previously, however those workers were unable to assign a reliable age to the Tuna pluton. Hawkins et al. (1996) reported that the age of the Tuna pluton ranged from 1750 – 1710 Ma with >2.0 Ga inheritance.

Our age of 1740 ± 14 Ma is consistent with both previous geochronologic constraints and field relations; the Tuna pluton displays both S_1 and S_2 foliations, and is thus interpreted to have been emplaced either before or during D_1 deformation (Karlstrom et al., 2003).

Elves Chasm Gneiss (K12-115L; K06-113):

The Elves Chasm gneiss is a lineated hornblende-biotite tonalite to quartz diorite which at 1840 ± 1 Ma is presently the oldest plutonic rock in the southwestern United States.

Zircons from the Elves Chasm gneiss range in size from long axes of approximately 60 – 200 µm with aspect ratios from 1:1 to 2:1. Grains are predominantly subhedral. Internal textures revealed by CL imaging show concentric igneous growth zoning commonly with CL-dark rims.

A total of 27 grains from the Elves Chasm gneiss were analyzed at the ALC, with 4 core-mantle pair analyses conducted for a total of 31 analyses. No core-mantle pairs passed the data reduction process; however, our results show that there was no distinct age population of cores. In all, 14 analyses passed the data reduction process. 16 analyses were discarded due to high ^{204}Pb counts, and 1 analysis due to low $^{206}Pb/^{204}Pb$ ratios. The remaining 14 grains yield a weighted mean age of 1850 ± 18 Ma (MSWD = 1.4). This age is within 2σ error of the 1840 ± 1 Ma age of Hawkins et al. (1996).

24 U-Pb ages were obtained from zircons analyzed at the GEMOC Key Centre. These ages yielded a weighted mean age of 1842 ± 5 Ma (MSWD = 0.9) in excellent agreement with the age of Hawkins et al. (1996).

Ruby Pluton (K06-107):

The 1716.6 ± 0.5 Ma Ruby pluton, exposed from river mile 102 – 108, comprises intermingled mafic to intermediate phases (Hawkins et al., 1996). The eastern margin of the pluton shows intrusive relations with supracrustal rocks. Meanwhile, the pluton is bounded in its western side by the Bass shear zone, and displays a weak magmatic foliation near the contact that is concordant with the S_1 fabric in the adjacent supracrustal rocks (Ilg et al., 1996). The Bass shear zone marks the western edge of the Tuna Creek metamorphic block, which is underlain mostly by the Ruby pluton and Tuna Creek plutons, and characterized by peak temperatures of 769 ± 188 °C.

Hawkins et al. (1996) described the zircon population from the Ruby pluton as large, clear, equant, and inclusion free grains. BSE imaging of zircons analyzed at the GEMOC Key Centre shows rounded equant to subhedral grains with some inclusions and ubiquitous fractures. Back scattered electron images (BSE) are less effective at revealing internal textures than CL images, however internal oscillatory zoning is displayed in most grains. Some show irregular zoning and nearly homogenous textures. No inherited grains or xenocrystic cores were identified in the Ruby pluton.

A weighted mean of 10 analyses yields an age of 1726 ± 14 Ma (MSWD = 0.1), in good agreement with the previous age of Hawkins et al. (1996).

$\varepsilon Hf_{(t)}$ values from the Ruby pluton yielded a tight cluster from 7.2 to 9.8, suggesting that the Ruby pluton is derived from juvenile 1.75 Ga crust.

Diamond Creek Pluton (K06-228.3):

The 1736 ± 1 Ma Diamond Creek pluton is exposed from river mile 212 – 228.5 (Karlstrom et al., 2003). It displays abundant magma mingling textures including local ultramafic cumulate texture.

Zircons separated from the Diamond Creek pluton are rounded to anhedral with abundant inclusions and fractures. Internal textures revealed by BSE are irregular, although igneous zoning is locally preserved. A weighted mean of 10 analyses yields an age of 1738 ± 14 Ma (MSWD = 0.2), in excellent agreement with the previous age of Karlstrom et al. (2003). One grain yielded an age of 1820 ± 50 Ma, which overlaps with the age of the Elves Chasm Gneiss, but no older xenocrystic grains were found.

$\varepsilon Hf_{(t)}$ values range from 5.0 to 10.3 and most are indistinguishable from the depleted mantle curve. The presence of a juvenile 1820 Ma zircon may suggest that the Diamond Creek pluton was in part derived from, or interacted with Elves Chasm age crust during its formation.

238-Mile Pluton (K06-238-2):

The 238-Mile pluton is a granitic gneiss from within the Gneiss Canyon shear zone. The Gneiss Canyon shear zone extends from river mile 234 – 242 and is a broad high strain zone with locally developed mylonite zones. A variety of supracrustal migmatitic gneisses are injected with granitic melts. The Gneiss Canyon shear zone represents the largest significant metamorphic discontinuity in the Grand Canyon region, where rocks to the west of the Gneiss Canyon shear zone record P-T conditions that correspond to ~15 – 20 km depths are juxtaposed against ~10 km rocks to the east.

Zircons separated from the 238-Mile pluton are primarily rounded with aspect ratios of 1:1 to 1:2. Some grains preserve pristine igneous zoning, and others yield more homogenous BSE textures.

The 238-Mile pluton has never been previously dated. A weighted mean of 21 analyses yields an age of 1731 ± 14. The 238-Mile pluton yielded 3 grains that overlap with the age of the Elves Chasm Gneiss, and an additional 2 ages of 2275 Ma and 2453 Ma. The latter corresponds well to the age peak found in the Vishnu Schist, and the age of 2275 is a globally rare age.

$\varepsilon Hf_{(t)}$ values in the primary 1730 Ma population range from 10.5 to -2.8; values indistinguishable from the depleted mantle to more evolved values that reflect the involvement of older crustal material in the pluton's genesis. Of the 3 grains that overlap with the Elves Chasm Gneiss, only one grain yielded a juvenile $\varepsilon Hf_{(t)}$ value. The oldest grains yield evolved $\varepsilon Hf_{(t)}$ values from -0.9 to -3.4, which is similar to the $\varepsilon Hf_{(t)}$ values of other xenocrystic grains found in the Tuna and 245-Mile plutons.

245-Mile Pluton (K06-245-2):

Zircons separated from the 245-Mile pluton are primarily subhedral and somewhat rounded, but two grains are extensively resorbed. Aspect ratios range from 1:1 to 1:3. Most grains contain inclusions and show some fracturing. Pristine igneous zoning is also displayed in all grains except the two that are extensively resorbed.

An age of 1720 ± 5 Ma was reported for the 245-Mile pluton (Karlstrom et al., 2003), which is in contrast to our weighted mean of 15 ages that yields 1741 ± 13 Ma, however the well-developed S_1 foliation preserved in the pluton may suggest that the older age is more accurate. Three older ages ranging from 2454 Ma to 2658 Ma were also obtained. One of these ages comes from a resorbed grain, however the other two are subhedral grains that display pristine igneous zoning indistinguishable from the younger population

$\varepsilon Hf_{(t)}$ values in the young population range from 2.0 to 7.2, which is somewhat lower than most of the other plutons in Grand Canyon. None of these primary grains yield $\varepsilon Hf_{(t)}$ values that are within error of the depeted mantle. In contrast, one of the older xenocrystic grains yielded a juvenile value of 8.9 at 2645 Ma. The other two grains yielded more evolved $\varepsilon Hf_{(t)}$ values ranging from 0.2 to -2.6.

REFERENCES

Andersen, T., Griffin, W.L., and Pearson, N.J., 2002, Crustal Evolution in the SW Part of the Baltic Shield : the Hf Isotope Evidence: Journal of Petrology, v. 43, p. 1725–1747.

Bahlburg, H., Vervoort, J.D., Andrew DuFrane, S., Carlotto, V., Reimann, C., and Cárdenas, J., 2011, The U–Pb and Hf isotope evidence of detrital zircons of the Ordovician Ollantaytambo Formation, southern Peru, and the Ordovician provenance and paleogeography of southern Peru and northern Bolivia: Journal of South American Earth Sciences, v. 32, p. 196–209, doi: 10.1016/j.jsames.2011.07.002.

Barovich, K.M., Patchett, P.J., Peterman, Z.E., and Sims, P.K., 1989, Nd isotopes and the origin of 1.9-1.7 Ga Penokean continental crust of the Lake Superior region: Geological Society of America Bulletin, v. 101, p. 333–338, doi: 10.1130/0016-7606(1989)101<0333.

Barth, A.P., Wooden, J.L., Coleman, D.S., and Fanning, C.M., 2000, Geochronology of the Proterozoic basement of southwesternmost North America, and the origin and evolution of the Mojave crustal province: Tectonics, v. 19, 616-629.

Barth, A.P., Wooden, J.L., Coleman, D.S., and Vogel, M.B., 2009, Assembling and disassembling California: A zircon and monazite geochronologic framework for Proterozoic crustal evolution in southern California: Journal of Geology 117, 221-239.

Bea, F., Montero, P., Gonzalez-Lodeiro, F., and Talavera, C., 2007, Zircon Inheritance Reveals Exceptionally Fast Crustal Magma Generation Processes in Central

Iberia during the Cambro-Ordovician: Journal of Petrology, v. 48, p. 2327–2339, doi: 10.1093/petrology/egm061.

Begg, G., Griffin, W.L., O'Reilly, S.Y., Natapov, L., 2007, Living with Archean Lithosphere: *in* Spencer, J., Titley, S., eds., Ores and Orogenesis: Circum-Pacific Tectonics, Geologic Evolution, and Ore Deposits, Arizona Geological Society Digest 22.

Begg, G.C., Griffin, W.L., Natapov, L.M., O'Reilly, S. Y., Grand, S., O'Neill, C. J., Hronsky, J.M.A, Poudjom Djomani, Y., Deen, T. & Bowden, P., 2009. The lithospheric architecture of Africa: Seismic tomography, mantle petrology and tectonic evolution. *Geosphere 5;23-50. doi:10.1130/GES00179.1*

Begg, G.C., Belousova, E.A., Griffin, W.L., O.Reilly, S.Y., Natapov, L., 2009, Continental versus crustal growth: understanding the paradox: Geological Society of America Abstracts with Programs, vol. 41, No. 7, p. 686.

Belousova, E. a., Griffin, W.L., Shee, S.R., Jackson, S.E., and O'Reilly, S.Y., 2001, Two age populations of zircons from the Timber Creek kimberlites, Northern Territory, as determined by laser-ablation ICP-MS analysis: Australian Journal of Earth Sciences, v. 48, p. 757–765, doi: 10.1046/j.1440-0952.2001.485894.x.

Belousova, E. a., 2005, Zircon Crystal Morphology, Trace Element Signatures and Hf Isotope Composition as a Tool for Petrogenetic Modelling: Examples From Eastern Australian Granitoids: Journal of Petrology, v. 47, p. 329–353, doi: 10.1093/petrology/egi077.

Belousova, E. a., Reid, a. J., Griffin, W.L., and O'Reilly, S.Y., 2009, Rejuvenation vs. recycling of Archean crust in the Gawler Craton, South Australia: Evidence from U–Pb and Hf isotopes in detrital zircon: Lithos, v. 113, p. 570–582, doi: 10.1016/j.lithos.2009.06.028.

Belousova, E. a., Kostitsyn, Y. a., Griffin, W.L., Begg, G.C., O'Reilly, S.Y., and Pearson, N.J., 2010, The growth of the continental crust: Constraints from zircon Hf-isotope data: Lithos, v. 119, p. 457–466, doi: 10.1016/j.lithos.2010.07.024.

Bennett, V.C., and DePaolo, D.J., 1987, Proterozoic crustal history of the western United States as determined by Nd mapping: Geological Society of America Bulletin, v. 99, p. 674–685.

Bickford, M.E., and Hill, B.M., 2007, Does the arc accretion model adequately explain the Paleoproterozoic evolution of southern Laurentia?: An expanded interpretation: Geology, v. 35, p. 167, doi: 10.1130/G23174A.1.

Bickford, M.E., Mueller, P.A., Kamernov, G.D., Hill, B.M., 2008, Crustal evolution of southern Laurentia during the Paleoproterozoic: Insights from zircon Hf isotopic studies of ca. 1.75 Ga rocks in central Colorado: Geology, v. 36, p. 555-558.

Bouvier, A., Vervoort, J.D., and Patchett, P.J., 2008, The Lu–Hf and Sm–Nd isotopic composition of CHUR: Constraints from unequilibrated chondrites and implications for the bulk composition of terrestrial planets: Earth and Planetary Science Letters, v. 273, p. 48–57, doi: 10.1016/j.epsl.2008.06.010.

Bowring, S.A., and Karlstrom, K.E., 1990, Growth, stabilization, and reactivation of Proterozoic lithosphere in the southwestern Unite States: Geology, v. 18, p. 1203–1206.

Cavosie, A.J., Wilde, S. a., Liu, D., Weiblen, P.W., and Valley, J.W., 2004, Internal zoning and U–Th–Pb chemistry of Jack Hills detrital zircons: a mineral record of early Archean to Mesoproterozoic (4348–1576Ma) magmatism: Precambrian Research, v. 135, p. 251–279, doi: 10.1016/j.precamres.2004.09.001.

Cavosie, A.J., Valley, J.W., and Wilde, S. a., 2006, Correlated microanalysis of zircon: Trace element, δ18O, and U–Th–Pb isotopic constraints on the igneous origin of complex >3900Ma detrital grains: Geochimica et Cosmochimica Acta, v. 70, p. 5601–5616, doi: 10.1016/j.gca.2006.08.011.

Cavosie, A.J., Valley, J.W., and Wilde, S.A., 2007, The oldest terrestrial mineral record: a review of 4400 to 4000 Ma detrital zircons from Jack Hills, Western Australia: In: Earth's Oldest Rocks, Developments in Precambrian Geology, v. 15, p. 91-111. doi: 10.1016/S0166-2635(07)15025-8.

Cecil, M.R., Gehrels, G., Ducea, M.N., and Patchett, P.J., 2011, U-Pb-Hf characterization of the central Coast Mountains batholith: Implications for petrogenesis and crustal architecture: Lithosphere, v. 3, p. 247–260, doi: 10.1130/L134.1.

Chamberlain, K.R., and Bowring, S.A., 1990, Proterozoic geochronologic and isotopic boundary in NW Arizona: Journal of Geology, v. 98, p. 399-416.

Corfu, F., Hanchar, J.M., Hoskin, P.W.O., Kinny, P., 2003, Atlas of zircon textures. In: Hanchar, J.M., and Hoskin, P.W.O. (eds) Zircon. Reviews in Mineralogy and Geochemistry, v. 53, p. 469-500.

Corrigan, D., Hajnal, Z., Németh, B., and Lucas, S.B., 2005, Tectonic framework of a Paleoproterozoic arc – continent to continent – continent collisional zone, Trans-Hudson Orogen, from geological and seismic reflection studies 1, 2, 3: v. 434, p. 421–434, doi: 10.1139/E05-025.

Corrigan, D., Pehrsson, S., Wodicka, N., and de Kemp, E., 2009, The Palaeoproterozoic Trans-Hudson Orogen: a prototype of modern accretionary processes: Geological Society, London, Special Publications, v. 327, p. 457–479, doi: 10.1144/SP327.19.

Crowley, J.L., Schmitz, M.D., Bowring, S. a., Williams, M.L., and Karlstrom, K.E., 2006, U–Pb and Hf isotopic analysis of zircon in lower crustal xenoliths from the Navajo volcanic field: 1.4 Ga mafic magmatism and metamorphism beneath the Colorado Plateau: Contributions to Mineralogy and Petrology, v. 151, p. 313–330, doi: 10.1007/s00410-006-0061-z.

Crowley, J.L., Brown, R.L., Gervais, F., and Gibson, H.D., 2008, Assessing Inheritance of Zircon and Monazite in Granitic Rocks from the Monashee Complex, Canadian Cordillera: Journal of Petrology, v. 49, p. 1915–1929, doi: 10.1093/petrology/egn047.

Dickinson, W.R., and Gehrels, G.E., 2009, Use of U-Pb ages of detrital zircons to infer maximum depositional ages of strata: A test against a Colorado Plateau Mesozoic database: Earth and Planetary Science Letters, v. 288, p. 115–125, doi: 10.1016/j.epsl.2009.09.013.

Duebendorfer, E.M., 2007, Research Focus : Crust formation in the western United States: Geology, doi: 10.1130/0091-7613(2007)35.

Duebendorfer, E.M., Chamberlain, K.R., and Fry, B., 2006, Mojave – Yavapai boundary zone, southwestern United States: A rifting model for the formation of an isotopically mixed crustal boundary zone: Geology, v. 34, p. 681-684.

Dumond, G., Mahan, K.H., Williams, M.L., and Karlstrom, K.E., 2007, Crustal segmentation, composite looping pressure-temperature paths, and magma-enhanced metamorphic field gradients: Upper Granite Gorge, Grand Canyon, USA: Geological Society of America Bulletin, v. 119, p. 202–220, doi: 10.1130/B25903.1.

DePaolo, D.J., 1981, Neodymium isotopes in the Colorado Front Range and crust-mantle evolution in the Proterozoic: Science, v. 291, p. 193–196.

Elston, D. P., 1989, Grand Canyon Supergroup, northern Arizona: Stratigraphic summary and preliminary pa- leomagnetic correlations with parts of other North American Proterozoic successions,in Jenney, J. P., and Reynolds, S. J., Geologic evolution of Arizona: Arizona Geological Society Digest, v. 17, p. 259–272.

Farmer, G.L., and DePaolo, D.J., 1983, Origin of Mesozoic and Tertiary granite in the western United States and implications for Pre-Mesozoic crustal structure: 1. Nd and Sr isotopic studies in the geocline of the Northern Great Basin: Journal of Geophysical Research, v. 88, p. 3379, doi: 10.1029/JB088iB04p03379.

Finger, F., 1997, Variscan granitoids of central Europe : their typology , potential sources and tectonothermal relations: Mineralogy and Petrology, v. 61, p. 67–96.

Fowler, A., Prokoph, A., Stern, R., Dupuis, C., 2002, Organization of oscillatory zoning in zircon: Analysis, scaling, geochemistry, and model of a zircon from Kipawa, Quebec, Canada. Geochemica et Cosmica Acta, v. 66, p. 311-328.

Friedman, R.M., Mahoney, J.B., and Cui, Y., 1995, Magmatic evolution of the southern Coast Belt: constraints from Nd-Sr isotopic systematics and geochronology of the southern Coast Plutonic Complex: Canadian Journal of Earth Sciences, v. 32, p. 1681–1698.

Gehrels, G.E., Valencia, V., Pullen, A., 2006, Detrital zircon geochronology by Laser-Ablation Multicollector ICPMS at the Arizona LaserChron Center, in Loszewski, T., and Huff, W., eds., Geochronology: Emerging Opportunities, Paleontology Society Short Course: Paleontology Society Papers, v. 11, 10 p.

Gehrels, G.E., Valencia, V. a., and Ruiz, J., 2008, Enhanced precision, accuracy, efficiency, and spatial resolution of U-Pb ages by laser ablation-multicollector-inductively coupled plasma-mass spectrometry: Geochemistry, Geophysics, Geosystems, v. 9, p. n/a–n/a, doi: 10.1029/2007GC001805.

Gehrels, G., Pecha, M., Canyon, W., and Mex, M., 2014, Detrital zircon U-Pb geochronology and Hf isotope geochemistry of Paleozoic and Triassic passive margin strata of western North America: Geosphere, v. 10, p. 49–65, doi: 10.1130/GES00889.1.

Gonzales, D.A., and Van Schmus, W.R., 2007, Proterozoic history and crustal evolution in southwestern Colorado: Insight from U/Pb and Sm/Nd data: Precambrian Research, v. 154, p. 31–70, doi: 10.1016/j.precamres.2006.12.001.

Griffin, W.L., Pearson, N.J., Belousova, E., Jackson, S.E., O'Reilly, S.Y., van Achterberg, E., and Shee, S.R. 2000. The Hf isotope composition of cratonic mantle: LAM-MC-ICPMS analysis of zircon megacrysts in kimberlites. Geochim. Cosmochim. Acta 64, 133-147.

Griffin, W., Wang, X., Jackson, S., Pearson, N., O'Reilly, S.Y., Xu, X., and Zhou, X., 2002, Zircon chemistry and magma mixing, SE China: In-situ analysis of Hf isotopes, Tonglu and Pingtan igneous complexes: Lithos, v. 61, p. 237–269, doi: 10.1016/S0024-4937(02)00082-8.

Griffin, W.L., Belousova, E. a., Shee, S.R., Pearson, N.J., and O'Reilly, S.Y., 2004, Archean crustal evolution in the northern Yilgarn Craton: U–Pb and Hf-isotope evidence from detrital zircons: Precambrian Research, v. 131, p. 231–282, doi: 10.1016/j.precamres.2003.12.011.

Griffin, W.L., O'Reilly, S.Y., Afonso, J.C., and Begg, G.C., 2008, The Composition and Evolution of Lithospheric Mantle: a Re-evaluation and its Tectonic Implications: Journal of Petrology, v. 50, p. 1185–1204, doi: 10.1093/petrology/egn033.

Griffin, W.L., Begg, G.C., Dunn, D., O'Reilly, S.Y., Natapov, L.M. and Karlstrom, K. 2011. Archean lithosperic mantle beneath Arkansas: continental growth by microcontinent accretion. Bull. Geol. Soc. America 123, no. 9-10, p. 1763-1775, doi:10.1130/B30253.1.

Hacker, B.R., Kelemen, P.B., and Behn, M.D., 2011, Differentiation of the continental crust by relamination: Earth and Planetary Science Letters, v. 307, p. 501–516, doi: 10.1016/j.epsl.2011.05.024.

Hanchar, J.M., and Rudnick, R.L., 1995, Revealing hidden structures, the application of CL and BSE imaging to dating zircons from lower crustal xenoliths: Lithos, v. 30, p. 289–303.

Hanchar, J.M., and Watson, E.B., 2003, Zircon saturation thermometry. In: Hanchar, J.M., and Hoskin, P.W.O. (eds) Zircon. Reviews in Mineralogy and Geochemistry, v. 53, p. 89-112.

Hawkins, D.P., 1996, U-Pb geochronological constraints on the tectonic and thermal evolution of Paleoproterozoic crust in the Grand Canyon, Arizona [Ph.D. thesis]: Cam- bridge, Massachusetts Institute of Technology, 320 p.

Hawkins, D.P., Bowring, S.A., Ilg, B.R., Karlstrom, K.E., and Williams, M.L., 1996, U-Pb geochronologic constraints on the Paleoproterozoic crustal evolution of the Upper Granite Gorge , Grand Canyon , Arizona: Geological Society of America Bulletin, v. 108, p. 1167–1181.

Hill, B.M., and Bickford, M.E., 2001, Paleoproterozoic rocks of central Colorado: Accreted arcs or extended older crust?: Geology, v. 29, p. 1015-1018.

Hoffman, P.F., 1988, UNITED PLATES OF AMERICA, and Growth of Laurentia: American Journal of Science, v. 16, p. 543 – 603.

Hoskin, P.W.O., 2000, Patterns of chaos: Fractal statistics and the oscillatory chemistry of zircon: Geochimica et Cosmochimica Acta, v. 64, p. 1905–1923.

Hoskin, P.W.O., and Schaltegger, U., 2003, The composition of zircon and igneous and metamorphic petrogenesis, In: Hanchar, J.M., and Hoskin, P.W.O. (eds) Zircon. Reviews in Mineralogy and Geochemistry, v. 53, p. 27-62.

Huntoon, P.W., Billingsley, G.H., Jr., Breed, W.J., Sears, J.W., Ford, T.D., Clark, M.D., Babcock, R.S., Brown, E.H., 1980, Geologic map of the eastern part of the Grand Canyon National Park: Grand Canyon, Arizona, Grand Canyon Natural History Association, scale 1:62 500.

Ilg, B.R., Karlstrom, K.E., Hawkins, D.P., and Williams, M.L., 1996, Tectonic evolution of Paleoproterozoic rocks in the Grand Canyon: Insights into middle-crustal processes: Geological Society of America Bulletin, v. 108, p. 1149–1166, doi: 10.1130/0016-7606(1996)108<1149.

Iriondo, A., Premo, W. R., Martinex-Torres, L.M., Budahn, J.R., Atkinson, Jr., W. W., Siems, D.F., Guaras-Gonzalez, B., 2004, Isotopic, geochemical, and temporal characterization of Proterozoic basement rocks in the Quitovac region, northwestern Sonora, Mexico: Implications for the reconstruction of the southwestern margin of Laurentia: Geological Society of America Bulletin, v. 116, p. 154-170.

Jackson, S.E., Pearson, N.J., Griffin, W.L., and Belousova, E. a., 2004, The application of laser ablation-inductively coupled plasma-mass spectrometry to in situ U–Pb zircon geochronology: Chemical Geology, v. 211, p. 47–69, doi: 10.1016/j.chemgeo.2004.06.017.

Jahn, B., Wu, F., Chen, B., 2000, Granitoids of the Central Asian Orogenic Belt and continental growth in the Phanerozoic: Geological Society of America Special Papers, 350, p. 181-193.

Jones, D.S., Barnes, C.G., Premo, W.R., and Snoke, A.W., 2011, The geochemistry and petrogenesis of the Paleoproterozoic Green Mountain arc: A composite(?), bimodal, oceanic, fringing arc: Precambrian Research, v. 185, p. 231–249, doi: 10.1016/j.precamres.2011.01.011.

Karlstrom, K.E., and Bowring, S.A., 1988, Early Proterozoic Assembly of Tectonostratigraphic Terranes in Southwestern North America Author: Journal of Geology, v. 96, p. 561–576.

Karlstrom, K.E., and Bowring, S.A., 1993, Proterozoic orogenic history of Arizona, *in* Reed, J.C., et al., eds., Precambrian: Conterminous U.S.: Boulder, Colorado, Geological Society of America, Geology of North America, v. C-2, p. 188-211.

Karlstrom, K.E., Heizler, M.T., and Williams, M.L., 1997, ^{40}Ar-^{39}Ar muscovite thermochronology within the Upper Granite Gorge of the Grand Canyon: Eos, (Transaction, American Geophysical Union), Fall Meeting Supplement, v. 78, no. 46, p. F784.

Karlstrom, K.E., Ilg, B.R., Williams, M.L., Hawkins, D.P., Bowring, S.A., and Seaman, J.S., 2003, Paleoproterozoic rocks of the Granite Gorges, *in* Bues and Morales, 2003: Grand Canyon Geology.

Karlstrom, K.E., Amato, J.M., Williams, M.L., Heizler, M., Shaw, C.A., Read, A.S., and Bauer, P., 2004, Proterozoic tectonic evolution of the New Mexico region: A synthesis, *in* Mack, G.H., and Giles, K.A., eds., The geology of New Mexico: A geologic history: Canada, New Mexico Geological Society, p. 1-34.

Karlstrom, K.E., Whitmeyer, S.J., Williams, M.L., Bowring, S. a., and Jessup, M.J., 2007, Does the arc-accretion model adequately explain the Paleoproterozoic evolution of southern Laurentia: An expanded interpretation: COMMENT AND REPLY: COMMENT: Geology, v. 35, p. e143–e144, doi: 10.1130/G23971C.1.

Kohút, M., and Nabelek, P.I., 2012, Geochemical and isotopic (Sr, Nd and O) constraints on sources for Variscan granites in the Western Carpathians - implications for crustal structure and tectonics: Journal of GEOsciences, v. 53, p. 307–322, doi: 10.3190/jgeosci.033.

Kovalenko V.I., Yarmolyuk V.V., Kovach V.P., Kotov A.B., Kozakov I.K., Salnikova E.B.,

Larin A.M., 2004, Isotope provinces, mechanisms of generation and sources of the continental crust in the Central Asian Mobile Belt: geological and isotopic evidence, J. Asian Earth Sci, Vol. 23, 605-627.

Lee, C.T., Yin, Q., Rudnick, R.L., and Jacobsen, S.B., 2001, Preservation of ancient and fertile lithospheric mantle beneath the southwestern United States.: Nature, v. 411, p. 69–73, doi: 10.1038/35075048.

Miller, C.F., Hatcher, R.D., Ayers, J.C., Coath, C.D., and Harrison, T.M., 2000, Age and zircon inheritance of eastern Blue Ridge plutons, southwestern North Carolina and northeastern Georgia, with implications for magma history and evolution of the southern Appalachian orogen: American, v. 300, p. 142–172.

Mueller, P.A., Wooden, J.L., Mogk, D.W., and Foster, D.A., 2011, Paleoproterozoic evolution of the Farmington zone: Implications for terrane accretion in southwestern Laurentia: Lithosphere, v. 3, p. 401–408, doi: 10.1130/L161.1.

Pupin, J.P., 1980, Zircon and granite petrology: Contributions to Mineralogy and Petrology, v. 73, p. 207 – 220.

Ramo, O.T., and Calzia, J.P., 1998, Nd isotopic composition of cratonic rocks in the southern Death Valley region; evidence for a substantial Archean source component in Mojavia: Geology, v. 26, p. 891-894.

Reymer, A., Schubert, G., 1986, Rapid growth of some major segements of continental crust: Geology, v. 14, p. 299-302.

Samson, S.D., McClelland, W.C., Patchett, P.J., Gehrels, G.E., and Anderson, R.G., 1989, Evidence from neodymium isotopes for mantle contributions to Phanerozoic crustal genesis in the Canadian cordillera: Nature, v. 337, p. 705–709.

Samson, S.D., Patchett, P.J., McClelland, W.C., and Gehrels, G.E., 1991, Nd isotopic characterization of metamorphic rocks in the coast mountains, Alaskan and Canadian cordillera: ancient crust bounded by juvenile terranes: Tectonics, v. 10, p. 770–780.

Scoates, J.S., and Chamberlain, K.R., 1995, Baddeleyite (ZrO_2) and zircon ($ZrSiO_4$) from anorthosistic rocks of the Laramie anorthosite complex, Wyoming: petrologic consequences and U-Pb ages. American Mineralogist, v. 80, p. 1319-1329.

Siebel, W., Shang, C.K., Thern, E., Danišík, M., and Rohrmüller, J., 2012, Zircon response to high-grade metamorphism as revealed by U–Pb and cathodoluminescence studies: International Journal of Earth Sciences, v. 101, p. 2105–2123, doi: 10.1007/s00531-012-0772-5.

Sommer, H., Wan, Y., Kroner, a., Xie, H., and Jacob, D.E., 2014, Shrimp Zircon Ages and Petrology of Lower Crustal Granulite Xenoliths From the Letseng-La-Terae Kimberlite, Lesotho: Further Evidence for a Namaqua-Natal Connection: South African Journal of Geology, v. 116, p. 183–198, doi: 10.2113/gssajg.116.2.183.

Shufeldt, O.P., Karlstrom, K.E., Gehrels, G.E., and Howard, K.E., 2010, Archean detrital zircons in the Proterozoic Vishnu Schist of the Grand Canyon, Arizona: Implications for crustal architecture and Nuna supercontinent reconstructions: Geology, v. 38, p. 1099–1102, doi: 10.1130/G31335.1.

Strickland, A., Wooden, J.L., Mattinson, C.G., Ushikubo, T., Miller, D.M., and Valley, J.W., 2013, Proterozoic evolution of the Mojave crustal province as preserved in the Ivanpah Mountains, southeastern California: Precambrian Research, v. 224, p. 222–241, doi: 10.1016/j.precamres.2012.09.006.

Vavra, G., 1990, On the kinematics of zircon growth and its petrogenetic significance: a cathodoluminescence study: Contributions to Mineralogy and Petrology, v. 106, p. 90–99.

Vavra, G., 1993, A guide to quantitative morphology of accessory zircon: Chemical Geology, v. 110, p. 15–28, doi: 10.1016/0009-2541(93)90245-E.

Vavra, G., 1994, Systematics of internal zircon morphology in major Variscan granitoid types: Contributions to Mineralogy and Petrology, v. 117, p. 331–344, doi: 10.1007/BF00307269.

Vervoort, J.D., Patchett, P.J., Blichert-toft, J., and Albare, F., 1999, Relationships between Lu – Hf and Sm – Nd isotopic systems in the global sedimentary system: Earth and Planetary Science Letters, v. 168, p. 79–99.

Wang, X., Griffin, W.L., O'Reilly, S.Y., Zhou, X.M., Xu, X.S., Jackson, S.E., and Pearson, N.J., 2002, Morphology and geochemistry of zircons from late Mesozoic igneous complexes in coastal SE China : implications for petrogenesis: Mineralogical Magazine, v. 66, p. 235–251.

Watson, E., B., and Harrison, T. M., 1983, Zircon saturation revisited: temperature and compositional effects in a variety of crustal magma types. Earth and Planetary Science Letters, v. 64, p. 295-304.

Whitehouse, M.J., Kamber, B.S., and Moorbath, S., 1999, Age significance of U–Th–Pb zircon data from early Archaean rocks of west Greenland—a reassessment based on combined ion-microprobe and imaging studies: Chemical Geology, v. 160, p. 201–224, doi: 10.1016/S0009-2541(99)00066-2.

Whitmeyer, S.J., and Karlstrom, K.E., 2007, Tectonic model for the Proterozoic growth of North America: Geosphere, v.3, p. 220–259, doi: 10.1130/GES00055.1.

Wooden, J.L., Barth, a. P., and Mueller, P. a., 2012, Crustal growth and tectonic evolution of the Mojave crustal province: Insights from hafnium isotope systematics in zircons: Lithosphere, v. 5, p. 17–28, doi: 10.1130/L218.1.

Wooden, J.L., and Miller, D.M., 1990, Chronologic and isotopic framework for early Proterozoic crustal evolution in the eastern Mojave Desert region, SE California: Journal of Geophysical Research, v. 95, p. 20133-20146.

Wooden, J.L., and DeWitt, E., 1991, Pb isotopic evidence for the boundary between the Early Proterozoic Mojave and central Arizona crustal provinces in western Arizona: Arizona Geological Society Digest, v. 19, p. 27-50.

Wooden, J. L., Nutman, A. P., Howard, K. A., Bryant, B., DeWitt, E., and Mueller, P. A., 1994, Shrimp U-Pb zircon evidence for Late Archean and Early Proterozoic crustal evolution in the Mojave province and central Arizona crustal provinces [abs.]: Geological Society of America Abstracts with Programs, v. 26, no. 6, p. 69.

Windley, B.F., 2003, Continental growth in the Proterozoic: a global perspective: Geological Society, London, Special Publications, v. 206, p. 23–33, doi: 10.1144/GSL.SP.2003.206.01.03.